The Preparation of Titanium Alloys and Composites via Non Melt Processing

David Tricker MEng

Thesis submitted in partial fulfilment of the
requirements for the degree of
Doctor of Philosophy
of the
University of London

July 2008

For

Mum

Abstract

The consolidation of affordable titanium (Ti) powder is essential for the fabrication of titanium components to reduce production costs. This thesis investigates the consolidation of titanium powder by non-melt processing routes.

An in-house canning and degassing procedure has been developed and employed for the encapsulation of Ti hydride-dehydride (HDH) powder for downstream processing. Degassing trials were conducted to determine the optimum degassing temperature of Ti HDH powder and cans of Ti HDH powder were extruded and analysed to prove consolidation. Compacts of Ti HDH powder were manufactured and extruded with different reduction ratios and a finite element (FE) model has been developed to predict the extrusion pressure and exit temperatures.

It is found that the degassing of Ti HDH powder at different temperatures has revealed that it is unnecessary to degas at temperatures above 500°C to minimise oxygen pick up. The consolidation of both canned and compacted Ti HDH powder is possible with non-melt consolidation routes (extrusion and hot isostatic pressing). However the formation of extrusion defects with regards to the canned material, at both the front and back ends of the extrude, would compromise the economics of industrial processes.

The mechanical properties of extruded Ti HDH powder compare well with wrought material, however the ductility is reduced due to the presence of embrittling inclusions found in the material. These are thought to be picked up during the milling of the Ti powder.

FE modelling has shown that the extrusion pressure is extremely sensitive to the extrusion speed, due to billet chilling. With current extrusion technologies, the high speed extrusion of titanium is the only way to process titanium; however, isothermal conditions would involve the development of a higher temperature container, and hence increase costs.

The thermomechanical processing of Ti-6Al-4V + 20 vol.% TiB composite manufactured via a non-melt processing route has been established, with the formation of the reinforcement phase via an *in-situ* reaction. The majority of TiB_2 converts to TiB during the consolidation with the remainder of the TiB formed during a high temperature conversion heat treatment. The distribution of the reinforcing phase, TiB, is extremely heterogeneous when there is no conversion heat treatment prior to extrusion, whereas the reinforcement phase is homogeneously distributed when the conversion heat treatment prior to extrusion, is applied to the material.

Acknowledgements

Firstly, thanks to my supervisors, Prof. Dicky Dashwood and Dr. Martin Jackson who have provided invaluable support over the years, especially with my inability to spell 'through' correctly. The PowdermatriX Faraday association and the EPSRC for funding the project through the CASE award scheme. Jon Silk and Andrew Tarrant at AMC for introducing me to the world of industry, and to QinetiQ for providing the material.

Also to Melvin Andrews, Richard Sweeney and Mahmoud Ardakani and especially to Garry Stakalls for help with all things technical. I would still be welding cans if not for Garry's help. Seema Raghunathan, Russell Talling and Ioannis Bantounas for help with popLA.

Thanks also to all my fellow members of the Materials Processing Group: Russell, Nick, Fatos, Tik, Rohit, Seema, Danny, Ioannis, Meurig and Dave, and not forgetting the staff at THC and other local establishments. A special mention must go to Betty, for being there through all the good times, and the bad times. Also to ICUC, which has provided a welcome relief for the 'odd weekend'.

A special thank you must goes to my family, and especially my Mum, who has been through so much more than I could ever imagine and has been a constant source of inspiration throughout writing up.

Contents

Abstract 3

Acknowledgements 4

Contents 5

List of Figures 9

List of Tables 15

1 Introduction 17

2 Literature Review 20

2.1 Titanium . . . 20

2.1.1 Classification of Titanium Alloys . . . 21

2.1.2 Microstructural Development in Titanium . . . 23

2.1.3 Commercially Pure Titanium Alloys . . . 24

2.1.4 Oxygen Diffusion in Titanium . . . 28

2.1.5 Ti-6Al-4V . . . 30

2.2 Titanium Powder . . . 32

2.2.1 Classification of Powders . . . 32

2.2.2 Powder Production Routes . . . 33

2.2.2.1 Hydride-dehydride . . . 33

2.2.2.2 Atomisation Routes . . . 33

2.2.2.3 Kroll Sponge/Sponge Fines . . . 34

2.2.2.4 Novel Routes for Powder Production . . . 34

2.3 Titanium Composites . . . 34

2.3.1 Particulate Reinforcement of Titanium Matrix Composites . . . 35

2.3.2 Titanium-Boron System . . . 36

2.3.2.1 Formation of TiB from TiB_2 . . . 37

2.3.2.2 Effect of Boron on the β Transus . . . 38

2.3.2.3 Manufacture of Ti/TiB Composites . . . 38

2.3.3 Mechanical Alloying 38
2.3.4 Load Transfer from the Matrix to the Reinforcement 40
2.4 Consolidation of Metal Powders 41
2.4.1 Theory of Powder Consolidation 41
2.4.2 Degassing and Compacting Powders 43
2.4.3 Vapour Pressure 45
2.4.4 Direct Powder Extrusion 45
2.4.5 Hot Isostatic Pressing 51

3 Experimental Techniques **54**
3.1 Summary 54
3.2 Materials Studied 54
3.2.1 Ti HDH Powder 55
3.2.2 Ti-6Al-4V and TiB_2 powders 56
3.3 Canning and Degassing 56
3.3.1 Can Manufacture 56
3.3.2 Welding 57
3.3.3 Canning 58
3.3.4 Argon Reflowing 59
3.3.5 Degassing 60
3.3.6 Crimping 60
3.4 Cold compacting 61
3.5 Consolidation routes 62
3.5.1 Hot Isostatic Pressing (HIP'ing) 62
3.5.2 Direct Particle Extrusion 62
3.6 Heat Treatments 64
3.7 Analytical techniques 65
3.7.1 Sample Preparation 65
3.7.2 Optical Microscopy 65
3.7.3 Electron Microscopy 65
3.7.4 X-ray Diffraction 65
3.7.5 Texture Analysis 66
3.8 Mechanical Testing 66
3.8.1 Tensile Tests 66
3.9 Thermomechanical Processing of Titanium Matrix Composites 67
3.9.1 Consolidation of Titanium Alloy Composites 67
3.9.2 Extrusion 67

3.9.3 Heat Treatments 68
3.9.4 Mechanical Testing of Ti MMC's 68
3.10 Finite Element Analysis 68
3.10.1 Compression Testing 69
3.10.2 Pre-Processing 69

4 The Consolidation of Canned Ti Powder **70**
4.1 Summary 70
4.2 Characterisation of Ti Powder 70
4.3 Degassing Trials 72
4.3.1 Effect of Temperature on Degassing 73
4.3.2 Deliberate Chloride Additions 77
4.4 Direct Powder Extrusion 80
4.5 Hot Isostatic Pressing 85
4.6 Consolidation of Canned Ti Powder 86
4.6.1 Analysis of Porosity in Consolidated Ti Powder 87
4.6.2 Microstructural Analysis of Consolidated Ti Powder 90
4.6.2.1 Microstructure of Ti HDH Consolidated *via* Extrusion and HIP'ing 90
4.6.2.2 Foreign Particles within the Powder 92
4.6.2.3 Oxygen Analysis on Extruded Canned Ti 93
4.6.2.4 Interface with the Can 93
4.6.3 Mechanical Properties 94
4.7 Conclusions 95

5 The Consolidation of Compacted Titanium Powder **96**
5.1 Summary 96
5.2 Billet Heating 96
5.3 Extrusion 98
5.4 Consolidation of Compacted Ti HDH Powder 100
5.4.1 Analysis of Porosity in Consolidated Ti HDH Powder 100
5.4.2 Microstructural Analysis of As-Extruded Ti HDH Powder 103
5.4.3 Mechanical Properties 104
5.5 Finite Element Modelling of Titanium Powder Extrusion 105
5.5.1 Determination of Constants from Thermomechanical Data Analysis 105
5.5.2 Predicted Extrusion Pressure 109
5.5.2.1 Determination of Heat Transfer Coefficient 109

5.5.2.2 Speed . . . 110
5.5.2.3 Die Temperatures . . . 111
5.5.2.4 Billet Temperature . . . 113
5.5.3 Predicted Temperature Profiles Across the Extrusion Width . . . 114
5.5.3.1 Extrusion Conditions . . . 114
5.5.3.2 Extrusion Speed . . . 120
5.5.3.3 Die Temperatures . . . 121
5.5.3.4 Billet Temperature . . . 122
5.5.4 Limitations of Finite Element Modelling . . . 123
5.6 Conclusions . . . 123

6 Thermomechanical Processing of Ti-6Al-4V+TiB Composites 125
6.1 Summary . . . 125
6.2 Characterisation of Ti-6Al-4V and TiB_2 Powder . . . 125
6.3 Processing Route for Ti-6Al-4V + 20 vol.% TiB . . . 126
6.4 As Extruded Ti-6Al-4V + 20 vol.% TiB . . . 127
6.4.1 Extrusion of Ti MMCs . . . 127
6.4.2 Microscopy of Ti MMCs . . . 132
6.5 Mechanical Properties . . . 139
6.6 Texture . . . 141
6.6.1 α Phase . . . 141
6.6.2 TiB . . . 142
6.7 Conclusion . . . 143

7 Conclusions and Further Work 145
7.1 Conclusions . . . 145
7.2 A Note on Titanium Powder . . . 147
7.3 Further Work . . . 149

A Appendix 151
References . . . 153

List of Figures

2.1 Cost breakdown for titanium processing, after Kraft [1] 21
2.2 Schematic of a beta isomorphous phase diagram, after Flower [17] 22
2.3 The effect of interstitial elements on the mechanical properties of pure titanium, after Finlay and Snyder [26] 26
2.4 Hall Petch strengthening of a grade 1 commercial purity titanium alloy, adapted from Polmear [19] 27
2.5 Titanium-oxygen phase diagram, after Murray [31] 28
2.6 Diffusion coefficient with temperature, the red line indicates the nominal β transus temperature for CP Ti grade 2 alloys 29
2.7 Thermomechanical processing routes for (a) bi-modal microstructure, (b) lamella microstructures and (c) equiaxed microstructures, after Lütjering [37] 31
2.8 Representative conditions of Ti-6Al-4V, (a) equiaxed α with intergranular β, (b) equiaxed and acicular α with small amounts of β, (c) equiaxed α in a transformed β matrix (duplex/bi-modal microstructure), (d) small amounts of equiaxed α in a transformed β matrix, (e) plate like acicular α, (f) Block, plate-like α showing a prior β grain boundary, after Donachie [21] 32
2.9 Titanium-boron phase diagram 37
2.10 Schematic illustration of the atomic arrangement of TiB, (a) TiB unit cell (B27), (b) basic triangular prismatic arrangement of Ti atoms around B and (c) arrangement of the basic triangular prismatic arrangement to form the TiB structure, after Decker [55] 38
2.11 Schematic of the mechanical alloying process, after Gardiner [61]. The schematic is explained in the section below 39
2.12 Idealised plot of fraction density against compaction pressure 42
2.13 Schematic of the extrusion process 46
2.14 Different die designs 47
2.15 Variation of flow with different die designs, after Sachs and Eisbein [71] . 48
2.16 Deformation zones in a billet, after [72] 49

2.17 Extrusion back end defect, after Pearson [73] 50
2.18 The effect of extrusion speed on the extrusion profile 51
2.19 Isostatic pressing of a powder compact showing a reduction in the volume of the envelope, after Atkinson [74] 52

3.1 Particle size distribution of Ti HDH powder 55
3.2 Process for welding mild steel cans to encapsulate Ti HDH powders, (a) degassing tube welded to the lid from the bottom, (b) bottom side welded onto the can (c) welding the lid onto the can with the position of the welding tip and turntable shown, (d) position of the welding tip 2 mm from the can 57
3.3 Ti HDH powder in the mild steel can, filled approximately up to 2 cm from the top of the can 58
3.4 A photograph of the can in the vertical tube furnace with the crimp placed over the degassing tube, also visible is a copper tube for cooling the degassing tube 59
3.5 Degassing and argon reflowing set-up for Ti HDH powder 59
3.6 Crimp used to seal the degassing tube 60
3.7 Crimping of the degassing tube, (a) can and crimp in the furnace, (b) crimp and can set up on the turntable and (c) hydraulic ram connected to the crimp before the load is applied 61
3.8 Cutting of the crimped degassing tube, (a) before cutting, (b) completed can 61
3.9 Tangye compaction equipment (i) ram, (ii) die, (iii) metal powder and (iv) example of powder compact 62
3.10 Enefco extrusion press 63
3.11 Extrusion set up 64
3.12 Tensile geometry for No.13's tensile specimens, all units are in mm 66
3.13 Tensile geometry for No.11's tensile specimens, all units are in inches . . . 67
3.14 Tensile geometry for AMC specimens, all units are in mm 68

4.1 Secondary electron images of the Ti HDH powder, (a) x50 magnification, indicating the angular morphology and (b) x160 magnification, showing the powder surface 71
4.2 Pressure tracking during degassing at 500°C prior to extrusion 74

4.3 Oxygen and nitrogen content of degassed Ti HDH powder, heated over a range of temperatures at a heating rate of 3°C/min, the dashed line at 1800 ppm indicates the maximum allowable oxygen content for CP Ti grade 1 alloys 75
4.4 Hydrogen content of Ti HDH powder, degassed over a range of temperatures 76
4.5 Vapour pressure of $MgCl_2$, NaCl and $CaCl_2$, from data shown in [83] . . . 79
4.6 Canned Ti HDH powder after degassing and crimping, ready for extrusion or HIP'ing 81
4.7 Extrusion pressure curves for the encapsulated cans of Ti HDH powder, degassed at (a) 500°C, (b) 700°C and (c) 900°C 82
4.8 (a) Load displacement profile of Ti HDH powder and (b) corresponding extrusion of canned Ti HDH powder indicating the different regions formed during extrusion 83
4.9 Front end of canned and extruded Ti HDH powder, illustrating the different parts of the front end defect 84
4.10 Cross section macrograph of partly extruded discard showing the flow of Ti powder and steel can though the die interface, the five regions are labelled on the figure are referred to in the discussion below 84
4.11 Cross section macrograph of discard of canned Ti HDH powder extrusion 85
4.12 (a) Can before HIP'ing, (b) can after HIP'ing at 920°C for 4 hours 86
4.13 Light micrograph illustrating an example of consolidated Ti HDH powder, region (i) equiaxed grains near the edge of the sample, region (ii) elongated grains towards the middle of the extrusion, region (iii) foreign particle . . 87
4.14 Porosity distribution of degassed and extruded Ti HDH powder, (a) 900°C, (b) 700°C, (c) 500°C, corresponding image analysis of porosity (d) 900°C, (e) 700°C, (f) 500°C 88
4.15 (a) Porosity in canned, degassed and HIP'ed Ti HDH powder and (b) corresponding image analysis 89
4.16 Light micrographs of canned, degassed and extruded Ti HDH powder, degassed at (a) 500°C, (b) 700°C, (c) 900°C and (d) degassed at 300°C and HIP'ed at 920°C for 4 hours 90
4.17 Light micrograph illustrating iron rich foreign particle in the consolidated Ti HDH powder 92
4.18 Light micrograph of the interface between the mild steel can and the Ti HDH powder, after HIP'ing at 920°C for 4 hours 93

5.1 Example of compacted Ti HDH, 72 mm diameter, powder billet 97

5.2 Extrusion pressure vs displacement during extrusion of Ti HDH powder compacts at 900°C 99
5.3 Porosity distribution of compacted and extruded Ti HDH powder, (a) 9:1, (b) 17:1, (c) 75:1, corresponding image analysis of porosity (d) 9:1, (e) 17:1, (f) 75:1 101
5.4 Volume fraction of porosity and average size of pores with the reduction ratio of extruded Ti HDH powder compacts 102
5.5 Light micrographs of as extruded Ti HDH powder at different reduction ratio (a) R=9:1, (b) R=17:1 and (c) R=75:1 104
5.6 Flow stress data for temperatures 700 - 900°C and strain rates of 0.05 to 5 106
5.7 Correlation between the predicted and experimental flow stress, using the Norton-Hoff Equation 108
5.8 Experimental and predicted extrusion pressure, with a heat transfer coefficient of 4250 $Wm^{-2}K^{-1}$ for three different reduction ratios (a) 9:1, (b) 17:1 and (c) 75:1 110
5.9 Predicted extrusion pressure of Ti HDH powder compacts, with different extrusion speeds (a) 3 $mm.s^{-1}$ and (b) 15 $mm.s^{-1}$, for reduction ratios of 9:1, 17:1 and 75:1 111
5.10 Predicted extrusion pressure with different die temperatures, (a) 500°C and (b) 900°C, the reduction ratios are shown in the figure 112
5.11 The predicted extrusion pressure of Ti HDH powder compacts at different billet temperatures (a) 900°C and (b) 800°C 113
5.12 Meshed billet with the material history points from the 9:1 reduction ratio die, (i) surface, (ii) midpoint and (iii) centre of the extrude width 114
5.13 Output data showing the temperature variations in the extrude, half way through the extrusion stroke, (a) R = 9:1 and (b) R = 75:1, the temperature key is shown in the figure 115
5.14 Temperature profiles across the extrusion width, (a) R = 9:1, (b) R = 17:1 and (c) R = 75:1, the red lines in each graph indicate the nominal β transus for CP Ti grade 2 alloys 116
5.15 The predicted surface temperatures as the Ti HDH extrusions exit the die, the red line indicates the nominal β transus temperature for Ti CP grade 2 alloys 117
5.16 The diffusion length of O in Ti, after t = 300 s, the red line indicates the nominal β transus for CP Ti grade 2 alloys 118

5.17 The variation in the exit surface temperature extrusion speed (a) 3 mm.s^{-1} and (b) 15 mm.s^{-1}, the red lines in each graph indicates the nominal β transus for Ti CP grade 2 alloys 120
5.18 The variation in the exit surface temperature with reduction ratio with different die temperatures (a) 500°C and (b) 900°C, the red lines in each graph indicate the β transus for Ti CP grade 2 alloys 121
5.19 The variation in the exit surface temperature with an initial billet temperature of 800°C, the red line indicates the β transus for Ti CP grade 2 alloys 122

6.1 Thermomechanical processing route for Ti-6Al-4V+TiB composites; the heat treatment conditions T1, T2 and T3 are described in Table 6.1 . . . 126
6.2 Extrusions of Ti-6Al-4V-TiB 128
6.3 X-ray diffraction trace of extruded Ti-6Al-4V + 20 vol.% TiB, T1 condition, transverse direction, the $\{101\}_{TiB_2}$ peak at 44.6° shows residual TiB_2 130
6.4 X-ray diffraction trace of extruded Ti-6Al-4V + 20 vol.% TiB, T2 condition in the transverse direction, conversion heat treatment converts the remaining TiB_2 to TiB 130
6.5 X-ray diffraction trace of extruded Ti-6Al-4V-20 vol.% TiB, T1 condition in the longitudinal direction, showing the disappearance of the $\{101\}_{TiB_2}$ peak at 44.6° 131
6.6 Optical micrographs of the as extruded titanium composites, (a) T1, (b) T2, (c) T3, with corresponding high magnification images (d) T1, (e) T2 and (f) T3 132
6.7 Backscattered electron micrographs of Ti-6Al-4V + 20 vol.% TiB (a) region of heterogeneous TiB reinforcement and (b) region of homogeneous reinforcement 133
6.8 Mechanical alloying, showing the (a) layered structure observed in Ti-TiB composites and (b) the optimal distribution of reinforcement phase, the alloy is in solid solution 135
6.9 Schematic illustration of TiB/TiB_2 distribution in the T1 condition . . . 135
6.10 Schematic illustration of the TiB distribution in the T2 condition 136
6.11 XRD trace of Ti-6Al-4V + 20 vol.% TiB in the T3 condition, transverse direction 138
6.12 Effect of the volume fraction of TiB on the stiffness and UTS of Ti-6Al-4V + 20 vol.% TiB in the T1 condition 139

6.13 Effect of the volume fraction of TiB on the ductility of Ti-6Al-4V + 20 vol.% TiB in the T1 condition 140
6.14 Texture of α phase in (a) Ti-6Al-4V + 20 vol.% TiB and (b) monolithic Ti-6Al-4V 142
6.15 TiB texture raw data file 143

A.1 Lid design 151
A.2 Can design 152

List of Tables

2.1 Commercial purity titanium grades [20,21] 24
2.2 The increase in strength per 1 wt.% of interstitial element [27] 26
2.3 Possible reinforcing phases for titanium matrix composites [49] 36
2.4 Predicted stiffness of Ti-6Al-4V reinforced with varying volume fractions of TiB using the rule of mixtures 40

3.1 Elemental analysis of HDH powders 56
3.2 TIG Welding Operating Parameters 57
3.3 Extrusion conditions for Ti alloy composites 68
3.4 Input parameters for Forge 2005 69

4.1 Elemental analysis of HDH powders 71
4.2 Chemical analysis for different size fractions of Ti HDH powder 72
4.3 Degassing runs information 73
4.4 Chemical analysis of Ti HDH powder degassed at various temperatures . 75
4.5 Remaining chloride content of HDH Ti powder + metal halide, after degassing at 700°C 78
4.6 Melting point and boiling point of $MgCl_2$, NaCl and $CaCl_2$ 79
4.7 Table of extrusion conditions for extrusion of encapsulated Ti HDH powder 80
4.8 Percentage porosity of extruded and HIP'ed Ti HDH powders 89
4.9 Chemical composition of foreign particle in the Ti HDH powder 92
4.10 Ultimate tensile strength and ductility of degassed and extruded Ti HDH powder 94

5.1 Table of oxygen analysis with different heating conditions of Ti HDH powder compacts 97
5.2 Ti HDH compact density with reduction ratio 98
5.3 Extrusion conditions for Ti HDH powder compacts 98

5.4 Breakthrough and maximum pressures for Ti HDH powder compacts extruded under different reduction ratios 99
5.5 Volume fraction and size of porosity of different reduction ratios of extruded Ti HDH powder compacts 102
5.6 The level of strain imparted to Ti HDH powder compacts when extruded at different reduction ratios 103
5.7 Tensile properties of compacted and extruded Ti HDH powder 105
5.8 Flow stress data for Ti HDH powder, extruded at R=9:1, the units of the flow stress are in MPa 107
5.9 Flow stress regression data obtained from compression testing 107
5.10 Simulation conditions for Forge 2005 modelling of Ti HDH powder compacts 108

6.1 Heat treatment conditions for the conversion heat treatment (CHT) of TiB_2 to TiB, pre and post extrusion 127
6.2 Extrusion conditions for CP Ti, Ti-6Al-4V and Ti-6Al-4V + 20 vol.% TiB 128
6.3 Breakthrough and maximum loads for CP Ti, Ti-6Al-4V and Ti-6Al-4V + 20 vol.% TiB 129
6.4 Morphology of TiB needles in the three different heat treatment conditions, T1, T2 and T3 134
6.5 Mechanical properties of Ti-6Al-4V+20 vol.% TiB, in both the T1 and T2 conditions 139
6.6 Specific stiffness of Ti-6Al-4V and Ti-6Al-4V + 20 vol.% TiB, the values for a steel alloy are also included as a comparison 141

Chapter 1

Introduction

Titanium (Ti) is the fourth most abundant structural metal on the planet, however, it is mostly used in niche applications where strong, lightweight components are a necessity, for example in the aerospace industry. This is due to the prohibitive cost of processing Ti and its alloys. One of the first alloys to be developed was the α+β alloy Ti-6Al-4V, which accounts for more than 50% of all Ti tonnage in the world. This alloy offers a wide variety of physical and mechanical properties by the control of microstructural development during thermomechanical processing. Titanium not only offers high strength to weight ratios, but also excellent corrosion resistance and is used in chemical and marine applications as well as high end sports equipment and medical prostheses. The recent requirements by western governments to make components, not just economically viable, but also environmentally friendly means that the titanium industry is experiencing a growth due to the high strength to weight ratio and excellent corrosion resistance. The titanium powder metallurgy (PM) industry has experienced a recent upturn as a result of the recent interest in Ti, due to the cost advantages of producing near-net-shape parts with similar, if not better, properties than conventional wrought components.

Until recently, the cost of titanium and, particularly, titanium powder, has prohibited the development of the Ti PM industry into low cost markets. However, several novel titanium metal reduction techniques are being investigated [1] with the possibility of producing Ti powder without the need for melting, thereby reducing the cost of Ti powder. In order to create a step change in the economics of Ti, non-melt processing from extraction to final component is a vital requirement for the manufacturing of cheap parts to open up the titanium market to a wide variety of industries. The consolidation of cheap titanium powder is therefore a vital part of the processing of titanium alloys and composites if there is to be a reduction in the total cost.

The consolidation of titanium powder is gaining interest in the field of titanium PM [2], although very little research has been published on the subject, as it is firstly, a new area of research and secondly, commercially sensitive due to the expected growth in the market. The extrusion of titanium is also a small field of research, which is mainly based on the extrusion of steel using a modified version of the Ugine-Sejournet process [3]. This has been modified for the extrusion of Ti-6Al-4V by Norley [4]. There is an array of literature on the subject of aluminium (Al) consolidation from Al powders [5–11] and it is these areas of research that forms the basis of much of the work presented in this thesis.

It is known that the extrusion process can consolidate Al powders, however, it has only recently been proven that this is a technique that can be applied to Ti powders [2]. Ti powder has been processed using traditional PM techniques, such as press and sintering, but if cheap power feedstock material could be consolidated using standard processes, such as extrusion, the total costs could be substantially reduced. This could open up the Ti market to a wide variety of non-traditional titanium industries.

A potential application of cheap titanium powder is in the use of metal matrix composites. These are materials which have high specific properties and as such, have the potential for increased weight savings in, not just the aerospace industry, but also other forms of transportation, for example the automotive industry. At present, the only viable commercial manufacturing route for titanium matrix powder is costly atomisation routes. In order to lower the final cost of these composites, not only do the raw materials need to come down in cost, but also the subsequent thermomechanical processing which is applied to these materials.

The thermomechanical processing of titanium alloy metal matrix composites (Ti MMCs) is also a new field of research, which has a vast potential due to increased specific stiffness and improved fatigue properties over conventional monolithic alloys. There is a need for the Ti industry to compete with the steel industry and as such improvements in the specific strength and stiffness of titanium components are needed. Several Ti MMCs have been developed to match these requirements, however, the cost of processing Ti MMC's is prohibitive for the majority of applications. At present, there are few commercial applications for Ti/TiB MMCs, the main one being exhaust valves in Toyota engines [12]. A low cost, non-melt process for developing Ti MMCs is required to enable the expansion of such materials into other markets.

The principle aims of this research are: (i) to develop a process by which Ti powder is consolidated using low cost processing routes and (ii) obtain a more detailed understanding of the thermomechanical processing conditions on the properties of Ti MMC's. The objectives can be summarised as follows:

Degassing conditions for Ti powder

- Determine the optimum temperature for degassing Ti powder.
- Obtain the degassing-microstructure relationship of Ti powder.

Compaction and consolidation of Ti powder

- Determine the effect of extrusion reduction ratio on the microstructure and mechanical properties of consolidated Ti powder.
- Development of a model to predict the extrusion pressure and temperature rise when consolidating Ti powder *via* extrusion.

Thermomechanical processing of Ti alloy composites

- Develop an understanding of the effect of heat treatments on the mechanical properties of extruded Ti alloy composite.

Integral to this research project was the development of an encapsulation and degassing facility at Imperial College London. This thesis explores for the first time the influence of degassing parameters and contaminants on the interstitial content of the powder and consolidated mechanical properties. A direct powder extrusion consolidation route for titanium powder has been explored and shown to be a viable route at the pilot scale. Whilst the application of powder metallurgy has been covered by previous workers, this thesis covers the extrusion processing of this class of material. This is an area which has received little attention in the past, particularly high ratio extrusion processing, the effect of conversion heat treatment and the evolution of texture.

This thesis is divided into six chapters. A review of the relevant literature giving an overview of the metallurgy of Ti, Ti powder and Ti alloy composites is presented in Chapter 2. Particular attention is paid to the extrusion process. Chapter 3 explains the experimental methodology used throughout this work. Chapter 4 covers the development of a canning process and optimisation of the degassing procedure with respect to Ti powder and the effects of degassing on the microstructural and mechanical properties of consolidated Ti powder. Chapter 5 details the effect of the reduction ratio during extrusion on the effect of microstructure and mechanical properties. The development of a finite element model to predict the flow stress and temperature variations within a titanium powder extrusion are also presented. The thermomechanical processing of a Ti MMC is discussed in Chapter 6. Finally, conclusions from this work are drawn and some suggestions for further work are presented in Chapter 7.

Chapter 2

Literature Review

2.1 Titanium

Titanium is a lightweight, strong and corrosion resistant metal, and as such is used frequently in applications where specific strength and corrosion resistance are required. The majority of titanium produced in its various forms is used in the aerospace industry due to it having a specific strength higher than that of most engineering steels. Titanium is the ninth most common element and the fourth most abundant metal, after iron, aluminium and magnesium. The mineral ores from which titanium is made are rutile (TiO_2) and ilmenite ($FeTiO_3$). In comparison with other metals, titanium is relatively young, being first discovered in 1791 by William Gregor in ilmenite [13]. However, it was not made into a pure metal until 1910 by the chemist Matthew Hunter [14], who heated $TiCl_4$ with sodium in a steel chamber at 700-800°C. In 1946, Wilhelm Kroll [15] developed the first commercially viable process for producing titanium, which is still the main process for producing the metal today. The Kroll process first treats the ore with carbon and chlorine gas to produce titanium tetrachloride ($TiCl_4$), called carbochlorination, Equ. 2.1. This is then purified to remove the iron chloride. The $TiCl_4$ is then reacted with magnesium in argon to produce porous titanium 'sponge', Equ. 2.2.

$$TiO_{2(s)} + 2Cl_{2(g)} + C \rightarrow TiCl_{4(g)} + CO_{2(g)} \tag{2.1}$$

$$TiCl_{4(g)} + 2Mg_{(l)} \rightarrow Ti_{(s)} + 2MgCl_{2(l)} \tag{2.2}$$

This titanium sponge is melted in a vacuum to form ingots for further processing.

The Kroll process is a time consuming batch process which is both costly and inefficient. Though several attempts have been made to find a commercially viable process

to produce titanium metal from its ore [1], the Kroll process still produces the majority of titanium.

The high cost of titanium stems not only from the inefficient reduction process, but also from the processing of the metal or alloy after it has been made. In fact, the majority of the cost of titanium alloy production is from the thermomechanical processing that it undergoes to obtain the necessary mechanical and chemical properties [16].

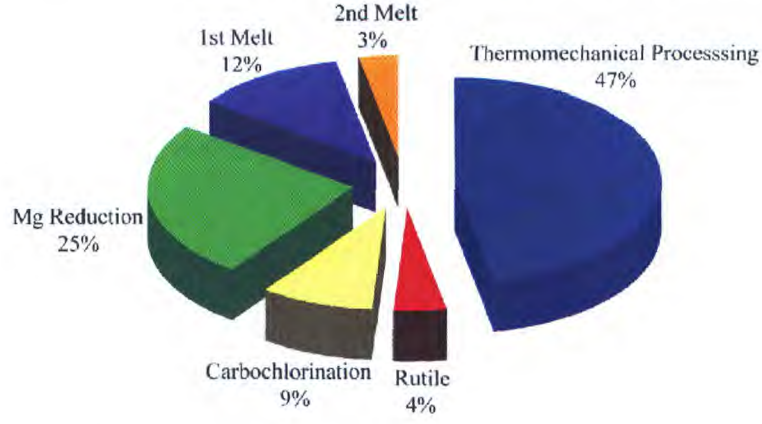


Fig. 2.1: Cost breakdown for titanium processing, after Kraft [1]

2.1.1 Classification of Titanium Alloys

Like a number of other metals, titanium is allotropic, so exists in different crystallographic forms. Titanium exhibits two allotropes, namely, the alpha (α) phase, which has a hexagonal close packed (hcp) structure and the beta (β) phase, which has a body centered cubic (bcc) structure. The two phases are only thermodynamically stable within their respective temperature ranges. The allotropic transformation temperature (β transus) for pure titanium is 882°C. The hcp α phase is stable below this temperature and the bcc β phase is stable above this temperature. This transformation dominates the physical metallurgy of titanium and its alloys [17].

There are several elements which can affect this allotropic transformation temperature. Elements, which when dissolved in titanium increase the β transus are known as α stabilizers, whereas elements which lower the transformation temperature are known as β stabilizers. Titanium is a transitional element and so has an incomplete outer electron shell. Generally, the number of bonding electrons of the alloying elements determines whether they stabilise the α or β phase. β stabilisers generally have four bonding electrons and are split into two different types of stabiliser; those which are isomorphous with titanium (V, Mo, Nb) and those which form a eutectoid reaction (Fe, Cr, Ni, Mn) and so can form intermetallics if their local concentration is high enough. In general, the

β isomorphous stabilisers are substitutional whereas eutectic formers are interstitials. There are exceptions to this rule; hydrogen does not have four bonding electrons, yet is a β stabiliser. This is most likely due to the size of the element. Elements with less than four bonding electrons (Al, O, N ,C) stabilise the α phase. There are also neutral stabilisers (Sn and Zr), which do not stabilise either phase but do provide a certain degree of solution strengthening. The stabilisation of the two phases leads to the broad classification of five main types of titanium alloy: (i) α, (ii) near-α, (iii) α+β, (iv) near-β and (v) β alloys. The five main alloy classes are shown in the phase diagram below, Fig. 2.2.

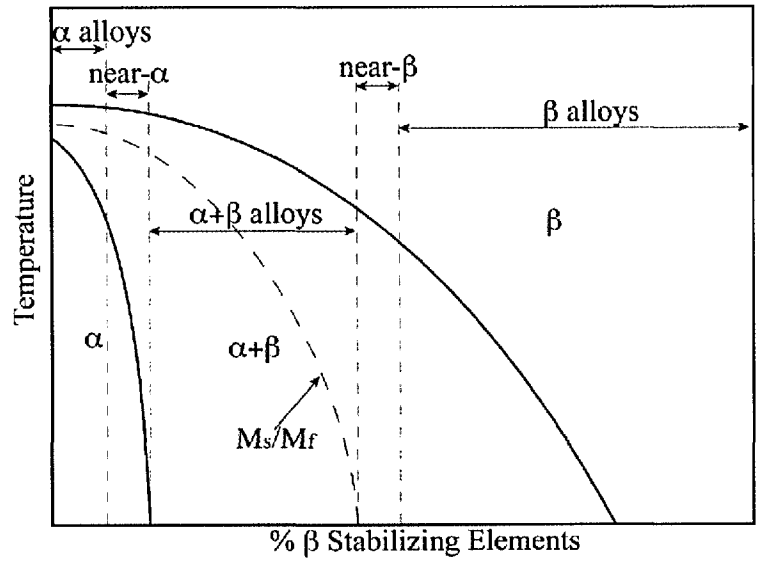


Fig. 2.2: Schematic of a beta isomorphous phase diagram, after Flower [17]

α alloys

α alloys have an *entirely* hexagonal crystal structure. The principle strengthening element for α alloys is oxygen in solid solution and a large proportion of α alloys consist of commercially pure (CP) grades of titanium and are discussed in Section 2.1.3.

Near-α

Near-α alloys contain small amounts of β stabilisers to widen the α+β thermomechanical processing window. These alloys can retain a small amount of β at room temperature. Near-α alloys were developed to meet the demand for higher operating temperatures, primarily for disk forging applications [13].

α+β alloys

These titanium alloys have sufficient β stabilisers to retain both α and β to below room temperature. A selection of α/β morphologies can be obtained depending on the

thermomechanical processing and heat treatment conditions [17]. Ti-6Al-4V is the most common α+β alloy and is discussed in more detail in Section 2.1.5.

Near-β

Near-β alloys are to the right of the martensitic start/finish line, near the α+β/β phase field in Fig. 2.2. The diffusion kinetics of these alloys is sluggish due to the large amounts of β stabiliser so metastable β can be retained upon quenching from the β phase. α phase can then be nucleated and grown during subsequent heat treatments. These constitute the strongest of all the titanium alloys as fine scale α can be precipitated to harden the material and are used in civil aircraft landing gears.

β alloys

β-alloys have such considerable amounts of β stabilisers that the β phase is retained down to room temperature. The β phase is technically metastable as the thermodynamically stable phase is still α+β.

2.1.2 Microstructural Development in Titanium

Depending on the alloy composition and processing treatment, the α phase in titanium alloys exists in three morphologies - primary alpha, secondary alpha and martensitic structures.

Primary α remains during heat treatments in the α+β field. The morphology is influenced exclusively by the thermomechanical history, primarily by the last working operation. The morphology can be lamella, equiaxed or mixed. Lamella α forms on cooling from above the transus or high in the α+β phase field, which then remains when subsequent heat treatments are applied. To obtain equiaxed α, heavy working below the β transus is required.

Secondary α (or transformed β) refers to α which is formed from a nucleation and growth mechanism from either martensite or metastable β regions and can take a variety of different forms. On cooling though the β transus or high in the α+β phase, α nucleates along grain boundaries and grows in to the β grains as laths. On slow cooling, the β transforms to α by a diffusion controlled partitioning of alpha stabilising elements to the α phase and β stabilising elements to the the remaining β. The β phase has the same crystal orientation as the original β grains and the α phase have orientations that are relative to the β grains, given by the Burger's relationship:

$(110)\beta$ // $(0001)\alpha$

$<111>\beta$ // $<1120>\alpha$

As a consequence of this relationship, there are twelve different variants on which α can grow from the β phase, and as a corollary there are different orientations that α can form from a β grain. These multiple orientations of α within a prior β grain often form basketweave structures that are characteristic of Widmanstätten structures. A cluster of α laths which have the same orientation are known as 'colonies'. These colonies are considered to be extremely important microstructural features as they effectively behave like individual grains [18].

On faster cooling from above the β transus, a martensitic transformation occurs and the α forms as lath-like or acicular martensite. In alloys with a low concentration of β stabilisers, the martensite is α prime and has a distorted hexagonal lattice. In alloys with higher concentrations of β stabilisers (e.g. 10 to 15 wt.% vanadium), the martensite forms an orthorhombic α''. Upon ageing, α prime decomposes to form α; this transformation cannot be distinguished with light microscopy.

In CP alloys, the number of microstructures is limited due to the single phase structure of α alloys. When quenched from the β field, a martensitic transformation occurs and α prime forms. On air cooling from the β field, the alpha forms as lath-like plates (Widmanstätten α). Equiaxed α can be formed by substantial working in the α phase field with a post deformation annealing treatment [19].

2.1.3 Commercially Pure Titanium Alloys

CP grades are α titanium alloys principally alloyed with oxygen as well as other elements such as iron and palladium which act as solid solution strengtheners [13]. CP grades are ranked according to the amount of alloying elements. Grade 1 alloys have the lowest concentrations of interstitial elements, and hence exhibits the lowest strength, but the highest resistance to corrosion. ASTM Grade 4 alloys have a higher oxygen content and higher strength but a lower resistance to corrosion. The first four grades of commercial purity alloys are shown in Table 2.1 along with the ultimate tensile strength (UTS) of the alloys. The increase in strength and the maximum interstitial content of four commercial

Table 2.1: Commercial purity titanium grades [20, 21]

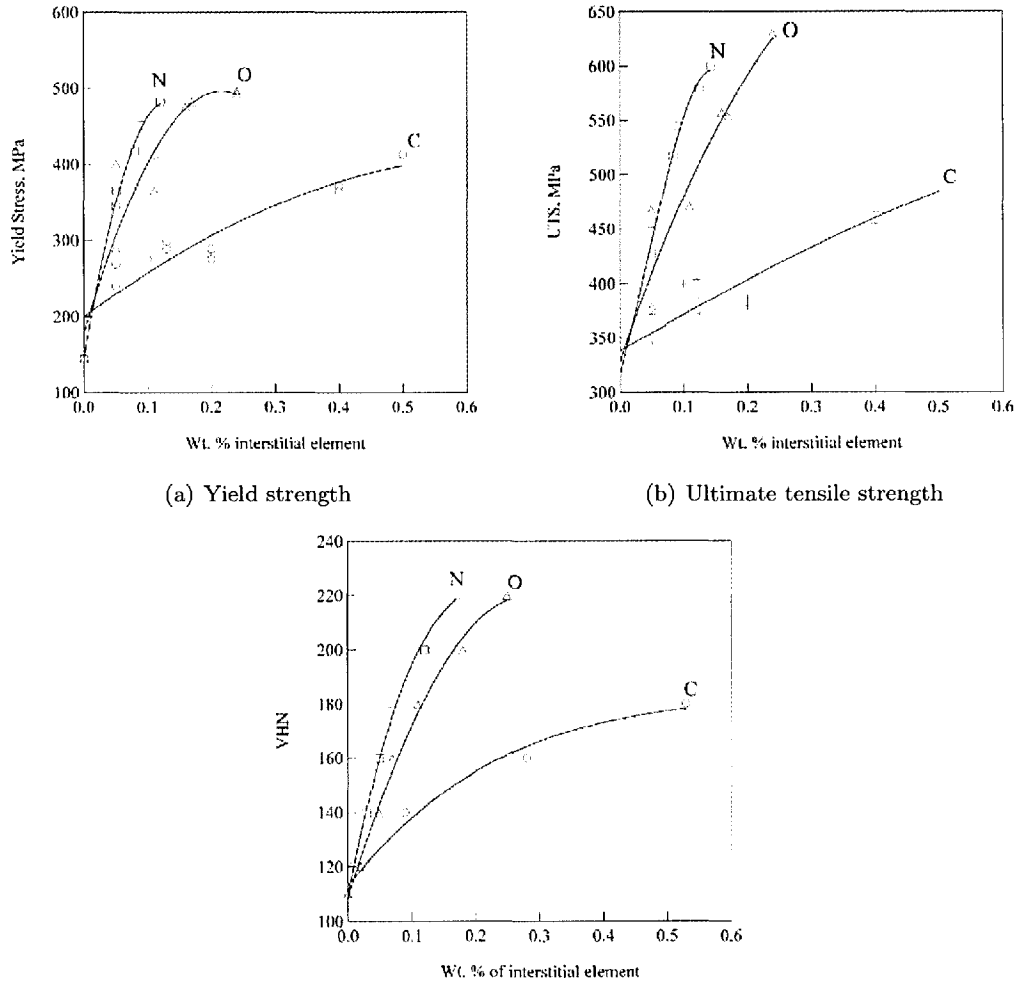
ASTM Grade	max wt.% O	max wt.% Fe	wt.% N	UTS, MPa
Grade 1	0.18	0.20	0.03	240
Grade 2	0.25	0.30	0.03	345
Grade 3	0.35	0.30	0.05	450
Grade 4	0.40	0.50	0.05	655

purity grades of titanium from ASTM standards are shown [20, 21]. There is a marked

increase in the strength with increasing interstitial concentration due to the solid solution strengthening effect. Other commercial grades of titanium exist, with varying grades of interstitial elements to alter the mechanical and chemical properties [22]. The higher the interstitial content the higher the strength but the lower the corrosion resistance. The maximum content of hydrogen in all ASTM grades of CP titanium is less than 100 parts per million (ppm) [22]. This is because hydrogen is a β stabiliser and forms a eutectic with titanium producing embrittling intermetallics. As these alloys are single phase alloys, they are the weakest of the titanium alloys, however they do retain substantial corrosion resistance. From a practical point of view, there is nearly always a small amount of β phase in CP alloys as α titanium has a very low solubility for iron (less than 0.06 wt.%) and therefore is rejected to form β phase [23].

Though the presence of interstitial elements dramatically increases the strength, there are some detrimental effects. For example, oxygen in solid solution deteriorates the tensile ductility, cold workability, fatigue strength and stress corrosion resistance in titanium and its alloys [24]. Though considerable hardening can be obtained by elements in solid solution, it is more difficult to harden the material in other ways, such as by precipitation hardening given the large amounts of solid solubility for α stabilisers hence α titanium alloys are generally non-heat-treatable.

It has long been known that of the three important interstitial elements, nitrogen has the greatest effect on the mechanical properties [25]. This has been quantified by Finlay and Snyder [26], represented in Fig. 2.3, which shows the effect of different interstitial elements on pure titanium.



(a) Yield strength

(b) Ultimate tensile strength

(c) Hardness

Fig. 2.3: The effect of interstitial elements on the mechanical properties of pure titanium, after Finlay and Snyder [26]

This has been verified by Ouchi *et al.* [27] who have attempted to quantify the respective influences of oxygen, nitrogen and carbon. The influence of nitrogen, illustrated in Fig. 2.3, is the reason why producers of titanium limit the nitrogen content by deliberately adding oxygen and iron as they have a less pronounced effect on the ductility of the final product.

Table 2.2: The increase in strength per 1 wt.% of interstitial element [27]

Element	0.2% PS, MPa	UTS, MPa
O	1360	1320
N	2530	2580
C	1120	590

With current production routes of titanium, the major interstitial contamination is from

oxygen, which is usually several orders of magnitude larger than either nitrogen or carbon. It is likely that the contribution of oxygen would outweight that of nitrogen and carbon combined [28], see Table 2.1. This is in broad agreement with the work of Finlay and Snyder [26].

Strengthening of pure titanium can also be obtained via grain refinement and can be predicted via the Hall-Petch equation [29]:

$$\sigma_{app} = \sigma_0 + kd^{-1/2} \tag{2.3}$$

Where σ_{app} is the increase in strength from grain refinement, σ_0 is the yield stress of a single crystal of similar composition, d is the grain size and k is the locking parameter, which effectively measures the hardening contribution of the grain boundaries. For grade 1 CP alloys, the room temperature yield strength can be predicted by the equation [19]:

$$\sigma_{YS} = 231 + 10.54d^{-1/2} \tag{2.4}$$

A plot of solid solution strengthening can be obtained from Equ. 2.4.

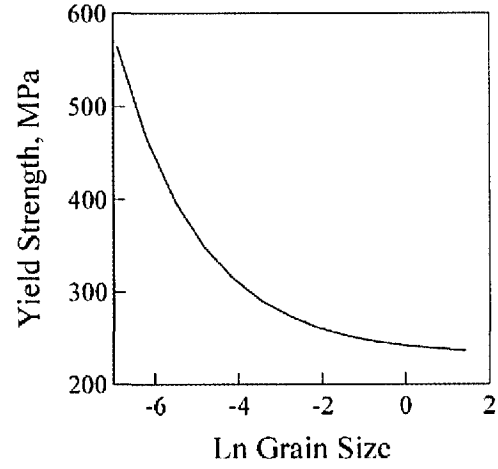


Fig. 2.4: Hall Petch strengthening of a grade 1 commercial purity titanium alloy, adapted from Polmear [19]

Fig. 2.4 shows an increase in strength with a decrease in grain size, from 241 to 349 MPa with a grain size of 1000 μm and 10 μm respectively. Grain refinement has successfully been demonstrated in pure titanium by massive deformation and recrystallisation [30] to increase the strength of the alloy. In titanium containing high iron contents, grain refinement can also occur by the presence of β phase which exists at grain boundaries after high temperature processing and annealing [28]. The β phase prohibits grain growth, but it is likely that the recrystallization temperature is raised due to the presence of interstitial elements which retard dislocation annihilation.

2.1.4 Oxygen Diffusion in Titanium

As can be seen from the titanium-oxygen system, Fig. 2.5, more than 10 wt.% oxygen can be contained in solid solution with pure titanium, which increases with elevated temperatures.

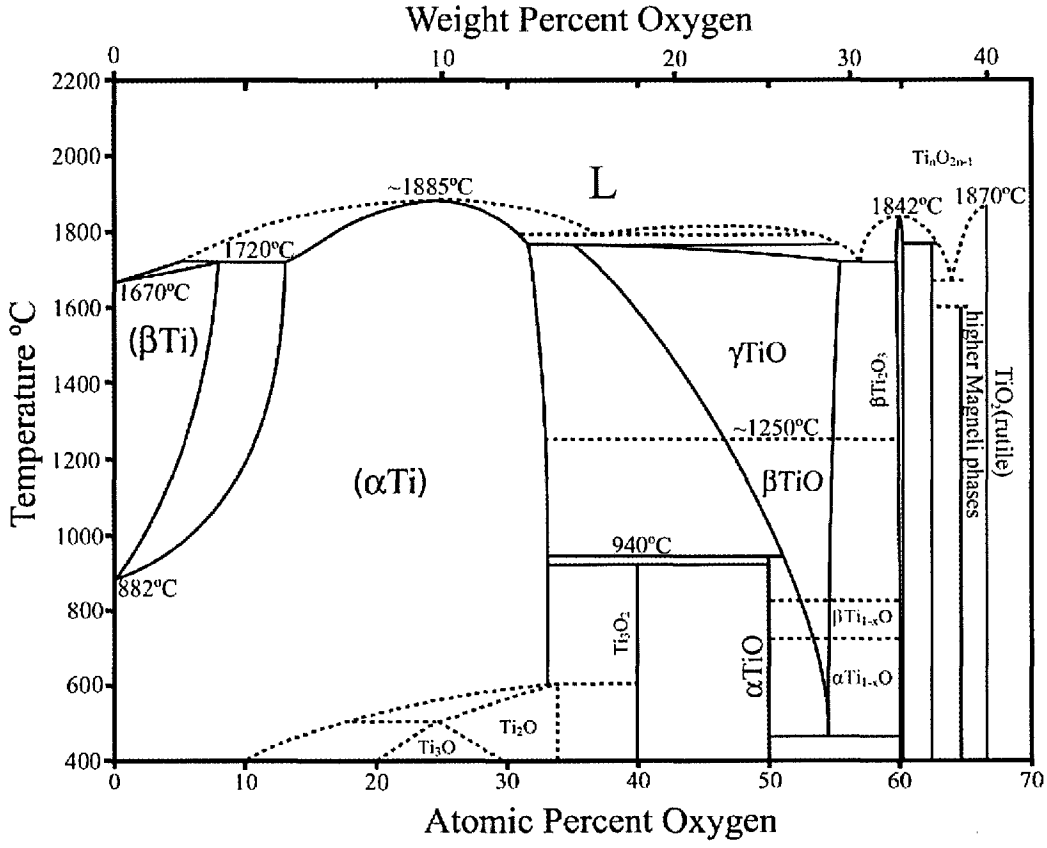


Fig. 2.5: Titanium-oxygen phase diagram, after Murray [31]

The effect of oxygen, nitrogen and carbon in solid solution on the properties of titanium have been reviewed in Section 2.1.3. Though nitrogen has a greater effect on the properties of titanium, oxygen is of more significance as diffusion of oxygen in titanium is several orders of magnitude greater than that of nitrogen [32,33]. Though some gains have been made to limit the contamination of oxygen, for example the near-α alloy IMI 834, the vast majority of titanium processing must be done in a vacuum or in an inert gas such as argon.

When oxygen diffuses into a titanium alloy, the local β transus is raised due to the stabilising effect of the oxygen to form an 'α case'. The local increase in oxygen concentration can change the mechanical properties, not only by increasing the oxygen in solid solution but also by altering the microstructure. It is therefore important to be able to predict the diffusion of oxygen in titanium at elevated temperatures so that the

necessary precautions can be taken to limit interstitial contamination. Diffusion can be predicted by the Arrhenius relationship, Equ 2.5:

$$D = D_o \exp\left(\frac{-Q}{RT}\right) \tag{2.5}$$

Where D is the diffusion coeffieient, D_o is the maximum diffusion coefficient, Q is the activation energy for diffusion, R is the molar gas constant and T is the absolute temperature. The investigations in to the diffusion in titanium has yielded varying results, sometimes by as much as several orders of magnitude [34], though it is likely that this is due to the presence of impurities in the experimental materials as a small amount of interstitial contamination can dramatically alter the diffusion coefficients in titanium [35]. The diffusion coefficients of α and β titanium are shown in Equs. 2.6 and 2.7 respectively, adapted from Dring [34]:

$$D_\alpha(cm^2/s) = 0.509 \exp\left(\frac{-200800}{RT}\right) \tag{2.6}$$

$$D_\beta(cm^2/s) = 3.3 \times 10^2 \exp\left(\frac{-246000}{RT}\right) \tag{2.7}$$

Where D_α and D_β are the diffusion coefficients in α and β titanium respectively.

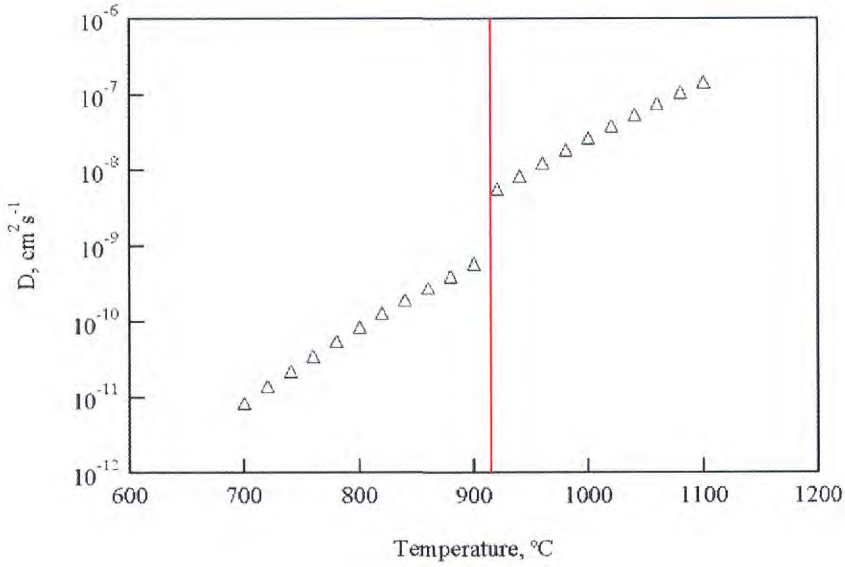


Fig. 2.6: Diffusion coefficient with temperature, the red line indicates the nominal β transus temperature for CP Ti grade 2 alloys

Fig. 2.6 shows the diffusion coefficients for oxygen in titanium, obtained from Equs. 2.6 and 2.7. Above the β transus, the diffusion coefficient increases by an order of magnitude. The data presented on this graph represent the lowest diffusion coefficients reported in the literature. Values an order of magnitude higher than this have been reported in the literature [34].

Powder has a much higher surface area than wrought material, and so any oxygen present on the surface of the powders will be transferred into the middle of the consolidated product hence there will be a local increase in the oxygen concentration in the middle of the consolidated product. With a solid product which has been exposed to an oxygen gradient, any oxygen present will be on the surface of the billet, thus can be machined away after processing

2.1.5 Ti-6Al-4V

As the development of titanium alloys has been largely financed from the aerospace industry and is inherently expensive, there has historically been a focus on microstructural rather than alloy development. Ti-6Al-4V was one of the first in a generation of titanium alloys and as such is the most widely used titanium alloy as there are many different microstructures that can be obtained from the alloy which have good overall properties. Ti-6Al-4V has 6 wt.% aluminium, an α stabiliser and 4 wt.% vanadium which stabilises the β phase. The β transus for this alloy is approximately 995°C [36] and both α and β phases are stable down to room temperature. As with all titanium alloys, the thermal and mechanical history determines the microstructure and texture of the material, and as the alloy has both α and β stabilisers present within the material, many different microstructures and morphologies can be obtained though thermomechanical processing. Some common microstructures are outlined below.

It is convenient to classify the main microstructures available in Ti-6Al-4V into three main classes. These are lamella, equiaxed and bi-modal microstructures [37]. Lamella microstructures consist of transformed β and are obtained by cooling from the β phase field. Slow cooling produces relatively coarse lamella grains and is commonly referred to as a 'Widmanstätten' or β-annealed structure. Quenching from above the β transus and subsequent annealing high in the α+β phase produces a much finer lamella microstructure and is termed a β-quenched structure. Equiaxed microstructures are worked high in the α+β phase field and a subsequent annealing at 700°C produces the so called 'mill-annealed' microstructure. Bi-modal microstructures consist of isolated grains of primary α in a lamella matrix and are obtained by hot working high in the α+β phase field, followed by annealing high in the α+β phase field and subsequent ageing at 600°C [37,38]. The heat treatment profiles are shown schematically in Fig. 2.7.

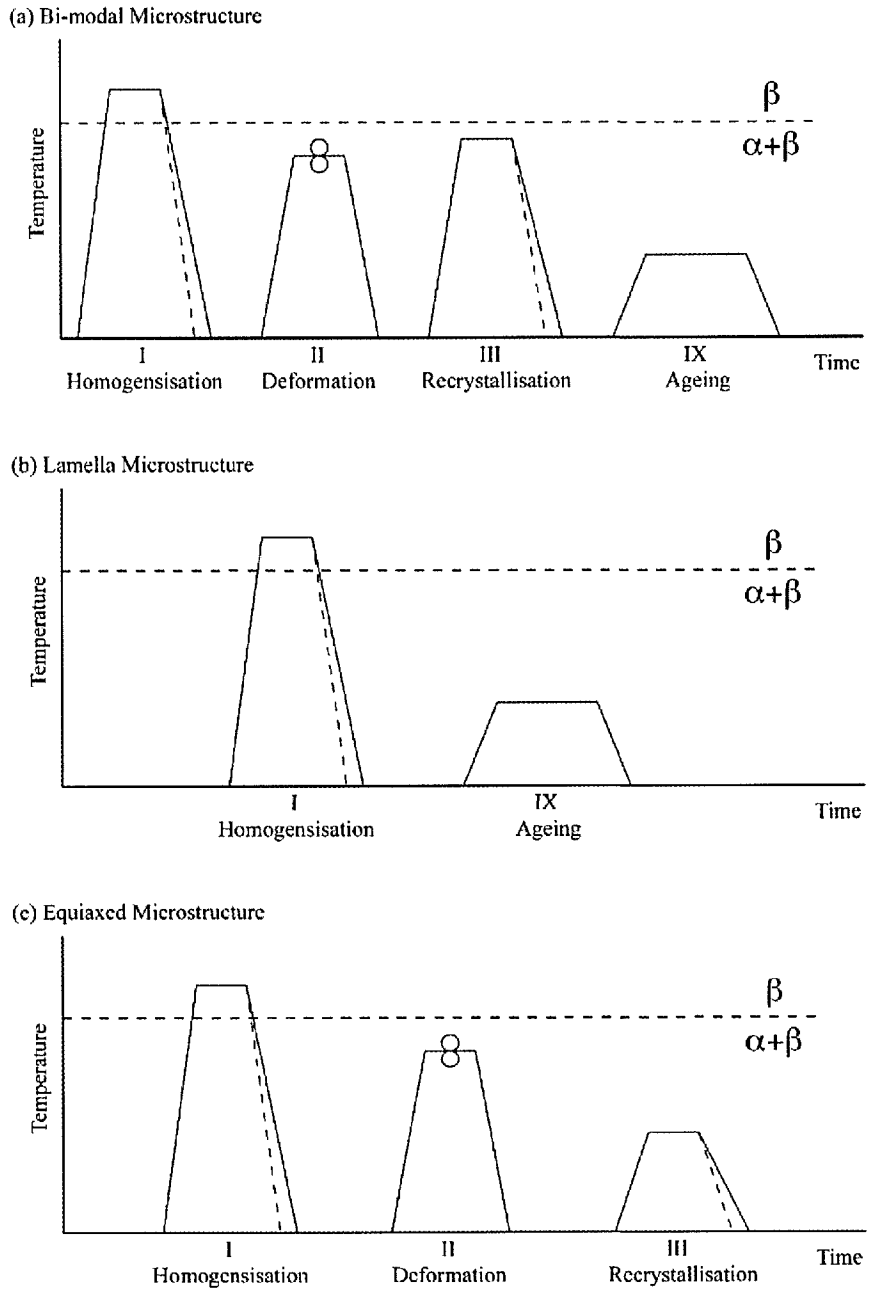


Fig. 2.7: Thermomechanical processing routes for (a) bi-modal microstructure, (b) lamella microstructures and (c) equiaxed microstructures, after Lütjering [37]

Fig. 2.8 shows some common metallurgical conditions of Ti-6Al-4V [21].

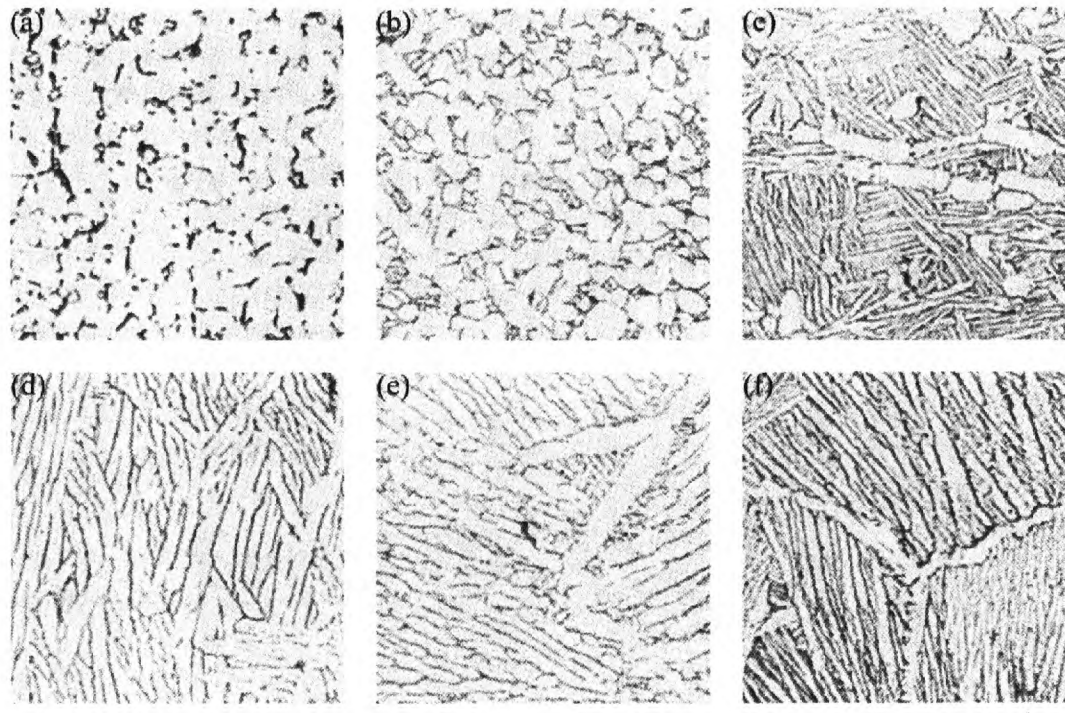


Fig. 2.8: Representative conditions of Ti-6Al-4V, (a) equiaxed α with intergranular β, (b) equiaxed and acicular α with small amounts of β, (c) equiaxed α in a transformed β matrix (duplex/bi-modal microstructure), (d) small amounts of equiaxed α in a transformed β matrix, (e) plate like acicular α, (f) Block, plate-like α showing a prior β grain boundary, after Donachie [21]

2.2 Titanium Powder

2.2.1 Classification of Powders

Metallic powders are characterised by their chemical, physical and process properties. The main physical and process characteristics of powders are: shape; size distribution; surface morphology; condition of the particles (e.g. work-hardened or annealed); packing density of particles (tap density) and flowability [39,40]. Section 2.2.2 explains the main powder production routes and the different kinds of powders that can be manufactured.

Above 700°C, titanium absorbs its own oxide and forms a metallurgical bond by inter-diffusion at the powder surface. Direct consolidation routes exploit this property by helping to bond the particulates together during consolidation. This property also inhibits the flow properties of the particulate at elevated temperatures as the material can agglomerate during pre-heating of the billet prior to consolidation. Titanium also absorbs large amounts of interstitial elements such as oxygen, (see Section 2.1.3), and as such processing titanium at any temperature above about 400°C requires an inert atmosphere. This places significant complications on the processing of these powders as any

oxygen that is in the surrounding atmosphere will be absorbed and change the chemistry of the powders. Thus, it is important to have either as high a vacuum as possible or an Ar atmosphere to limit the oxygen pick up when processing titanium powders.

2.2.2 Powder Production Routes

2.2.2.1 Hydride-dehydride

Hydride-dehydride (HDH) powder is made from solid titanium material that has been heated to above 400°C in a hydrogen atmosphere. The hydrogen diffuses through the material along grain boundaries. As hydrogen is very embrittling, the material can be easily pulverised into a particulate form. Once the powder is formed, the material is heated in a vacuum to drive the hydrogen off. This forms powders ranging in particle size from a few millimetres down to a few micrometres, reflecting the initial grain size of the feedstock material. The powder is generally angular in shape with a smooth surface morphology. Due to the angular shape of the powders, interlocking can occur which can be extremely beneficial for certain modes of consolidation. Common impurities of HDH powders are mainly hydrogen and oxygen as part of the process involves heating the titanium; however other elements commonly found are Fe, Ni, Cr and Al. These mainly come from the steel reactor in which the ore is reduced to metal. The hydride-dehydride process is commonly used to manufacture not only commercial purity powders but also alloys, such as Ti-6Al-4V [21,41].

2.2.2.2 Atomisation Routes

Rapid solidification routes involve the solidification of the liquid metal at extremely high cooling rates, as high as 10^5°Cs^{-1} [42]. Gas atomisation (GA) makes use of a gas jet into which a molten metal stream is injected, where it is atomised by the gas pressure. Rotating electrode techniques melt the electrode and liquid metal droplets are formed when the electrode is rotated. The rotating electrode process (REP) utilises a tungsten arc to melt the feedstock material, whereas the plasma rotating electrode process (PREP) uses a plasma arc to melt the electrode. GA powders have the highest concentration of contaminants, mainly from the tungsten electrode, REP powders are contaminated from the ceramic container nozzle. Both REP and PREP powders contain low interstitial contents and usually produce coarser powders than GA products. Powders produced by atomisation routes are spherical, pack to a consistently high density and flow readily. Atomised powders do not compact well at low temperatures using techniques such as cold isostatic pressing (CIP) and are usually processed by hot isostatic pressing (HIP'ing)

[19,43].

Atomisation routes have also been used to produce alloy powders as the feedstock material for metal matrix composites by atomising the alloy powder with the reinforcement phase [44].

2.2.2.3 Kroll Sponge/Sponge Fines

Kroll sponge is 'powder' that is obtained directly from a Kroll reactor. The particle size is generally very large (approximately between 1 mm and 12 mm) and this is the starting material for all titanium alloys. Kroll sponge is rarely used as a powder feedstock material as the flow and packing properties are so poor; however, given that the material has very little contamination, there is no reason as to why this material could not be used as a powder feedstock material.

Sponge fines are the smaller particles which are leftover of the Kroll process. They generally have the same shape and morphology as HDH powders but due to the different manufacturing processes, they contain lower interstitial contaminants as the powders have not been heated.

2.2.2.4 Novel Routes for Powder Production

There are many novel titanium powder processes that are currently the subject of much research [1,45]. Possibly the most well known electrochemical method to produce titanium is the Fray-Farthing-Chen Cambridge (FFC Cambridge) process [46]. The process involves the electrochemical reduction of titanium oxide in molten $CaCl_2$ salt bath to form metallic titanium. This titanium could potentially be made into a powder which can then be used as cheap feedstock powder material. However, the only company currently pursuing commercialisation of direct powder reduction is International Titanium Powder (ITP) using the Armstrong process, which is a continuous version of the Hunter process [47] . This is similar to the Kroll process, but the $TiCl_4$ is injected into a stream of molten sodium rather than magnesium (as in the Kroll process) and this has showed promising results that could be expanded into automotive applications [48].

2.3 Titanium Composites

Metal matrix composites (MMC) utilize the properties of a stiff ceramic reinforcement phase in a tough ductile metal matrix to form a material with superior properties than those of either the single parent materials that make up the composite. There is a need

to make titanium alloys competitive with high strength steels which demand properties beyond those provided by conventional titanium alloys. Titanium matrix composites (TMC) are very promising as they provide significant strength and stiffness improvements over conventional alloys and the possibility of significant cost reductions obtainable *via* an *in situ* reaction to form the reinforcing phase has driven recent developments in whisker/particulate reinforced titanium composites [44].

2.3.1 Particulate Reinforcement of Titanium Matrix Composites

Titanium composites are gaining popularity in the aerospace and automotive industries as they significantly enhance high temperature and specific strength properties over conventional materials. Titanium composites are now being used by Toyota for exhaust components [49] and continuously reinforced titanium composites are of interest in high end aerospace components such as blisks and landing gears. It is widely believed that for the majority of applications, the reinforcing phase for a metal matrix composite should have the following properties [50] :

- be stiffer than the matrix
- have a similar coefficient of thermal expansion (CTE) to the matrix so cracking does not occur when processing the material at temperature or during service temperatures
- have a low solubility in the matrix to limit any interfacial reactions between the reinforcing phase and the matrix

A list of possible reinforcing phases for particulate reinforced titanium composites is shown in Table 2.3. For comparison, typical values for a monolithic titanium alloy are included.

Table 2.3: Possible reinforcing phases for titanium matrix composites [49]

Reinforcing Particle	Young's Modulus (GPa)	CTE K^{-1}	Max. Solubility (at.%)	Estimation ✓ ×
TiB	371	8.6	<0.001	✓
TiC	460	7.4	1.2	✓
TiN	250	9.3	22.0	×
SiC	420	4.3	Unstable in Ti	×
Si_3Ni_4	320	3.2	Unstable in Ti	×
TiB_2	529	6.4	Unstable in Ti	×
B_4C	449	4.5	Unstable in Ti	×
Al_2O_3	350	8.1	Unstable in Ti	×
Ti-6Al-4V	110	8.2	-	-

From the data in Table 2.3, it is clear that most of the candidates are not suitable as they react with the matrix (a common problem with SiC continuous fibre composites [51]). TiB and TiC are potential candidates for reinforcement phases; however titanium can accommodate up to 0.4 wt.% of carbon in solid solution whereas less than 0.05 wt.% of boron can be in solid solution with α titanium [31]. Even though TiC is reported to have a higher stiffness, TiB has a very similar CTE and the possibility of forming the reinforcement *in-situ* leads it to being a more suitable candidate for a reinforcement phase in titanium matrix composites manufactured by a mechanical alloying route.

2.3.2 Titanium-Boron System

The titanium-boron phase diagram (Fig. 2.9) shows that boron has less than 0.05 wt.% solubility in both α and β titanium up to its melting point. Of the three intermetallic compounds (TiB, Ti_3B_2 and TiB_2) which can be present in equilibrium, TiB is the most thermodynamically stable phase and will form where there is less than 18.4 at.% boron in the material. When the matrix is intimately mixed with either boron or TiB_2, TiB will form from via an *in situ* reaction when there are excess moles of titanium present [52].

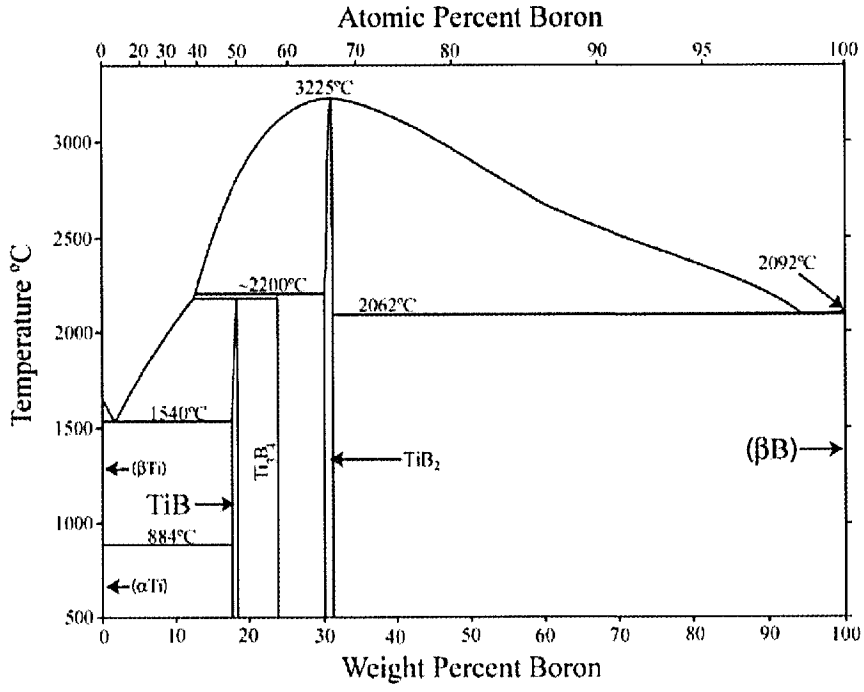


Fig. 2.9: Titanium-boron phase diagram

From the titanium-boron phase diagram it is clear that there are no phases exist between Ti and TiB, so there can be no interfacial reaction and hence a very clean interface is observed in these materials [53]. The narrow compositional range of TiB also means that the stoichiometry of the TiB reinforcing phase is the same, i.e. each TiB particle will have very nearly the same chemistry and so the mechanical and thermal properties of each TiB particle reinforcing phase will be the same.

Both TiB and TiB_2 exhibit a high degree of thermal stability up to the melting point of the materials. This is a beneficial for any high temperature applications, as the reinforcement phase will not react with the matrix.

2.3.2.1 Formation of TiB from TiB_2

Brandstötter and Lengauer [54] observed the formation of TiB needles emanating from the TiB_2 particles but not the presence of Ti_3B_4 at the Ti/TiB_2 interface. The structure of TiB is orthorhombic and is characterised by diffusion of boron atoms parallel to the 'b' direction, forming 'zigzag' chain of boron atoms, Fig. 2.10(a), surrounded by six titanium atoms [55], Fig. 2.10(b). TiB forms from a reaction between TiB_2 and the matrix and the morphology of the TiB phase is needle-shaped. A high temperature anneal is required to fully convert the TiB_2 to TiB.

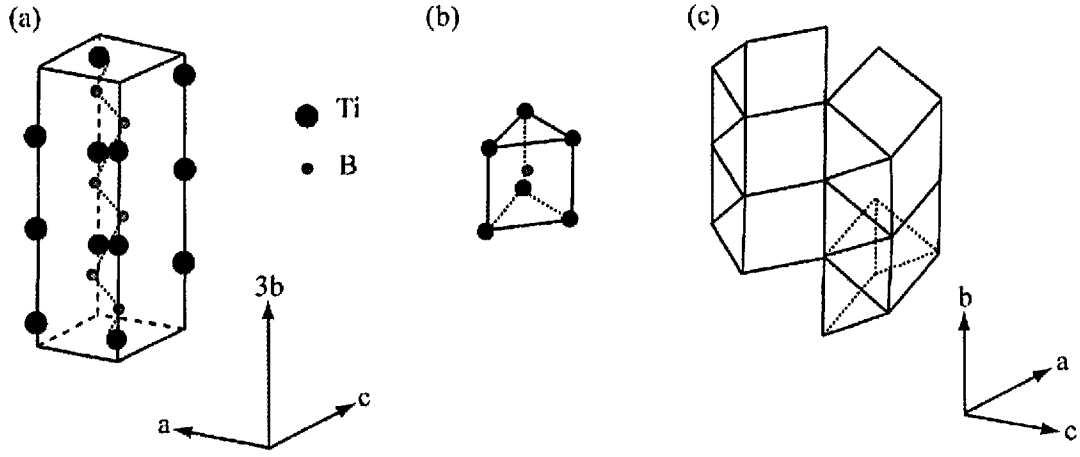


Fig. 2.10: Schematic illustration of the atomic arrangement of TiB, (a) TiB unit cell (B27), (b) basic triangular prismatic arrangement of Ti atoms around B and (c) arrangement of the basic triangular prismatic arrangement to form the TiB structure, after Decker [55]

2.3.2.2 Effect of Boron on the β Transus

Boron is chemically an α stabiliser, but due to the low solubility of boron in titanium, it should have a negligible effect on the β transus [56]. Whang [57] is reported to have achieved up to 10 at.% solubility of boron in titanium with a rapid solidification technique. This level of boron in solid solution would increase the β transus although no value is reported. Tamirisakandala *et al.* [58] have reported an increase of 60°C in a Ti-6Al-4V-1.7B powder manufactured via inert gas atomisation. Even though there is a low solubility of boron in titanium, it is still believed that the β transus will be raised, though the exact temperature of the transus will also depend on the purity of the constituent materials, for example the oxygen content of the Ti-6Al-4V.

2.3.2.3 Manufacture of Ti/TiB Composites

There are two methods that are used to manufacture Ti/TiB composites. These are rapid solidification (RS) [44,57] and mechanical alloying (MA) [59,60]. It is clear that a much more intimate mixture of boron is seen in RS techniques and it has been demonstrated that finer TiB can be formed [44] - however, the cost of RS techniques is prohibitive for the majority of applications.

2.3.3 Mechanical Alloying

Mechanical alloying was originally developed to produced oxide (yttria) strengthened nickel based superalloys in which the oxide phases did not coarsen at service tempera-

ture. Mechanical alloying is a solid state technique in which the constituent phases are mixed together with a high energy ball mill and are alloyed together. This is shown schematically in Fig. 2.11.

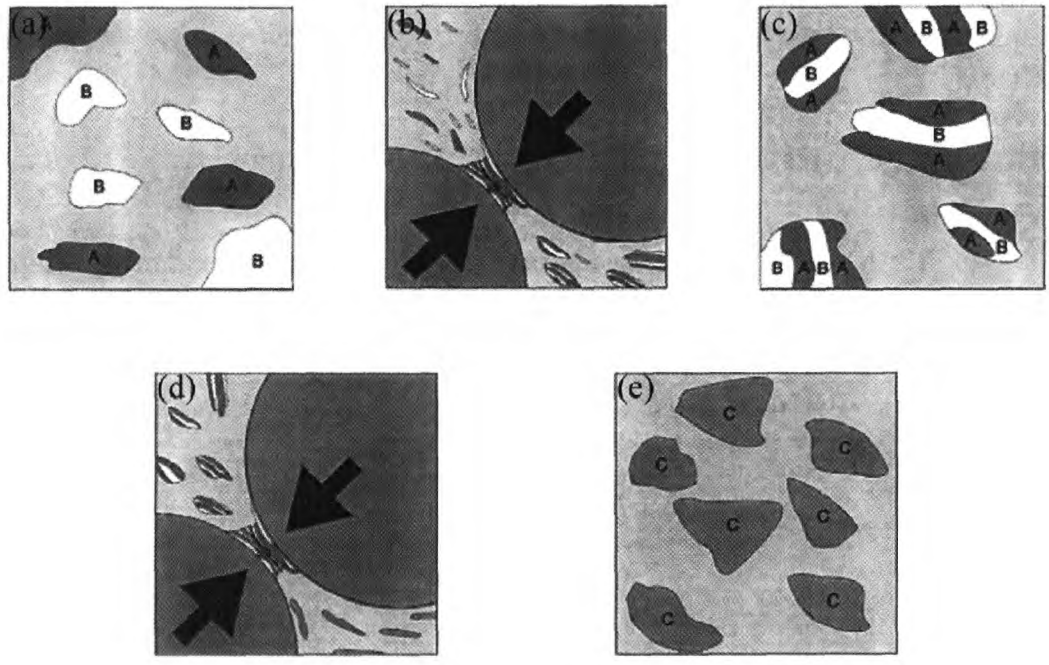


Fig. 2.11: Schematic of the mechanical alloying process, after Gardiner [61]. The schematic is explained in the section below

Initially, the two different elements, A and B, in Fig. 2.11(a) are mechanically alloyed as in Fig. 2.11(b). The elements are milled together and a layering of the elements occurs Fig. 2.11(c). Milling continues, Fig. 2.11(d), until there is a homogeneous distribution of the elements, giving alloy of composition C, as shown in Fig. 2.11(e). Mechanical alloying has been extensively employed for Al alloy SiC reinforced composites [62].

For ductile powders, alloying is achieved by deformation, fracture and cold welding. This results in the elemental powders having a lamellar structure (illustrated in Fig. 2.11(c)). Layering continues until a homogeneous distribution of the elemental powders is obtained. Mechanical alloying of brittle powders consists of powder fracture and welding so layering does not occur. Mechanical alloying is a balance between fracture and cold welding. With ductile powders, which readily cold weld, particles weld together. This balance of fracturing and welding is difficult to achieve so process control agents can be used to limit particle agglomeration. With mechanical alloying of titanium powders, TiH_2 can be used as it is embrittling and breaks up the welded particles, however, the material requires degassing to remove the TiH_2 from the powder afterwards.

Godfrey [59] determined that even with long milling times, it was not possible to get an even distribution of either B or TiB_2 in the titanium matrix. The distribution of B in

the Ti powder is more likely to resemble the layered structure observed in Fig. 2.11(c) rather than the homogeneous distribution observed in Fig. 2.11(e)

2.3.4 Load Transfer from the Matrix to the Reinforcement

When a stress is applied to the material, the load is transferred to the reinforcement phase across the matrix/reinforcement interface. The amount of load that can be transferred is proportional to the volume fraction of the reinforcement phase and can be predicted by the rule of mixtures:

$$E_c = (1 - f)E_m + fE_r \tag{2.8}$$

Where E_c is the stiffness of the composite, E_m is the stiffness of the matrix, E_r is the stiffness of the reinforcement phase and f is the volume fraction of the reinforcement phase. When numerical values are inserted into Equ. 2.8, from Table 2.3, the stiffness of the Ti-TiB composite can be predicted:

Table 2.4: Predicted stiffness of Ti-6Al-4V reinforced with varying volume fractions of TiB using the rule of mixtures

Volume Fraction. %	Stiffness, GPa
0	110
10	136
20	162

This predicts a 23% and 47% rise in the stiffness for a 10 vol.% and 20 vol.% reinforced composite respectively. This model crudely predicts an increase in the stiffness for a whisker reinforced metal matrix composite but is known to be more effective with fibre reinforced composites.

The interfacial bonding between the matrix and the reinforcement is important in the transfer of the load from the matrix to the reinforcement. An interface which is too weak will de-laminate when a load is applied and load transfer will be inefficient across the boundary. An interface which is too strong will make inelastic processes more difficult and make the composite brittle. With metal matrix composites, it is usually desirable to have a strong interface to obtain maximum load transfer to the reinforcing phase. Any microstructural changes which occur between the matrix and the reinforcing phase will also weaken the interface [50].

As the boundary between the titanium matrix and the TiB needles is a strong interface, due to the crystallographic coherency of the Ti-6Al-4V and the TiB, load transfer should be relatively efficient.

2.4 Consolidation of Metal Powders

Metal powders are characterised by their physical, chemical and process properties. The main physical properties of powders are the shape of the particles, the size distribution and hardness of the powders [39]. The shape of the powder is generally predetermined by the manufacturing method, the size and size distribution by the process conditions. The methods for manufacturing titanium powders are described in Section 2.2.2.

It should be noted that the 'compaction' of powder is a term used to describe the incomplete consolidation of the material, in the case of titanium, this is usually due to the lack of shear in breaking the oxide layer on the powder inherent on the surface of each powder particle. Consolidation is a term that is used to describe the complete compaction to the theoretical density of the material. It is, however, possible to compact the powder to near full density but not break the oxide layer so that the material is not 'consolidated' - as is the case of extruding powder which is compacted to near 100% density but is poorly bonded together [5]. In order to fully consolidate the material, temperature, pressure and, to some extent, shear is required. In the case of titanium powders, sintering is the most common commercial method used to consolidate the material to full density. Though powder metallurgy routes are not commonly used to consolidate titanium alloy powders, there is currently much research using PM processes to consolidate metal matrix composites, see Chapter 6.

There are several advantages of powder metallurgy routes over wrought or cast products, these are summarised below:

- Near-net shaping capability
- Fine grain size possibility
- Isotropic properties
- Range of possible size parts
- Can produce highly alloyed components which are difficult when using ingot metallurgy routes
- Cost-effective components

2.4.1 Theory of Powder Consolidation

It is generally considered that the compaction of powders follows four distinct stages [42, 63].

1. Rearrangement
2. Localised plastic deformation
3. Homogeneous deformation
4. Consolidation

Figure 2.12 shows that an idealised plot of the fraction of density increases with increasing compaction pressure, which tails off with increasing pressure until the theoretical density is reached. The cold compaction of metals powders has been studied by various authors and is outlined below [63–65].

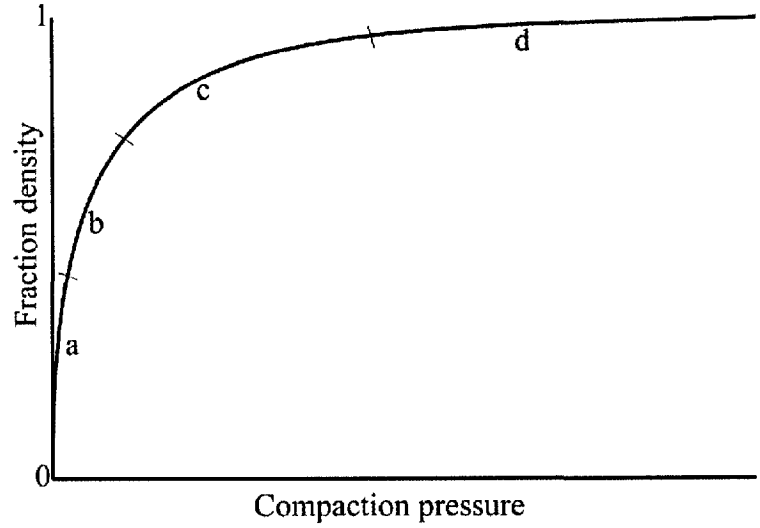


Fig. 2.12: Idealised plot of fraction density against compaction pressure

Initially, elastic deformation occurs at the points between particles. This is when particles are rearraged into a greater packing density until the maximum packing density is achieved, shown in Fig. 2.12(a); this is the rearrangment stage of the densification process and occurs due to particle rearrangement and sliding. The tap density is often cited as the upper limit of the rearrangement stage and is a measure of the greatest possible packing possible with a particular powder type. The second stage, Fig. 2.12(b), is localised plastic deformation. Asperities are flattened where there are points of contact between particle. For ductile materials, the stress will increase above the yield stress and material will flow into neighbouring areas that are empty, hence the stress in the material is not uniformly distributed. This flow of material eliminates the larger pores and there is an inherent shift to a smaller pore size distribution. Brittle materials fracture at the onset of plastic deformation and the particles can fragment and the particles are repacked as the smaller particles move into unoccupied spaces between the larger particles. Homogeneous deformation, Fig. 2.12(c), occurs with higher pressures. It is

characterised by deformation thoughout the particle mass and an increase in bulk properties. As the material becomes more and more strain hardened, resistance to further deformation increases. At larger compaction pressures, the oxide layer breaks exposing fresh metal, which increasces the interatomic forces and cold welding between particles can occur, Fig. 2.12(d).

The amount of densification in the early stages of consolidation is primarily a function of the particle geometry whereas during the later stages, the material properties (e.g. work hardening characteristics) are more important [63].

2.4.2 Degassing and Compacting Powders

In the literature, the majority of degassing work carried out is on titanium matrix composites. Most of the data presented in this section is from experimental methodologies used in the manufacture of the composites rather than studies of the degassing parameters on final properties and microstructures. Degassing procedures prior to consolidation appear to be either at low temperatures (approximately 300°C) [58] or high temperatures [57]. The majority of degassing conditions used in industry are proprietary and so a parametric study into the effect of degassing conditions on final properies has never been published.

Prior to consolidation, powders generally require preparation to remove air and moisture from the powder surface to limit interstitial contamination during downstream processing. For some materials (e.g. Al), powders can be compacted at room temperature and processed in air [66], for other metal powders, removal of air and moisture and total isolation during processing is necessary [57]. Titanium has traditionally been considered to fall in to the latter category.

Lee and Peters [67] have investigated the degassing of Ti-6Al-4V PREP powder. They found that several reactions occurred at various temperatures up to 730°C. At low temperatures from 40°C to 320°C, H_2O emission was predominant. Two possible reasons for this are the dissociation of physically adsorbed titanium hydroxide at the powder surface,

$$2Ti(OH)_2 \rightarrow Ti + TiO_2 + H_2O \tag{2.9}$$

or the separation of combined water from the surface of the powder particles,

$$Ti/TiO_2.(H_2O) \rightarrow (Ti + TiO_2) + H_2O \tag{2.10}$$

At temperatures between 320 and 500°C, H_2 emission was predominant due to the oxidation of titanium at the powder surface with emitted water vapour as part of the

dehydration process. The partial pressure of water vapour decreases over this temperature range.

$$Ti + 2H_2O \rightarrow TiO_2 + 2H_2 \tag{2.11}$$

At 500°C there is a sharp drop in the H partial pressure being emitted from the can, corresponding to the hydration process,

$$Ti + H_2 \rightarrow Ti(H) \tag{2.12}$$

The H_2 emission increased again to a maximum at 780°C, corresponding to the dehydration process,

$$Ti(H) \rightarrow Ti + H_2 \tag{2.13}$$

Lee and Peters [67] therefore postulated that the optimum temperature for degassing PREP Ti-6Al-4V powder is 500°C so as to avoid recombination with any hydrogen that is driven off at temperatures above this. Also at this temperature, there is appears to be minimal contamination from oxygen and nitrogen, although no value is reported. It is important to note that in Equs 2.9, 2.10 and 2.11, TiO_2 is formed which is not removed during subsequent hot degassing. It is virtually impossible to remove oxide once it has formed on the surface of the powders so it is important to reduce the amount of oxide reacting with the powder in the first place. Suppressing the reactions shown in Equtions 2.9, 2.10 and 2.11 is the only way to limit the build up of oxide on the powder surface. If there are temperature gradients in the can, gases can be evolved from powders at lower temperatures which, instead of exiting the can, react with the powders at higher temperatures. Minimising the temperature gradients can be achieved with the correct heating rate during the degassing. Heat transfer in the can, however, is minimal due to both the poor conductivity of titanium and the vacuum within the can, so a slow heating rate is required to keep the temperature gradients to a minimum.

Clearly, it is necessary to limit the amount of interstitial elements in the titanium powder as these have a dramatic effect on the mechanical properties of the final product, as shown in Fig. 2.3. Therefore, it is important to get the correct degassing parameters for titanium powder. There is insufficient evidence to suggest that the temperature proposed by Lee and Peters [67] is incorrect, as the majority of information on degassing is kept in-house. Logic dictates that the higher the degassing temperature, the faster the removal of air, moisture and other compounds from the surface of the powder; but the likelihood of interstitial contamination increases dramatically above approximately 500°C.

Powder that has been compacted to a level where the porosity is closed rather than open cannot be degassed, as the moisture and air cannot escape from the compacted powder mass. There is, therefore, a maximum compact density to which degassing can

be suitably applied. It is not possible to estimate the amount of compaction required to begin to close porosity in a compact as the only suitable technique for accurately quantifying porosity is X-ray micro tomography, and currently there is no technique which allows for large enough sample sizes. Therefore, it is not wise to compact titanium powder into a can to increase the density before degassing, as the air would not be able to escape from the pores.

Recent research by Wilson *et al.* [2] showed that it is not necessary to can and outgas titanium powders prior to consolidation. With a suitably protective atmosphere, it is possible to extrude titanium compacts to produce a consolidated fine grained microstructure with little contamination from oxygen, they have even reported a decrease in the nitrogen content after extrusion. If powder is not canned prior to extrusion, then it must be compacted to a suitable green strength to allow for handling of the powder.

If powder were to be compacted into the can to a specific density, then the air within the pores of the compact would be absorbed into the the titanium during processing. The fact that Wilson *et al.* have reported only minimal oxygen pick up when extruding compacts proves that only minimal air remains within a compact and that the majority of interstitial contamination occurs from the surrounding atmosphere of the billet during processing. This indicates that air is squeezed out of the compact when the powder is subjected to the uniaxial pressure during compaction. If a suitable method can be developed to limit the oxygen pick up during processing then it would be possible to develop techniques to consolidate powder without canning or degassing.

2.4.3 Vapour Pressure

The vapour pressure of a compound is the pressure at which the compound will change state from a solid/liquid to a gas. The degassing of powders thus also allows for compounds mixed in with the powders to be removed from the surface of the powders if the pressure is low enough. This is particularly useful for compounds that maybe left over from the metal reduction processes, for example $MgCl_2$ from the Kroll process; or for compounds that may be added to the powders to aid the manufacturing process, e.g. TiH_2 is added to some titanium alloys to aid the mechanical alloying process, Section 4.6.3.

2.4.4 Direct Powder Extrusion

Direct particulate extrusion (DPE) is a similar process to conventional extrusion where the material is pushed though a die into a rod or bar shaped product. With DPE, the

powder is consolidated and shaped in one operation [42] and has been extensively studied for a variety of different metal powders [5,6,8–10,68,69]. A schematic of the extrusion process is shown in Fig. 2.13.

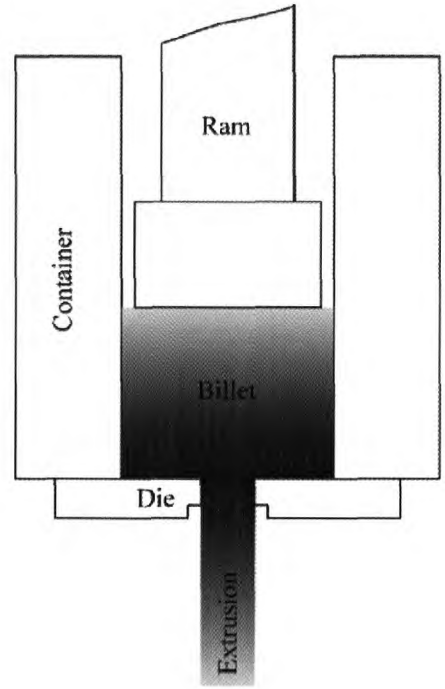


Fig. 2.13: Schematic of the extrusion process

With powder extrusion, the powder either requires containment in a can to protect the powder from oxidation during heating [68,70], cold compacting so that the powder has green strength for easy handling [11] or a combination of both [68]. There are advantages to both methods. With canned extrusion, the can is degassed to remove the atmosphere and moisture from the powder surface so that the extruded product is likely to have fewer contaminants. A mild steel can may act as a lubricant [4,68], increasing the life of the die, when the powder materials are hard. Containing powder in a can also inherently means that the powder will have a lower starting density compared to powder compacts, which have been compacted to a higher density. Canning powder prior to extrusion will require removal of the can after the working operation whilst compacting the powder will produce longer lengths of bar compared to extruding loose powder [68].

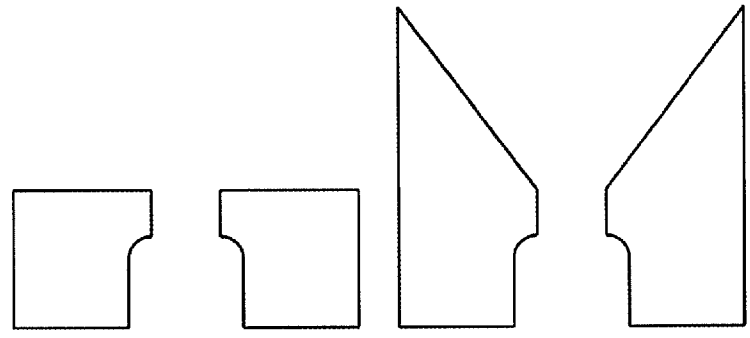
Sheppard and Chare [6] have shown that the powders are compacted to near 100% density prior to extrusion, though the particles remain poorly bonded. As the densified material passes though the die, redundant work is done on the particles which welds, breaks and re-welds the particles until there has been enough shear work done on the particles, at which point the product will have metallurgically sound bonds and be completely consolidated. The amount of work done on the material is dependent on the

reduction ratio of the extrusion. The reduction ratio, R, is defined as the reduction in area of the extrusion to the billet, Equ. 2.14.

$$R = \frac{A_{billet}}{A_{extrusion}} \tag{2.14}$$

where A_{billet} is the area of the billet and $A_{extrusion}$ is the cross sectional area of the extrusion. There is a general rule that a minimum reduction ratio of 10 is required to consolidate compacted powder billets.

The smaller the die diameter, the greater the reduction ratio and so the more work done on the material as it passes though the die. The shape of the die is also important in determining the work done on the material as it passes through the die.



(a) Flat Die (b) Conical Die

Fig. 2.14: Different die designs

The different die designs generate different deformation zones and flow patterns, illustrated in Fig. 2.15.

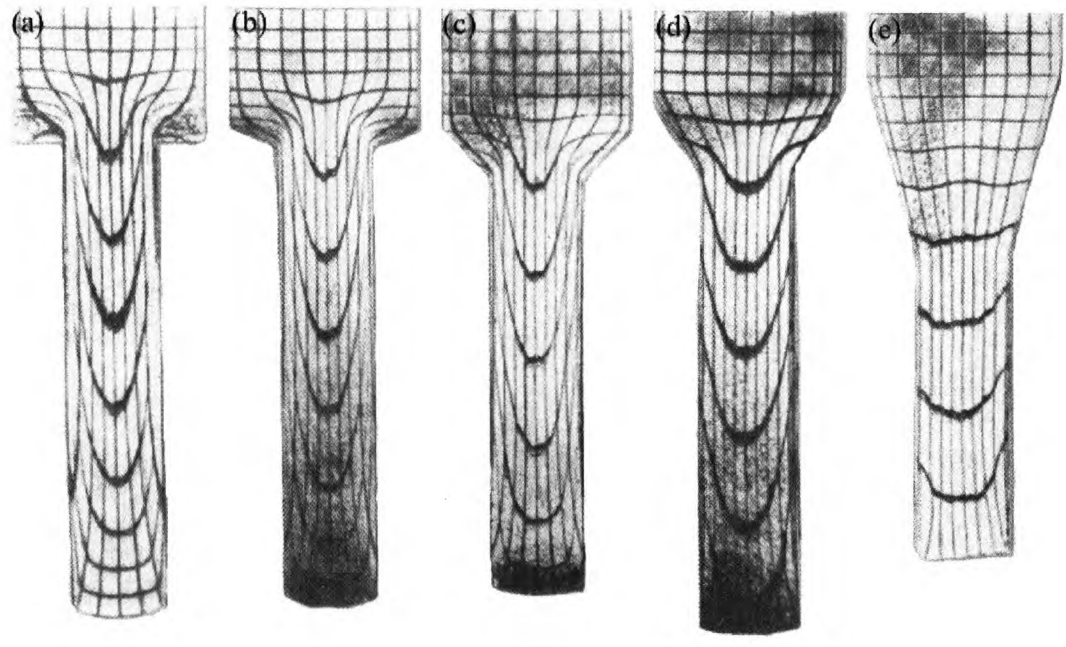
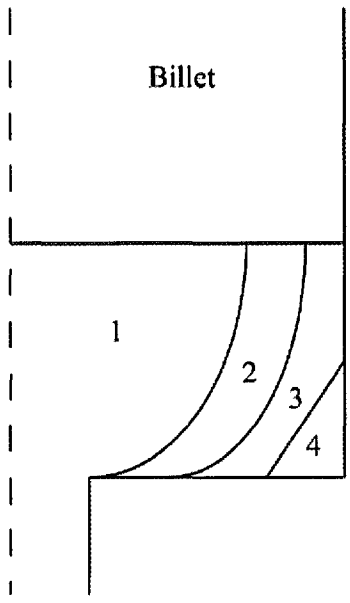


Fig. 2.15: Variation of flow with different die designs, after Sachs and Eisbein [71]

Fig. 2.15 shows the die becoming more conical, with Fig. 2.15(a) being a flat faced die though to Fig. 2.15(e) being a conical die. The different deformation zones can be seen at the front of the dies. Flat dies lead to turbulent flow, in which the central part of the billet travels faster than the edge which is retarded due to the friction at the billet/liner interface, Fig 2.15(a). This results in the formation of a dead-metal zone in which there is no flow of metal, and a highly sheared zone in which the metal flows though the die. The different deformation zones for Al alloys have been reviewed by Thackray [72] and are briefly described in Fig. 2.16.



1. Centre - Metals in this zone flow through the die with no frictional influence from the container walls. This is the first part of the billet to exit the die and forms the front of the extrusion.

2. Co-extrusion - This part of the material has its flow restricted compared to the central zone, therefore more deformation and shear is applied to this part of the billet. This part of the extrusion forms the surface layer of the extrusion. As a result of this restriced flow, this area does not immediately flow though the die, even though it is adjacent to the die.

3. Slow-flowing - Though heavily deformed, the material in this zone is not always extruded and forms most of the discard.

4. Elastic zone - This region remains undeformed during the extrusion cycle and also forms the discard.

Fig. 2.16: Deformation zones in a billet, after [72]

The previously mentioned dead metal zone is formed by zones 3 and 4. Steady state extrusion occurs when material flows though the dead metal zone.

A practical result of turbulent flow which occurs with flat faced dies is the back end defect or piping defect. This is caused by the tendency of the the outer surfaces of the billet to remain relatively stationary compared to the centre of the billet, which results in a build up of the surface layers at the billet/die interface. When a certain percentage of the extrusion stroke is complete (approximately 70 - 80%) the outer layers build up and flow though the die. The surface of the billet contains oxide materials and these can be folded in to the centre of the extrusion by shear deformation, Fig 2.17. This can lead to up to 30% of the extrusion having to be discarded [73]. Conical dies (Fig. 2.15(e)) generate minimal shear as there is no dead metal zones at the billet/liner interface. Titanium is usually extruded using conical dies to minimise flow stresses.

The amount of shear generated as the material passes thought the dead metal zone is extremely important in determining the amount of deformation the material undergoes. Flat faced dies produce more shear so they are more appropriate for powder consolidation.

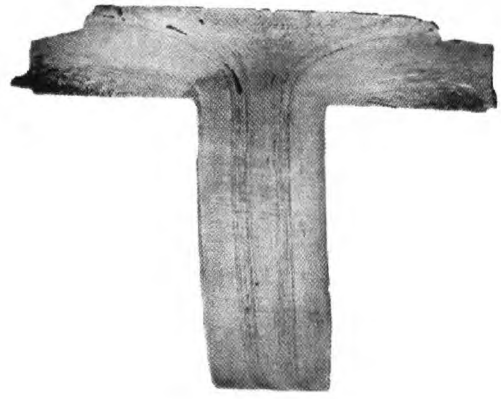


Fig. 2.17: Extrusion back end defect, after Pearson [73]

The temperature of the extrusion is one of the most important parameters in determining the final properties of the extrudate. The higher the temperature, the lower the extrusion load as the material becomes more plastic. There are, however, some detrimental microstructural effects of extruding at higher temperatures. Extruding at higher temperatures results in a larger grain size and with respect to titanium, the extrusion at higher temperatures could result in massive grain growth. The extrusion of titanium is usually achieved at 920°C as this is below the β transus of Ti-6Al-4V. It is generally accepted that extrusions should be attempted at the lowest possible temperature for any given press capacity to firstly, reduce wear on the container and dies and secondly, to limit microstructural changes in the material. It is important to maintain the billet temperature during the extrusion as there will be a drop in temperature as heat transfers to the container. Such billet chilling is detrimental to the extrusion profile and can cause microstructural variations along the length of the extrusion. Billet chilling leads to an increasing load on the extrusion profile, due to increased flow stresses, thus the greater the required press capacity, illustrated in Fig. 2.18.

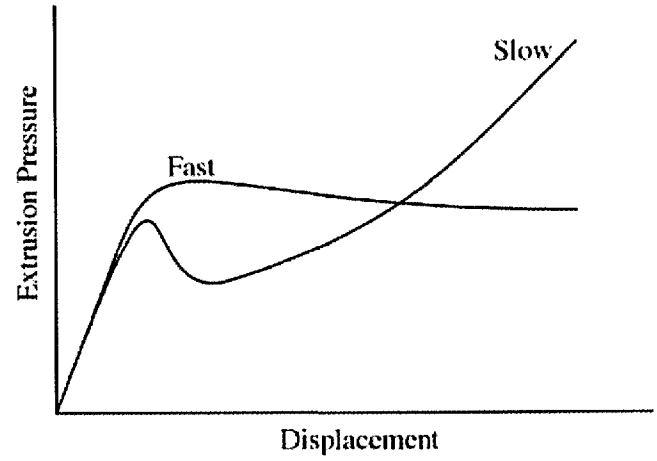


Fig. 2.18: The effect of extrusion speed on the extrusion profile

Fig. 2.18 shows that for a fast extrusion, where there is minimal billet chilling, the load increases to a breakthough load and steadily decreases, representing the reducing friction between the container wall and the billet as the material is forced though the die. With slower extrusions, there is a breakthough load and then a slight decrease in the load, but as billet chilling occurs the load starts to increase due to the increasing flow stress. This clearly illustrates how extrusion speed is an important parameter in determining the extrusion load and therefore the press capacity required.

As material is forced though the die, there is a local increase in temperature at the billet die interface due to the friction between the die and the billet.

2.4.5 Hot Isostatic Pressing

Hot isostatic pressing (HIP) is a solid state consolidation process that utilises the application of temperature and isostatic pressure to consolidate the powder to the theoretical density of the material. The pressure is applied though an inert gas, such as argon. HIP'ing is a technique that is usually carried out on wrought or cast products to reduce porosity [74], increasing fatigue life, and is not commonly used for powder consolidation [20]. However the process has successfully been applied to metal matrix composites [44] which are difficult to process by conventional ingot metallurgy and for bonding dissimilar materials together.

HIP'ing is concerned with the removal of pores from within a material. These may originate from shrinkage porosity in castings to porosity within a powder compact, the driving force for the removal of porosity is the reduction in surface area. During the process, the Ar atoms used to transmit the pressure can be thought of as mini forges; when they collide with the material, they impart kinetic energy into the material which

plastically deforms the material. In the case of powder compacts, there is also a volumetric change in the material to increase the density of the powder. It is the isostatic nature of the process which allows complex shapes to be HIP'ed. Although the process is isostatic, the deformation of the material is not always if it is encased with a canning material [74]. Fig. 2.19 shows the reduction in volume of a HIP'ed complex shape.

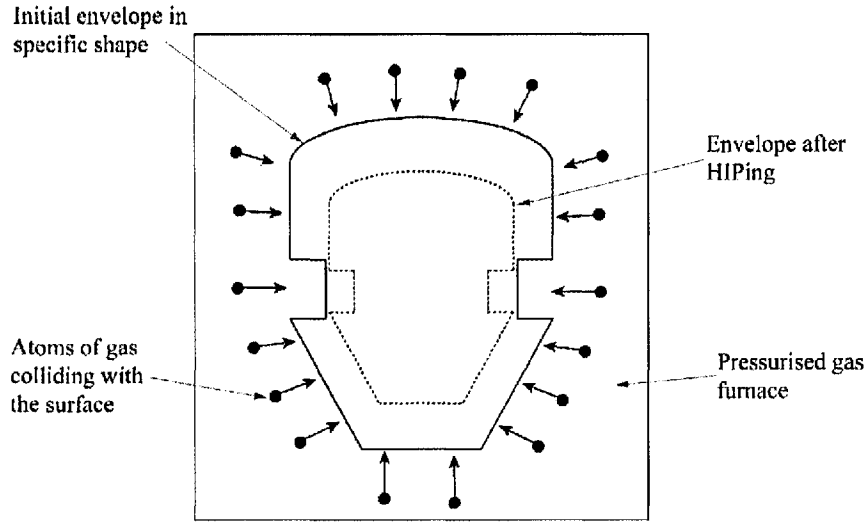


Fig. 2.19: Isostatic pressing of a powder compact showing a reduction in the volume of the envelope, after Atkinson [74]

The majority of densification occurs during the early stages of the process with a significant contribution from particle rearrangement and then plastic deformation up to approximately 90% density [75]. In order to fully densify the material beyond this level, creep mechanisms dominate, with mass transport via lattice diffusion and along grain boundaries [76].

The pressures that are usually used for HIP'ing operations are in the order of 100 MPa for most metallic powders, slightly higher pressures are used for ceramic powders. The temperatures used are usually greater than 0.7 T_m, to ensure that the material is plastic enough to deform under the pressure applied. Titanium alloys, such as Ti-6Al-4V, are usually HIP'ed at 920°C (which is high in the α+β phase field) which is approximately 0.7 T_m (as T_m for Ti is 1668°C). This temperature is chosen because at the pressing temperature there is a 50% volume fraction of α and 50% of β which enables favourable deformation mechanisms, such as grain boundary sliding and diffusional creep to occur, and β grain growth to be minimised. The HIP'ing temperature will determine the volume fraction of primary α and the cooling rate will determine the morphology of secondary α. The cooling rate during HIP'ing processes is limited due to the design of the press. Quenching is not possible, but cooling rates of up to 10°C/min are obtainable.

There are several advantages to HIP'ing over other consolidation routes: the mechan-

ical properties are as good as, if not better, than wrought products. The material is isotropic, it produces a better surface finish which decreases stress concentrations and increases fatigue strength, as stated earlier, near-net-shaped products can be produced which reduces machining costs [74]. Generally, the temperature and pressure are the variables during the HIP'ing process. Froes *et al.* [77] has suggested that spherical powders produced by RS processes are the most suitable, as they flow to a consistently higher packing density than angular powders. However, with non-melt processing, the use of angular particles is more viable as only costly atomisation routes produce spherical powder feedstock.

Chapter 3

Experimental Techniques

3.1 Summary

This chapter summarises the experimental and computation techniques utilised in this thesis. The canning, degassing and crimping procedure, used to produce canned powder for downstream consolidation is detailed. The compaction of powder billets for extrusion is also described. Experimental procedure for the extrusion and hot isostatic pressing (HIP'ing) are explained. The characterisation techniques used to examine the materials shown in Chapters 4-6, X-ray diffraction (XRD), electron microscopy, light microscopy and mechanical testing, are also detailed. Finally, the finite element analysis set up is discussed, along with the details of compression testing that was employed to determine the rheology behaviour of the extruded powder.

3.2 Materials Studied

The hydride de-hydride (HDH) titanium powder used for this investigation was supplied by QinetiQ Ltd, Farnborough (originally supplied by Hereford Metal Powder Company Ltd), its production route has already been described in Section 2.2.2, on page 33. Secondary electron images (SEI) of the powder are shown in Fig. 4.1 in Section 4.2. Initial trials used relatively low grade Kroll sponge fines. Kroll sponge fines are similar in size and surface morphology to the HDH powder, it was acceptable material for initial scoping trials.

3.2.1 Ti HDH Powder

One hundred grams of HDH powder was sieved using an Octagon digital shaker with 8 inch diameter sieves for 1 hour to determine the size fraction of the titanium powder. The sieves used were 2000, 1000, 900, 800, 710, 600, 500, 400, 300, 200 and 100 μm. The mass of each sieve was measured before and after the powder was sieved and the mass of powder recorded. The particle distribution of the Ti HDH powder is shown in Fig. 3.1. The mean particle size was measured to be 400 μm.

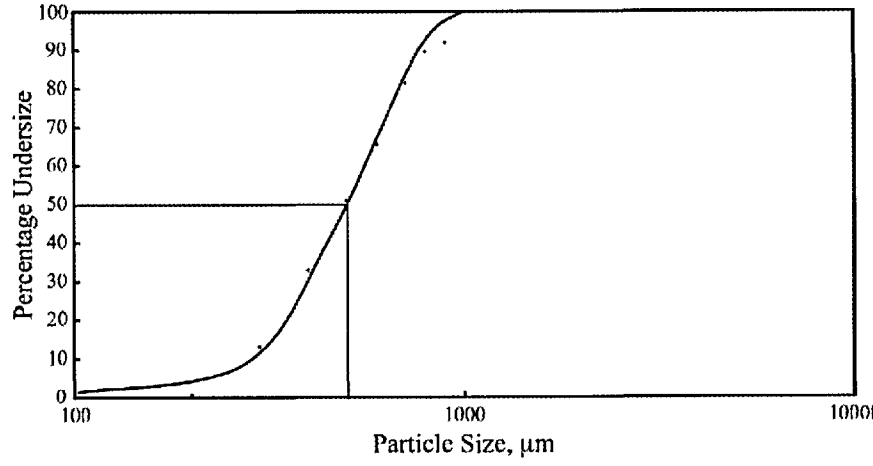


Fig. 3.1: Particle size distribution of Ti HDH powder

Chemical analysis of the powders was performed by IncoTest for the interstitial and rare earth elements and UK Analytical for the chlorine analysis. Approximately 5 g of powder was used for each chemical analysis test. Oxygen and nitrogen were analysed using a LEC2 test, hydrogen was analysed using a LEC3 test. All other elements were tested by the ICP test (OES analyser).

Table 3.1 shows the chemical analysis for the Ti HDH powder.

Table 3.1: Elemental analysis of HDH powders

Element	Composition	Element	Compositions
Fe	0.35	Si	0.01
Cr	0.05	Mn	<0.01
Mg	0.033	P	<0.001
N	240 ppm	Al	<0.01
O	1300 ppm	B	<0.001
H	65 ppm	Ca	<0.001
Cl	<0.005	Co	<0.01
Cu	<0.01	Mo	<0.01
Nb	<0.01	Sn	<0.01
Ta	<0.0.1	V	<0.01
W	<0.01	Y	<0.001
Zr	<0.01	Ti	Balance

All chemical compositions are in wt.% unless otherwise stated.

3.2.2 Ti-6Al-4V and TiB_2 powders

The Ti-6Al-4V used as the matrix of the composites was in the form of inert gas atomised powder, with a typical particle size of 100-120 μm, an oxygen content of 0.1-0.12 wt.% and was supplied by Crucible Research. The TiB_2 used in the manufacture of the composites was 5 μm in diameter, manufactured by H. C. Stark. The two powders were mechanically alloyed by Aerospace Metals Composites (AMC) with a small amount of TiH_2 to break up the agglomerates that form during the mechanical alloying stage. The mechanical alloying was done at room temperature and in an argon atmosphere (less than 200 ppm oxygen).

3.3 Canning and Degassing

3.3.1 Can Manufacture

All cans, lids and tubes were machined from EN1A mild steel. The design of the cans is shown in Fig. A.1 and Fig. A.2 on pages 151 and 152 respectively. The can was originally machined from steel bar which was bored out to make the can, however this was deemed to be too time consuming. So a welded can method was developed.

3.3.2 Welding

All welding was done with a tungsten inert gas (TIG) welding machine (Lincoln TIG-355). A table of the operating parameters for welding the different parts of the can is shown in Table 3.2. The inert gas used was alushield light (Ar-30%He) flowing at a rate of 6 l/min. The cans were welded on a turntable set at approximately 2 mm/s.

Table 3.2: TIG Welding Operating Parameters

Part	Current, A
Degassing Tube	88
Base and Lid	60
Crimp Welding	30

A diagram of the welding process is shown in Fig. 3.2

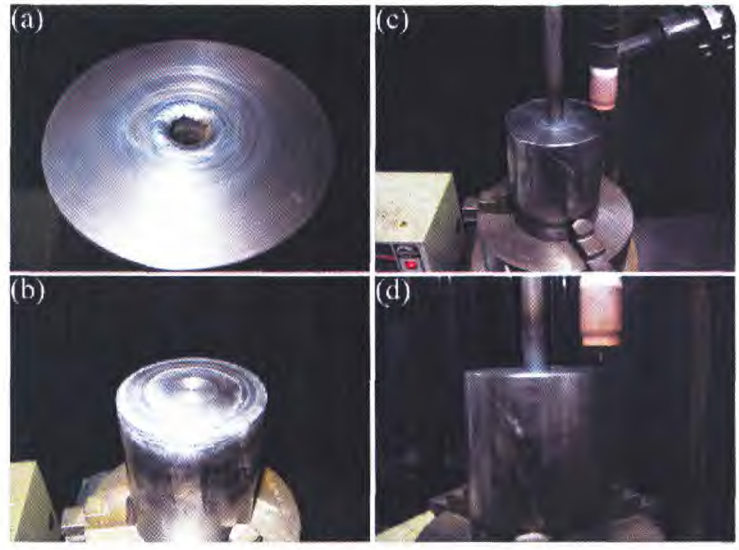


Fig. 3.2: Process for welding mild steel cans to encapsulate Ti HDH powders, (a) degassing tube welded to the lid from the bottom, (b) bottom side welded onto the can (c) welding the lid onto the can with the position of the welding tip and turntable shown, (d) position of the welding tip 2 mm from the can

In order to manufacture a can, first, the degassing tube is welded to the lid, Fig. 3.2(a). The weld line is made underneath the lid due to the difficulty of TIG welding a 90° bend, as it is much easier to weld a flat surface and it was determined that it makes no difference to the quality of the weld. The bottom side of the can is then welded onto the body of the can. The dimension of the bottom side are the same as the lid but without the degassing tube in the centre, Fig. 3.2(b). The welding tip for TIG welding needs to be approximately 2-3 mm from the metal, shown in Fig. 3.2(d). Fig. 3.2(c) shows the

lid being welded onto the can after the Ti HDH powder has been put into the can.

3.3.3 Canning

When the bottom side has been welded to the can, the powder is poured in and tapped until there is no visible decrease in the height of the powder. The can is filled with powder up to approximately 2 cm for the top of the can, Fig 3.3. Such a gap was necessary so that the lid could be welded to the can without heating the adjacent powder. The lid was then welded onto the can, Fig. 3.2(c).



Fig. 3.3: Ti HDH powder in the mild steel can, filled approximately up to 2 cm from the top of the can

After welding the lid onto the can, the remaining powder was poured thought the top of the degassing tube using a funnel. The can was tapped until there was no further decrease in the powder height. The can was filled up until the powder just passed the top of the can to ensure that the powder entirely filled the can. After the completion of the canning, the can with the Ti HDH powder was placed in a vertical tube furnace. Before the degassing tube was attached to the the vacuum pump, the crimp was placed over the degassing tube so that the pump could continue to evacuate the can when crimping, Fig. 3.4.

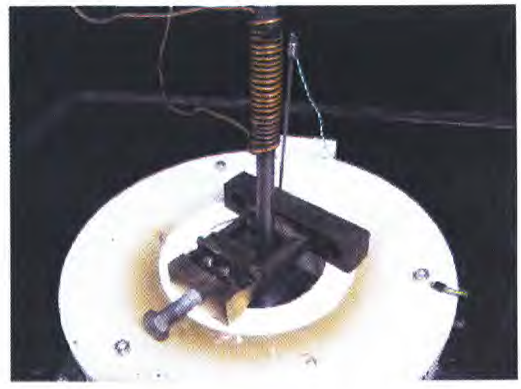


Fig. 3.4: A photograph of the can in the vertical tube furnace with the crimp placed over the degassing tube, also visible is a copper tube for cooling the degassing tube

The copper pipe visible in Fig. 3.4 is a water cooling system to cool the degassing tube so that the heat from the vertical tube furnace did not affect the join to the vacuum pump.

3.3.4 Argon Reflowing

Argon was reflowed over the titanium powder by connecting a pureshield argon bottle supply (purity level 99.995%) to the can via a three way valve that separated the vacuum pump from the argon, so that either the vacuum pump or the argon was connected to the can, but not both at the same time, Fig. 3.5.

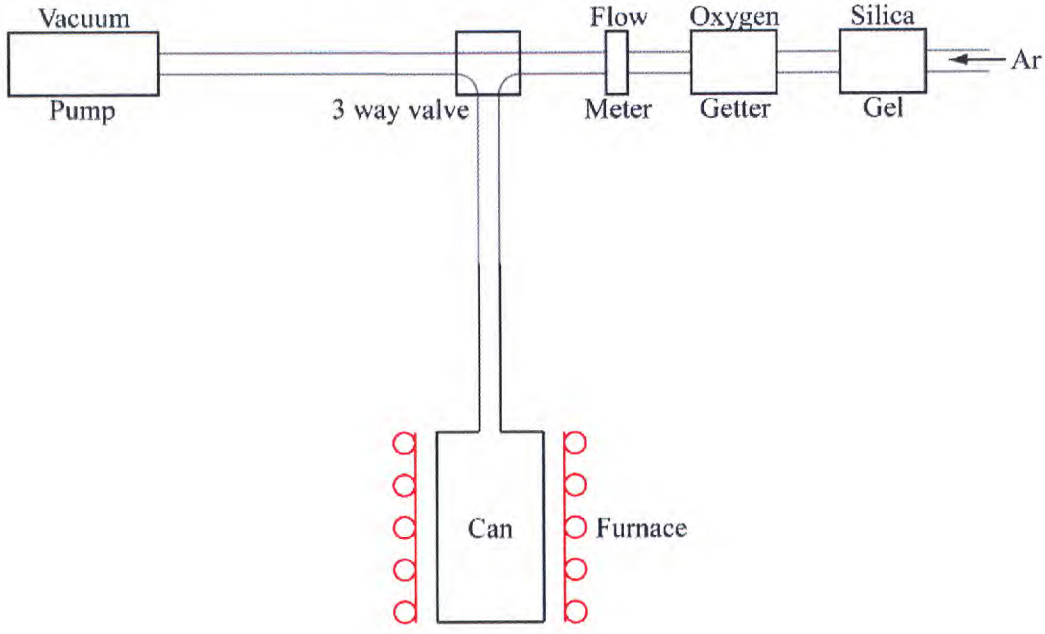


Fig. 3.5: Degassing and argon reflowing set-up for Ti HDH powder

The vacuum pump was switched on and the can was evacuated. When the can had reached a stable pressure, approximately 10^{-1} mbar, argon was flowed over the Ti HDH powder three times to displace any remaining oxygen in the can. The argon flow was passed over silica gel to absorb moisture and titanium turnings (heated to approximately 800°C) to remove primarily oxygen, but also other interstitial gases in the bottled argon supply. The argon used was conventional bottled argon and was flowed over the titanium powder for 1 minute each time, at the beginning of the degassing procedure when the powder was at room temperature.

3.3.5 Degassing

After argon reflowing, the can was ready for degassing. The heating rate for the furnace was either 3°C/min or 25°C/min to the degassing temperature. Degassing was done with a rotary/diffusion pump connected to the can via a series of reinforced PVC tubes. For some degassing runs, only the rotary or diffusion pump was used, for others, both types of pump were used, this was to obtain different pressures within the can.

3.3.6 Crimping

When degassing was complete, the can was removed from the furnace and placed on the turntable. The crimp, Fig. 3.6, and is shown placed over the degassing tube in Fig. 3.4.

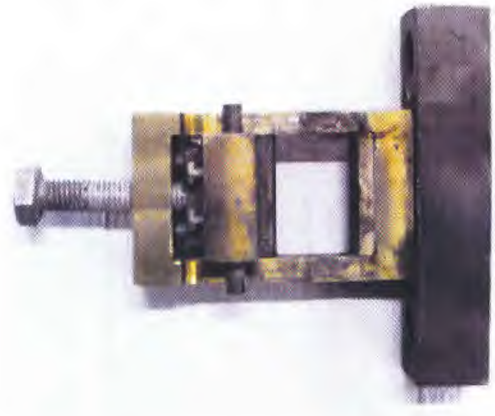


Fig. 3.6: Crimp used to seal the degassing tube

A hydraulic ram was used to press the crimp into the degassing tube. An oxy-acetylene torch was used to heat the tube before the hydraulic load applied to the crimp, sealing the can, Fig.3.7(c). The tube was crimped twice and the bottom crimp bent through 90°, seen in Fig. 3.8(a). The remaining tube was cut away using tin snips, Fig. 3.8(b).

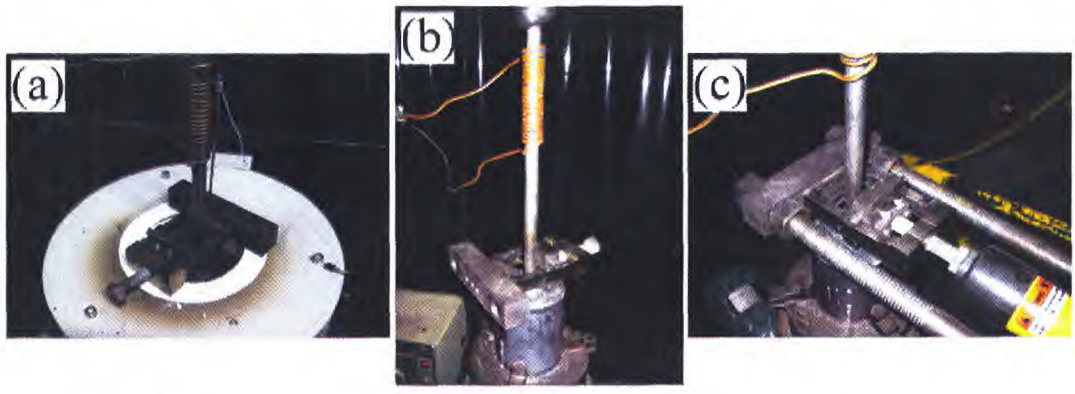


Fig. 3.7: Crimping of the degassing tube, (a) can and crimp in the furnace, (b) crimp and can set up on the turntable and (c) hydraulic ram connected to the crimp before the load is applied



Fig. 3.8: Cutting of the crimped degassing tube, (a) before cutting, (b) completed can

3.4 Cold compacting

Cold compacting of the titanium powder was done in a Tangye hydraulic press with a 73 mm die. The inside of the die, the plug and the ram were coated with zinc stearate lubricant. Approximately 500 g of titanium powder was poured into the die and tapped until no further reduction in powder height was observed and then compacted to 320 MPa which achieved an approximate density of 76%. A photograph of the compacting equipment is shown in Fig. 3.9



Fig. 3.9: Tangye compaction equipment (i) ram, (ii) die, (iii) metal powder and (iv) example of powder compact

3.5 Consolidation routes

3.5.1 Hot Isostatic Pressing (HIP'ing)

The cans of HDH titanium powder were HIP'ed at 920°C for 4 hours, at a heating rate of 9°C/min and a cooling rate of approximately 10°C/min to 300°C when the can was removed from the furnace and allowed to air cool. The chamber was first evacuated and purged with argon prior to HIP'ing in order to minimise reactions with the can.

3.5.2 Direct Particle Extrusion

Extrusion of both titanium powder and the titanium composites were done on a 5 MN Enefco hydraulic press mounted vertically over an accessible pit. The driving software allowed variation of the extrusion speed and discard length as well as data logging of the extrusion pressure and displacement. A photograph of the extrusion press used throughtout the experimental work is shown in Fig. 3.10.



Fig. 3.10: Enefco extrusion press

The billets were coated in Achesons Deltaglaze 3418 and allowed to dry prior to heating to prevent oxidation during billet heating and transfer to the press. The billets were preheated in a furnace at 900°C in the case of the titanium powder and between 900-1060°C for the titanium alloy composites. Transfer to the container took approximately 5 seconds with a further 5 seconds of ram operation before the ram reached the billet and extrusion proceeded. Graphite dag (Acheson Dag 1559) was painted onto the inside of the container lining and the die face to lubricate the billet and the dummy block during the extrusion. A glass pad was placed between the billet and the die, this was to lubricate the billet as it passed though the die. The set up for the extrusion is schematically shown in Fig. 3.11.

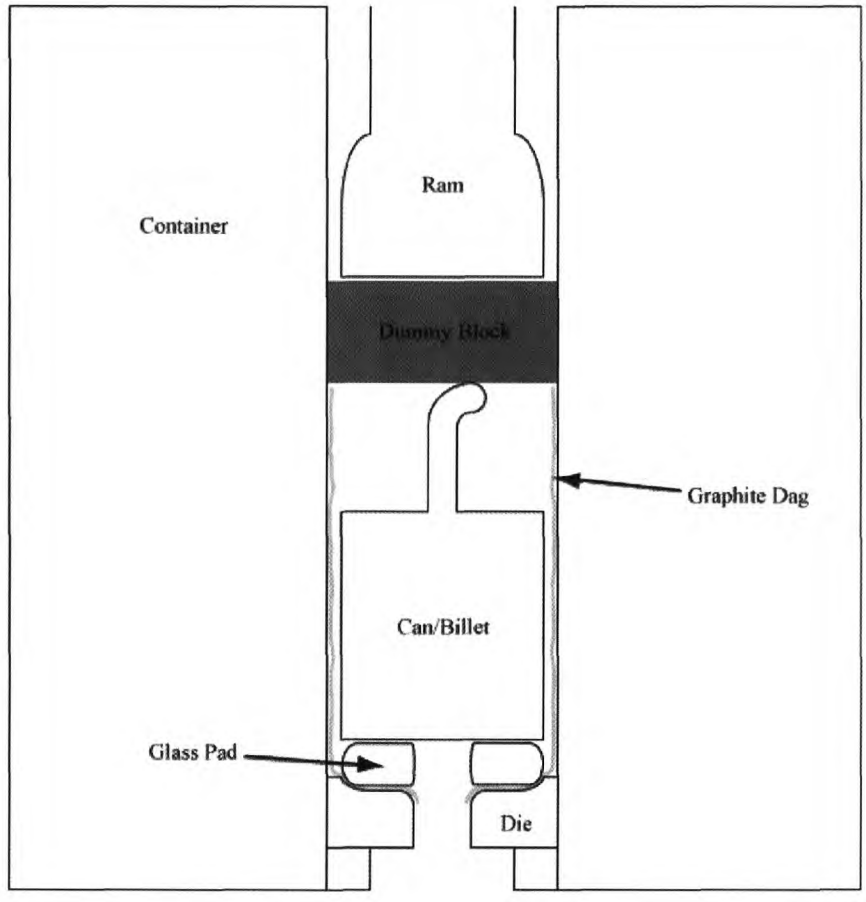


Fig. 3.11: Extrusion set up

The glass pad had an approximate composition of 64% SiO_2, 12% N_2O, 12% CaO, 10% B_2O_3, 1%Al_2O_3, 1% K_2O, as described by Norley [4]. On exiting the press, all extrusions were allowed to air cool.

3.6 Heat Treatments

Samples were coated in Deltaglaze glass lubricant and put into a preheated furnace with an air atmosphere. After the Deltaglaze lubricant was applied, each sample was dried in an oven at 100°C.

3.7 Analytical techniques

3.7.1 Sample Preparation

Samples for light and electron microscopy analysis were sectioned using either a cut-off blade or a Struers accutom (precision cutting machine) and then mounted in bakelite. Samples were ground to 4000 grit using SiC paper and finally polished with OPS, a 0.25 μm colloidal silica suspension.

3.7.2 Optical Microscopy

An Olympus BX51 optical microscope was used throughout the experimental procedure and was performed on both unetched and etched samples. Samples were etched with Kroll's reagent of composition:

2% HF, 5%HNO_3, balance H_2O for 2-5 seconds.

Light micrographs were captured with polarised light and optimised using image analysis software.

3.7.3 Electron Microscopy

Electron microscopy was performed on a JEOL 840 scanning electron microscope or a high resolution LEO field emission gun scanning electron microscope (FEGSEM) operating at 8 kV.

3.7.4 X-ray Diffraction

X-ray diffraction was performed on a Philips PW 1710 diffractometer, using $Cu_k\alpha$ radiation and a Ni filter. The wavelength of the radiation was 1.54055 Å. Typical operating conditions was a 2θ range from 30 - 100°, 0.04 degrees per increment and 5 seconds between each step. Calibration was first performed on a polycrystalline silicon standard. Phase identification employed the used of powder diffraction files from the International Centre for Diffraction Data cards: α-Ti (44-1294), β-Ti (44-1288), TiB_2 (35-741) and TiB (5-0700).

3.7.5 Texture Analysis

X-Ray diffraction to analyse texture was performed on a Philips X'pert MRD diffractometer, using $Cu_k\alpha$ radiation. The wavelength of the radiation was 1.54055 Å. Once texture files for at least three poles were obtained, they were inserted into the program popLA (preferred orientation package - Los Alamos). As the measured pole figures are incomplete, i.e. the scanned angles are only between 0 and 80°, a harmonic analysis was performed in popLa, to fit the remaining data. Once the pole figures were obtained, a WIMV analysis was performed to assign weights to obtain pole figures.

3.8 Mechanical Testing

3.8.1 Tensile Tests

Tensile tests were performed on both extruded and HIP'ed samples on a Zwick/Roell Materialprfung 1474 tensile testing machine. Samples were machined and tested at an initial speed of $5x10^{-4}$ mm/s. The specimen geometry for the canned and extruded Ti HDH tensile specimens is shown in Fig. 3.12.

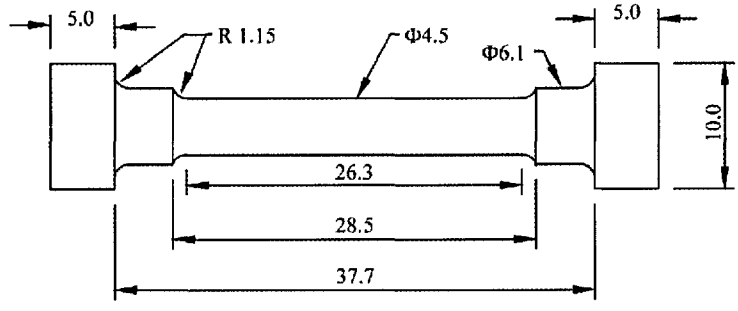


Fig. 3.12: Tensile geometry for No.13's tensile specimens, all units are in mm

The specimen geometry for the compacted and extruded and HIP'ed Ti HDH powder is shown in Fig. 3.13.

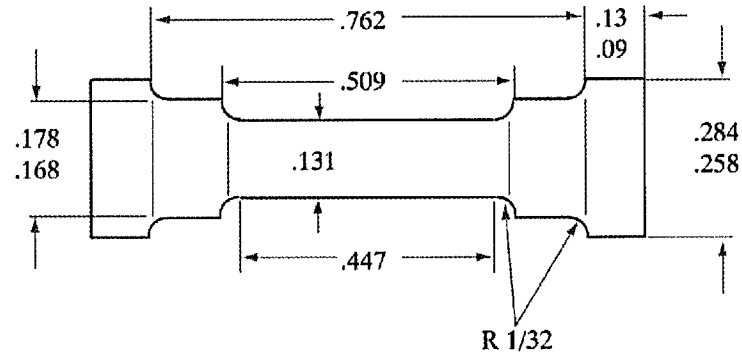


Fig. 3.13: Tensile geometry for No.11's tensile specimens, all units are in inches

3.9 Thermomechanical Processing of Titanium Matrix Composites

3.9.1 Consolidation of Titanium Alloy Composites

The gas atomised (GA) Ti-6Al-4V was blended with 12.8 wt.% TiB_2 and 6.4 wt.% TiH_2 and mechanically alloyed. The resulting powder mass was encapsulated in either stainless steel or mild steel cans and then degassed at 800°C for 2 hours at a heating rate of 10°C/min under a vacuum of approximately $1x10^{-3}$ mbar. Ar was reflowed into the cans before a final cold degas before crimping. The cans were hot isostatically pressed at 920°C for 2 hours to consolidate the powder to the theoretical density of the material. All the Ti-6Al-4V and Ti-6Al-4V-TiB cans were HIP'ed by Bodycote. The billets canned in stainless steel were then heat treated at 1200°C for 4 hours in a vacuum furnace to fully convert the TiB_2 to TiB. The billets were then quenched with a nitrogen blast. The billets canned in mild steel were not conversion heat-treated and were thus left in the as HIP'ed condition. A schematic of the processing route for the composite billets is shown in Fig. 6.1.

3.9.2 Extrusion

The commercial purity (CP) Ti, Ti-6Al-4V and Ti-6Al-4V+TiB composites were extruded under the conditions shown in Table 3.3 using the same techniques described in Section 3.5.2.

Table 3.3: Extrusion conditions for Ti alloy composites

Billet Temperature:	950-1060°C
Loading Time:	50 seconds
Tooling Temperature:	280°C
Ram Speed:	2.5-5 mm/s
Ratio:	14:1

These conditions were chosen as AMC required a final diameter of 20 mm and an exit velocity of approximately 70 mm/s.

3.9.3 Heat Treatments

A conversion heat treatment (CHT) to convert TiB_2 to TiB, post extrusion, was carried out at 1200°C in an argon furnace at a heating rate of 5°C/min with an Ar flow rate of 6 l/min. No Deltaglaze coating was applied to the samples for conversion heat treating.

3.9.4 Mechanical Testing of Ti MMC's

Tensile testing was carried out by AMC using their in-house sample geometry, shown in Fig. 3.14.

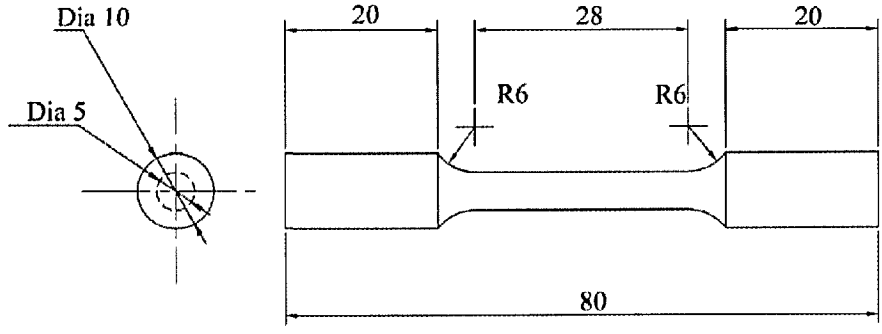


Fig. 3.14: Tensile geometry for AMC specimens, all units are in mm

3.10 Finite Element Analysis

Modelling of the extrusion process using a range of processing conditions was performed with the commercial finite element package Forge 2005, developed by Transvalor, France.

3.10.1 Compression Testing

In order to obtain rheology data for the physical properties inputs for Forge 2005, compression tests were performed on Ti HDH, extruded at a reduction ratio of 9:1. Compression samples of dimensions 10 mm high by 8 mm in diameter were tested using a servo-hydraulic Mayes machine with an infra red (IR) furnace attached. Compression tests were performed at temperatures ranging from 700 to 900°C and at strain rates from $5x10^{-2}$ to 5 s^{-1}. The heating rate for the samples was 25°C/min with a 100 N pinch load and with a 5 minute dwell time at temperature before the test was started.

3.10.2 Pre-Processing

In order to run a simulation, there are several required inputs defining the starting material, rheology data for the material, thermal data relating to the material, tooling and tooling/material interface, frictional behaviour at the material/tooling interface [78]. The thermal input parameters are shown in Table 3.4.

Table 3.4: Input parameters for Forge 2005

Thermal Property	Value	Units	Source
Density	4510	Kgm^{-1}	[79]
Tresca Friction	0.2	-	[80]
Specific Heat Capacity	600	$Jkg^{-1}K^{-1}$	[79]
Thermal Conductivity	20	$Wm^{-1}K^{-1}$	[79]
Heat Transfer Coefficient	7500	$Wm^{-2}K^{-1}$	[81]
Material Emissivity	0.3	-	[82]

Chapter 4

The Consolidation of Canned Ti Powder

4.1 Summary

In this chapter, the degassing of Ti powder is presented and the optimum degassing conditions established. The degassing of three different chlorides which are potential contaminants from three different metal reduction processes are also analysed. The extrusion of canned and degassed Ti powder is considered in terms of the pressure-displacement curves with reference to the extrusion length. The effects of degassing conditions on the porosity, microstructure and mechanical properties of extruded Ti powder are also discussed. A can of Ti powder was also manufactured for hot isostatic pressing as a comparison.

4.2 Characterisation of Ti Powder

The particle size distribution of the Ti HDH powder is shown in Fig. 3.1 . The particle size of the powder varies from approximately 1000 μm to less than 100 μm. The majority of the powder, however, is in the size range 900 μm to 200 μm. The average particle size (at 50% percentage undersize) is 400 μm. The broad particle size range of this powder is beneficial for the packing properties as small particles can fit between the larger particles. Secondary electron images (SEI) of the Ti HDH powder are shown in Fig. 4.1.

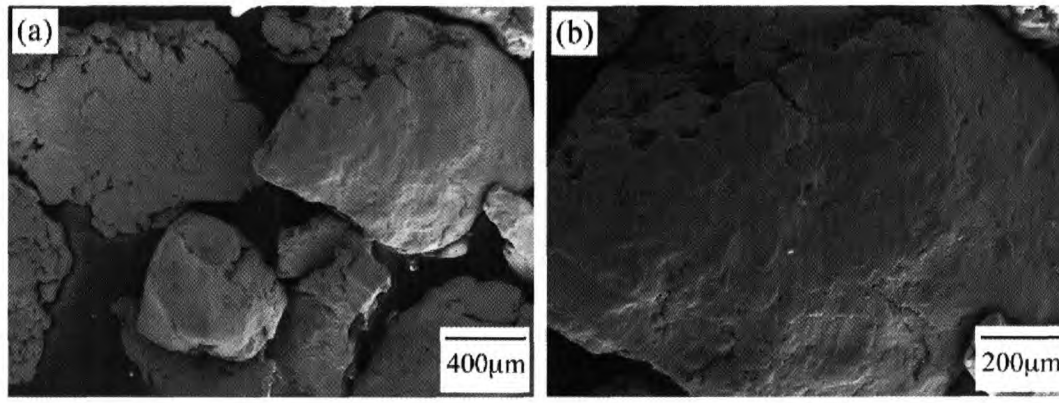


Fig. 4.1: Secondary electron images of the Ti HDH powder, (a) x50 magnification, indicating the angular morphology and (b) x160 magnification, showing the powder surface

From the secondary electron images in Fig. 4.1 it can be seen that HDH powder has an angular shape but with a smooth surface topography. The angular shape of the powder enhances the interlocking capabilities of the material. However, on the downside, packing and flow properties are inferior to spherical powders. The shape of this Ti powder is characteristic of Ti HDH powder. The chemical composition of the Ti HDH powder is shown in Table 4.1.

Table 4.1: Elemental analysis of HDH powders

Element	Composition, wt.%
Fe	0.35
Cr	0.05
Mg	0.033
N	240 ppm
O	1300 ppm
H	65 ppm
Cl	<0.005

All values are in wt.% unless otherwise stated.

Chemical analysis of the Ti HDH powder, Table 4.1, indicates that the powder has a high iron content, which is considerably higher than would be expected for a commercial purity (CP) Ti grade 1 alloy and also much higher than for Kroll sponge, which is approximately 0.04-0.10 wt.% [1]. The oxygen content is also higher than expected. The high oxygen content of the Ti HDH powder is inherent of to the hydride-dehydride manufacturing process. The powder is heated up under a positive pressure of H to form TiH_2, and then degassed to remove the H from the Ti. Heating the powder in

such an atmosphere enables any residual oxygen around the powder to be absorbed into the powder and thus, increase the oxygen content of the powder. The HDH process is reviewed in Section 2.2.2. All the other elements are within the allowable range for a grade 1 CP alloy [21].

Table 4.2: Chemical analysis for different size fractions of Ti HDH powder

Size Fraction	-2000+1000	-800+710	-500+400
Element	Large	Medium	Small
O, ppm	1600	1400	1800
N, ppm	350	50	400
H, ppm	67	69	73

The oxygen content of the different powder sizes do not vary significantly and are all below the allowable limit for CP Ti grade 1 alloys. The nitrogen content does not vary significantly, and it is believed that the value low value of 0.005 wt.% for the medium size fraction is an anomalous reading from the analysis which does not reflect the value of the nitrogen content in the powder. There is no explanation as to why the medium sized powder would have a significantly lower nitrogen content compared with the other size fractions. There is a slight increase (5%) in the hydrogen content of the material as the material decreases in size. This is most likely due to the initial starting grain size. The surface area of smaller particles is greater than the larger particles and as the powder size reflects the initial starting grain size, so there will be more hydrogen absorbed per surface area for smaller particles than for larger particles. The increase in hydrogen content with smaller particle sizes is not significant as all the values are all less than the maximum hydrogen content for CP Ti alloys.

4.3 Degassing Trials

Degassing trials were performed on canned Ti powder. Photographs of the experimental procedure for canning and degassing are shown in Section 3.3. Ti HDH powder was placed in a small mild steel can for the degassing trials. The powder was held at temperature for 1 hour. For degassing larger amounts of powder, the can was held at temperature for 2 hours.

Two different kinds of pumps were used to achieve a vacuum in the can: a rotary and diffusion pump. The rotary pump provided a vacuum of approximately 10^{-1} mbar and the diffusion pump generated a pressure of approximately 10^{-6} mbar; thus five orders of magnitude difference in generated pressure exists between the two types of pump used

in this study.

Before degassing, Ar was flowed over the Ti powder three times for 1 minute, to displace any air that was in the can. The Ar was first purified and dehydrated by passing the Ar over a molecular sieve and secondly by passing over hot Ti swarf to remove residual oxygen that may be in the Ar supply. Runs 7 to 9, $MgCl_2$, $CaCl_2$ and NaCl, respectively, were deliberately added to the Ti powder to determine whether these chlorides could be removed from the powder. All the degassing runs are detailed in Table 4.3.

Table 4.3: Degassing runs information

Run No.	Degassing Temperature, °C	Heating Rate, °Cmin^{-1}	Pump Type rotary/diff.	Final Pressure, mbar
1	Room Temp	-	rotary/diff	5x10^{-5}
2	110	3	rotary/diff	5x10^{-5}
3	300	3	rotary/diff	5x10^{-5}
4	500	3	rotary/diff	5x10^{-5}
5	500	25	rotary/diff	5x10^{-5}
6	700	3	rotary/diff	5x10^{-5}
7	700	3	rotary/diff	5x10^{-5}
8	700	3	rotary/diff	5x10^{-5}
9	700	3	rotary/diff	5x10^{-5}

An oxygen analysis was obtained for all degassing runs as well as a nitrogen and hydrogen analysis for runs 1 to 6. The results of runs 1-6 and 7-10 are shown in Table 4.4 and 4.5, respectively.

4.3.1 Effect of Temperature on Degassing

The pressure in the can, degassed (for extrusion) at 500°C, was monitored in order to ascertain at which temperatures degassing events occurred. The pressure-time graph is shown in Fig. 4.2.

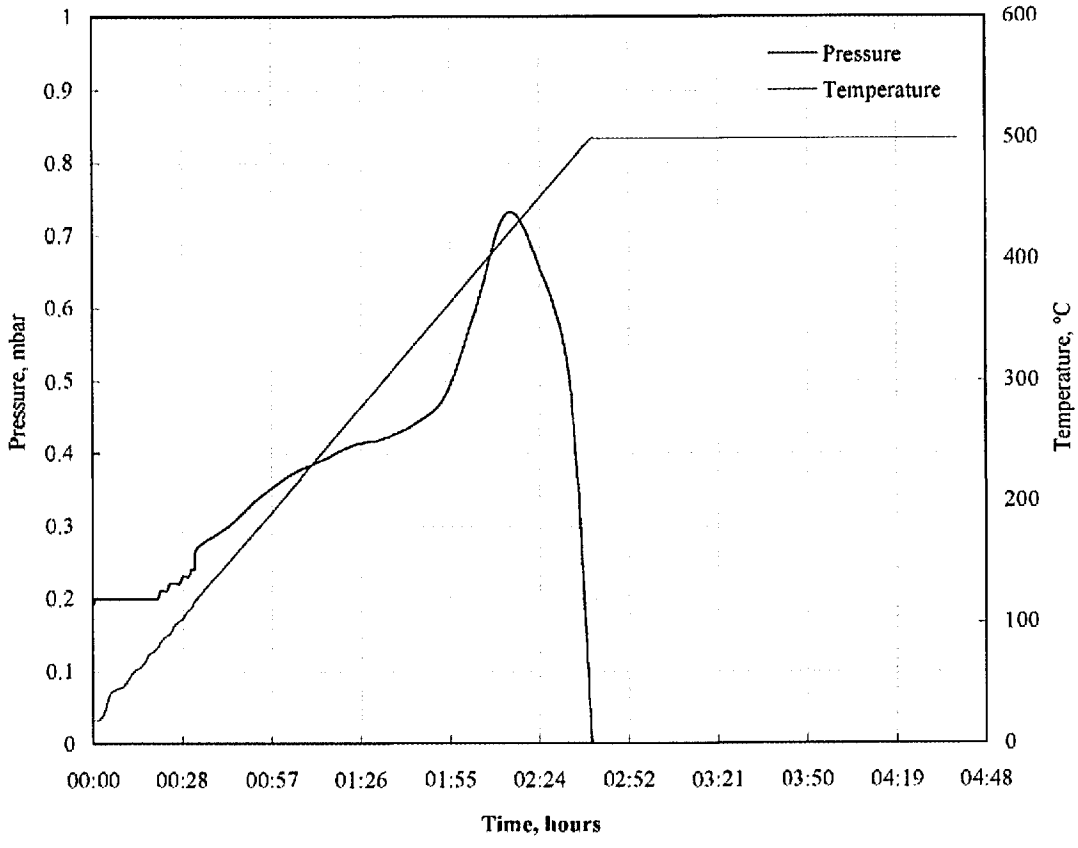


Fig. 4.2: Pressure tracking during degassing at 500°C prior to extrusion

From 20°C to approximately 80°C, there is no change in pressure inside the can, which remains at 0.2 bar. As the can is heated up, there is an increase in the pressure beginning at 80°C to 0.45 bar. This increase in pressure is believed to be due to H_2O being driven off from the surface of powders, as observed previously by Lee and Peters [67]. The pressure begins to steady off at 230°C as the majority of the H_2O has been driven off. At 270°C the pressure increases again up to 0.73 bar, most likely due to compounds, such as $Ti(OH)_2$ disassociating into Ti and H_2O [67]. The pressure in the can peaks at 480°C. As the can is continuously heated from room temperature, there are likely to be temperature gradients in the can, so reactions occur over a broad temperature range. The temperature gradients are exacerbated by the poor thermal conductivity of Ti and the vacuum generated in the can, both of which reduce the overall thermal conductivity of the canned powder. At 500°C, there is a marked drop in the pressure when the diffusion pump is switched on, down to $4x10^{-6}$ mbar. Any interstitial contamination of the powder is likely to be picked up during the heating stage.

Table 4.4: Chemical analysis of Ti HDH powder degassed at various temperatures

Run No.	Degassing Temperature, °C	Heating Rate, °Cmin^{-1}	O ppm	N ppm	H ppm
1	Room Temp	-	1700	340	89
2	110	3	1600	340	54
3	300	3	1600	340	56
4	500	3	2000	500	61
5	500	25	2000	400	57
6	700	3	1900	500	50

Fig. 4.3 shows the oxygen and nitrogen concentration of Ti HDH powder degassed over a range of temperatures.

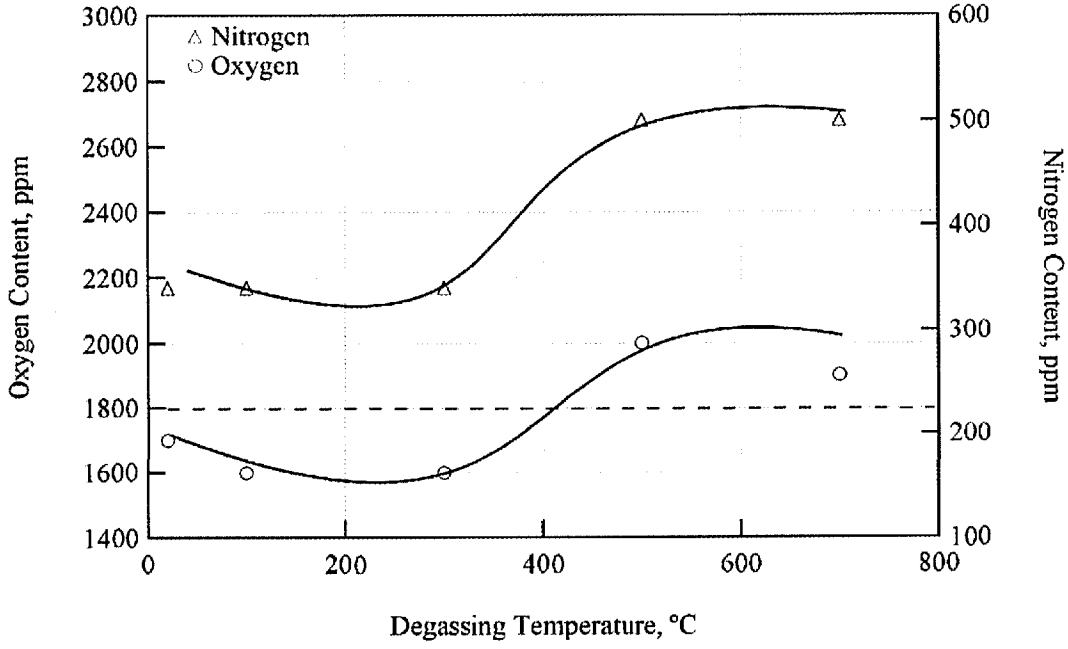


Fig. 4.3: Oxygen and nitrogen content of degassed Ti HDH powder, heated over a range of temperatures at a heating rate of 3°C/min, the dashed line at 1800 ppm indicates the maximum allowable oxygen content for CP Ti grade 1 alloys

Fig. 4.3 shows that the oxygen and nitrogen of Ti powder degassed from room temperature to 700°C. There is a minimum oxygen content at a degassing temperature of 300°C. Above this temperature, there is an increase in the oxygen content of the Ti powder up to 0.20 wt.%. The nitrogen curve shows a similar profile to that of the oxygen, i.e. there is a minimum at 300°C rising to a maximum of 500 ppm at 700°C.

As the can is continuously heated, there is a temperature gradient across the powder

mass. Powder which is at a lower temperature would evolve gases which are absorbed by powder at higher temperatures in the can. At a degassing temperature of 300°C, recombination of evolved gases is unlikely as diffusion in Ti is extremely slow at temperatures below 550°C, so it is postulated that there is time for the evolved gases to be drawn out of the can rather than being adsorbed into the powder. Degassing Ti powder at higher temperatures shows an increase in the oxygen content due to recombination of evolved gases. The maximum oxygen pick up, however, is still only 400 ppm.

The maximum oxygen content for Ti grade 1 commercial purity alloys is 1800 ppm. Degassing Ti HDH powder above 300°C shifts the oxygen content to above the maximum oxygen content for CP Ti grade 1 alloys. It is extremely important to limit the oxygen pick-up during degassing as a small contamination can have a dramatic effect on the mechanical properties of the final product, as illustrated on Table 2.2 on page 26. Also, further downstream processing of the powder will inevitably lead to additional oxygen pick up. The nitrogen content of the degassed Ti powder shows a similar trend to oxygen, but several orders of magnitude lower than oxygen, due to the significantly lower diffusion coefficient of nitrogen compared with oxygen in Ti [32], Section 2.1.4. Though nitrogen has a greater effect on the properties of Ti, limiting the oxygen pick up is more important, as oxygen contamination is far more prevalent in Ti than nitrogen.

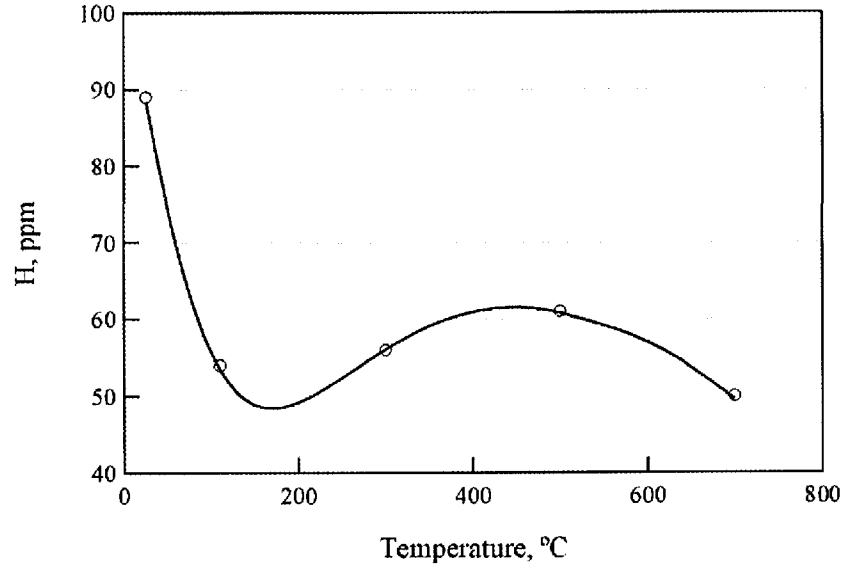


Fig. 4.4: Hydrogen content of Ti HDH powder, degassed over a range of temperatures

The hydrogen content of the powder decreases as the degassing temperature increases from 89 ppm at room temperature to 50 ppm at 700°C. There is a small increase in the hydrogen concentration at 500°C, most likely due to the reaction:

$$Ti + H_2 \rightarrow Ti(H) \tag{4.1}$$

At higher temperatures, the hydrogen content decreases again, due to the de-hydration process:

$$Ti(H) \rightarrow Ti + H_2 \tag{4.2}$$

which is known to occur above 600°C. It is encouraging that the hydrogen content is substantially less than the maximum content allowed for all CP Ti grade alloys when degassing within this temperature range.

From the result in Table 4.4, the heating rate does not effect the interstitial content after canning at a final degassing temperature of 500°C. This is most likely due to the small quantities of powder being degassed for these trials. It is believed that it is still necessary to limit the heating rate of large powder masses to approximately 3°C/min to minimise the temperature gradients across the canned powder and limit re-absorption of interstitial elements from low to high temperature powders.

From the data presented in Fig. 4.3 and 4.4, it is clear that the optimum degassing temperature for Ti HDH powder is 300°C, so as to avoid oxygen contamination by re-absorption, as well as having an acceptably low hydrogen content. It is clear that degassing procedures need to be optimised for each particular powder type and mix of powders.

The smaller the particle size, the greater the surface area of the powder and therefore more absorption is likely to occur. The particle size of the Ti HDH powder is relatively coarse compared to gas atomised powder, which is approximately 100-200 μm in diameter, and thus, the latter is likely to have increased oxygen contamination during a degassing procedure. It is also important to consider the mean free path of the gases during evolution from powder surfaces and the can. Smaller powders will pack to a greater density and so the mean free path of the evolved gases will be more tortuous compared to coarser particles. This is an important consideration in determining the time at temperature and the heating rate, especially when degassing large quantities of powder on an industrial scale.

It would be beneficial to determine the effect of degassing on the different particles sizes. This could be achieved by degassing a powder mass and then sieving the powder into its constituent size fractions. Also, sieving the powder prior to degassing would reveal the effect of the particle size on the degassing temperature.

4.3.2 Deliberate Chloride Additions

In the Kroll process, Mg is reacted with $TiCl_4$ to form Ti and $MgCl_2$, as stated in Equ. 2.2, and so there is likely to be residual $MgCl_2$, this is distilled off at approximately

800°C. In other reduction processes, the Ti metal is subjected to other metal halides, which could potentially contaminate the respective powder products. In order to ascertain the possibility of removing residual chlorides, Ti HDH powder was mixed with three chlorides, which represent three reduction processes, the Kroll process ($MgCl_2$), the Armstrong Process (NaCl) and the FFC Cambridge Process ($CaCl_2$). These processes are reviewed in Section 2.2.2.

Table 4.5 shows the results of degassing Ti powder with deliberate additions of the three different chlorides. One weight percent of each chloride was added to the Ti HDH powder, the ground using a pestle and mortar before mixing in a tumbler. The powder mixture was then degassed at 700°C. This temperature was chosen rather than the optimal temperature of 300°C in order to improve the chances of removing any chloride.

Table 4.5: Remaining chloride content of HDH Ti powder + metal halide, after degassing at 700°C

Run No.	Metal Chloride	Remaining Cl, wt.%	Remaining Cl, % of starting amount
7	$MgCl_2$	0.162	22
8	$CaCl_2$	0.440	68
9	NaCl	0.380	62

Table 4.5 shows that it is possible to remove some of the chloride from the powder surface, however, some residual chloride remains. $MgCl_2$ has 0.162 wt.% Cl remaining, $CaCl_2$ and NaCl have 0.440 and 0.380 wt.% respectively. The differences in the remaining chloride contents are due to the vapour pressures of the metal halides. The vapour pressure of the different metal halides are shown in Fig. 4.5

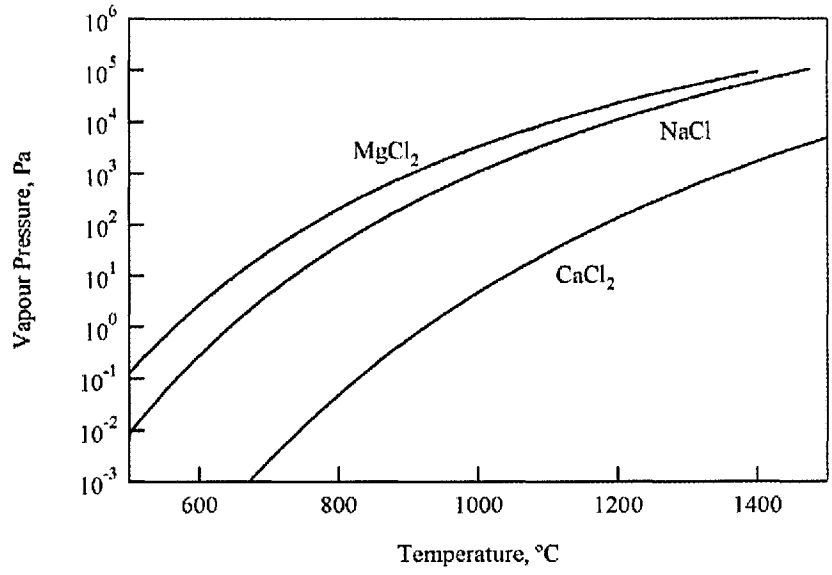


Fig. 4.5: Vapour pressure of $MgCl_2$, NaCl and $CaCl_2$, from data shown in [83]

The data represented in Fig. 4.5 shows the vapour pressures of the three metal halides. The data is only available for the metal halides when they are molten, so the data has been extrapolated to the degassing temperature concerned. Fig. 4.5 shows that $MgCl_2$ has a higher vapour pressure than the other two chlorides, which is why $MgCl_2$ is used in the Kroll process as it is easier to distil off after the reduction, (Equ. 2.2). There is still a considerable amount of $MgCl_2$ remaining in the powder after degassing at 700°C. The likely reason is the comparatively low degassing temperature of 700°C (compared to commercial production processes) and that the titanium/chloride mix was held at temperature for 1 hour (the vacuum distillation during the Kroll process usually takes days to complete). It is unlikely that lower degassing temperatures will remove this amount of metal halide in this short timescale. But, with a high enough vacuum and longer times, it is believed that the $MgCl_2$ would eventually be evolved from the powder surface. The NaCl and $CaCl_2$ have significantly lower vapour pressures than $MgCl_2$ and so, even with a high enough vacuum and degassing temperature, it is unlikely that all the metal halide would be evolved from the powder.

Table 4.6: Melting point and boiling point of $MgCl_2$, NaCl and $CaCl_2$

Metal Halide	Melting Point, °C	Boiling Point, °C
$MgCl_2$	714	1418
NaCl	801	1465
$CaCl_2$	772	>2000

Critically, all the metal halides are still solid at this temperature, this would mean that the metal halides must sublime rather than vapourise at this degassing temperature. The melting and boiling points of the three metal halides are shown in Table 4.6

As a final note, aside from optimising degassing procedures for a particular powder, there is little that can be done to further limit the interstitial pick-up prior to consolidation. Ti powder will absorb moisture and other compounds onto the powder surfaces, even at storage temperatures; so proper storage and handling of any powder is extremely important in any industrial process to limit oxygen contamination.

4.4 Direct Powder Extrusion

Three cans were manufactured for direct powder extrusion to ascertain the effect of degassing temperature on the microstructure and properties of Ti HDH powder. The three degassing temperatures were 500, 700 and 900°C. The cans were filled with 582 grams of Ti powder, which filled the can up to a level just above the lid, so that the powder was just inside the degassing tube. In all three cans, this equated to an apparent density of 80%. The extrusion conditions are shown in Table 4.7.

Table 4.7: Table of extrusion conditions for extrusion of encapsulated Ti HDH powder

Reduction Ratio:	17:1
Extrusion Temperature:	900°C
Extrusion Speed:	7 mms^{-1}
Container Temperature:	350°C

The manufacturing process, developed in-house, is shown in Section 3.3. An example of a can used for extrusion after canning, degassing and crimping is shown in Fig. 4.6.



Fig. 4.6: Canned Ti HDH powder after degassing and crimping, ready for extrusion or HIP'ing

The load-displacement curves obtained from the press were converted to plots of extrusion pressure against displacement, shown in Fig. 4.7.

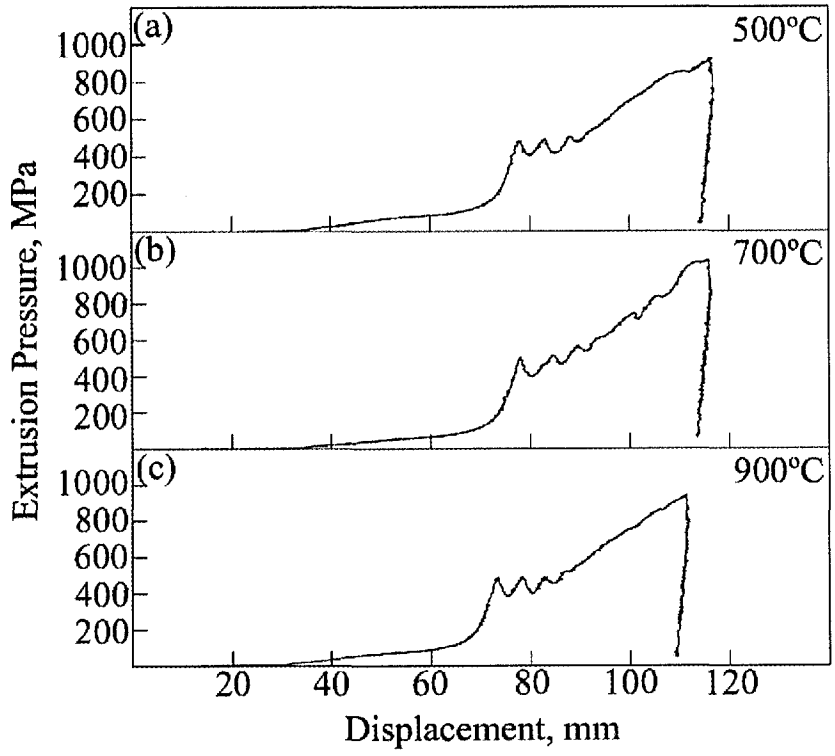


Fig. 4.7: Extrusion pressure curves for the encapsulated cans of Ti HDH powder, degassed at (a) 500°C, (b) 700°C and (c) 900°C

All the extrusions of degassed cans exhibit a breakthough pressure at 480 MPa and have similar extrusion profiles. The general trend of the pressure-displacement curves show an increasing extrusion pressure as the extrusion proceeds. This increase in pressure is a direct result of billet chilling, due to a slow extrusion speed, as illustrated in Fig. 2.18. Billet chilling occurs when the temperature of the billet exceeds the temperature of the container. Heat is transferred to the container down the thermal gradient that exists, the higher the temperature of the billet compared to the container, the larger the thermal gradient and so the quicker the billet chilling. Billet chilling also depends on the interface between the billet and the container. A 'strong' interface means that there is a high heat transfer coefficient, a weak gradient means that there is a low heat transfer coefficient and so billet chilling is reduced. It is thought that the Deltaglaze glass coating acts as a thermal insulator, providing a low heat transfer coefficient. The heat transfer coefficient of Deltaglaze glass is discussed further in Chapter 5.

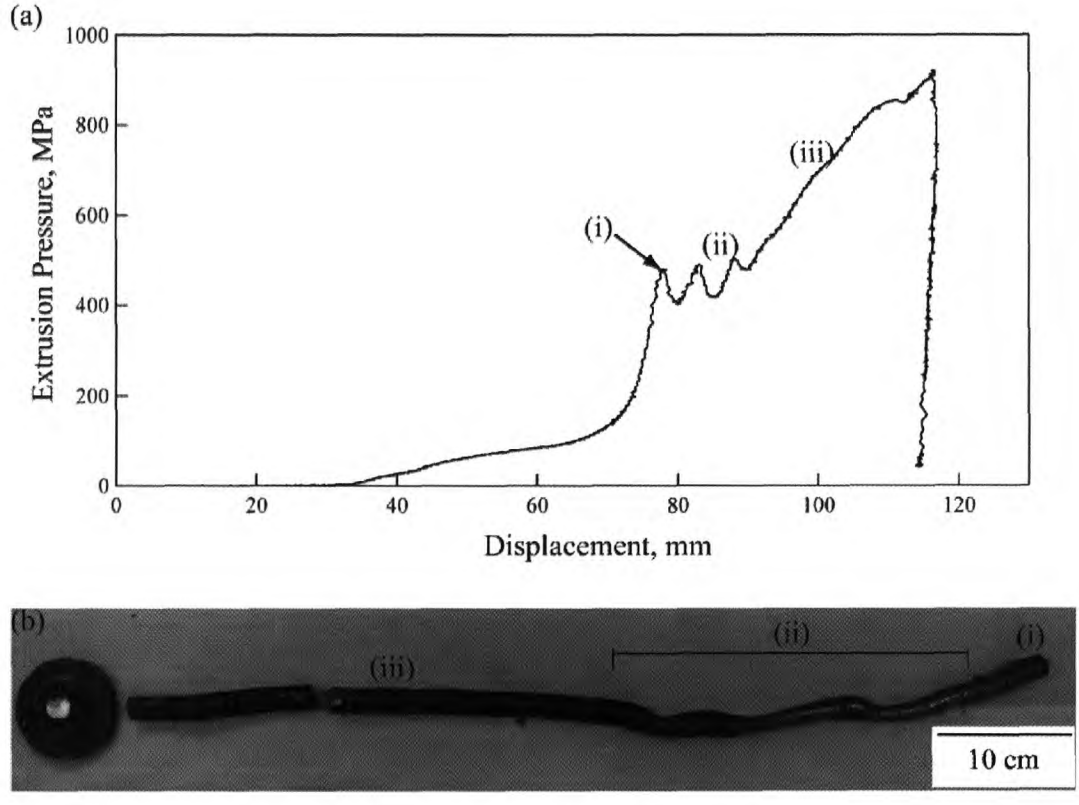


Fig. 4.8: (a) Load displacement profile of Ti HDH powder and (b) corresponding extrusion of canned Ti HDH powder indicating the different regions formed during extrusion

The three regions noted on the extrusion profile in Fig. 4.8(a) are events that correspond to the three regions labelled in the extrusion in Fig. 4.8(b).

All three degassed cans which were extruded show a similar extrusion profile along the length of the extrusion, illustrated in Fig. 4.8(b). The build up in pressure at the start of the extrusion stroke is due to the degassing tube being forced into the can and the compaction of the powder in the can, prior to the front end of the can being forced though the die. This is the upsetting stage, when the billet fills up the die container before the onset of extrusion. When the material reaches the breakthough pressure, the extrusion begins as material is forced though the die, represented as (i) in Fig. 4.8(a). The first part of the billet to enter the die is the region directly in front of the die, as illustrated in in Fig. 2.16.

After the first part of the billet has exited the die, the diameter of the extrusion decreases from the diameter of the die, 20 mm, to between 10 and 18 mm. The front end has been 'punched though' the die and very little deformation has occurred, represented by region (ii) in Fig. 4.8. At this point in the extrusion profile, the pressure fluctuates as the extrusion proceeds. The surface of the front end of the extrusion is uncoated Ti as

canned Ti has perforated though the can, as illustrated in Fig. 4.9(b).

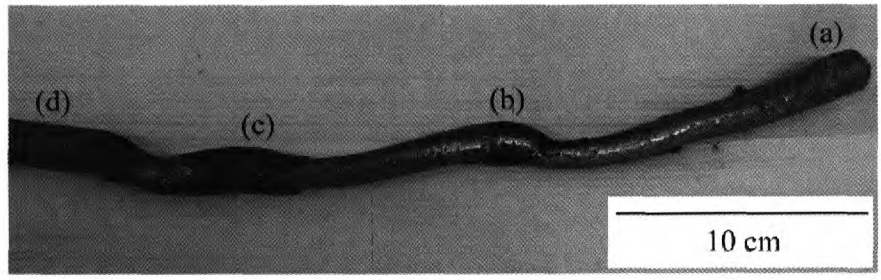


Fig. 4.9: Front end of canned and extruded Ti HDH powder, illustrating the different parts of the front end defect

The extrusion profile increases in diameter from 10 mm to 18 mm in Fig. 4.9(b), and there is no steel on the outside of the extrusion. The diameter decreases again from Fig. 4.9(b) to Fig. 4.9(c). At Fig. 4.9(c), the steel can starts to be extruded, after a third of the length of the extrusion when equilibrium flow is established, represented in Fig.4.9(d). The front end defect that results is due to the lack of shear generated in the Ti HDH powder. As the can passes though the die, the front end experiences little shear deformation as the material has not passed though the deformation zone. Only material that has passed though the deformation zone will have been fully sheared, which is underlined by the observation that the extrusion diameter is less than the die.

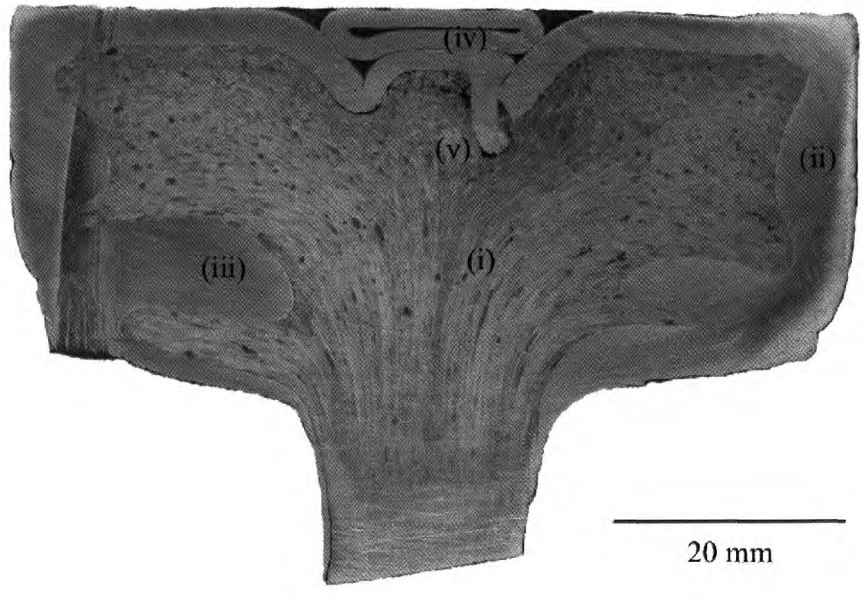


Fig. 4.10: Cross section macrograph of partly extruded discard showing the flow of Ti powder and steel can though the die interface, the five regions are labelled on the figure are referred to in the discussion below

Fig. 4.10 shows a discard from a partial extrusion of canned Ti HDH powder. There are various aspects of the discard which are worth noting with respect to Fig. 4.10. Area (i) shows the flow lines of the Ti powder as it flows though the die. Region (ii) is the steel can, from which some flow into the Ti powder is observed in area (iii), where the edge of the billet is drawn in to the middle of the extrusion and eventually forms the back end defect. The partially extruded can shows the back end defect starting to form even before half the stroke cycle has been completed. The back third of the extrusions showed the back end defect in the extruded Ti powder. The discard for the powder degassed at 500°C, in Fig. 4.11, shows the resultant back end defect and is discussed below. Other interesting features of the partly extruded discard are the degassing tube shown in (iv), which has been deformed in to the Ti and the back of the discard and is starting to show a second back end defect (v).



Fig. 4.11: Cross section macrograph of discard of canned Ti HDH powder extrusion

Fig. 4.11 shows the steel can infiltrating the centre of the Ti powder extrusion. This back end defect was observed in all three cases of canned and extruded Ti HDH powder. A possible way of reducing the back end defect is to extrude the can until the back end defect forms, leaving a large discard, or to cut off the back third of the extrusion. When more than half the extrusion needs to be discarded due to the front end defect and the back end defect, the economics of canned powder extrusion are severely affected.

4.5 Hot Isostatic Pressing

The experimental method for HIP'ing Ti HDH powder canned in mild steel cans is discussed in Section 3.5.1. A photograph of the can before and after HIP'ing is shown in Fig. 4.12.

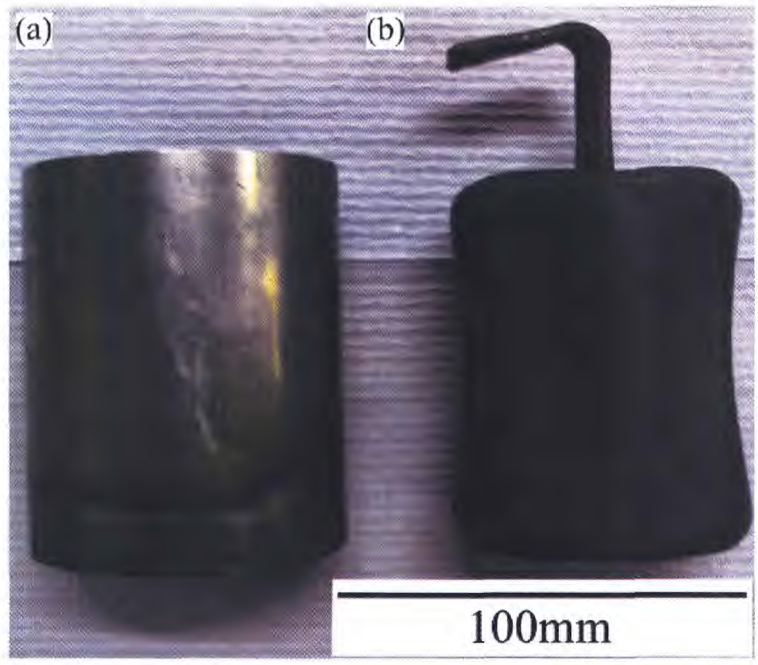


Fig. 4.12: (a) Can before HIP'ing, (b) can after HIP'ing at 920°C for 4 hours

Fig. 4.12 shows a comparison between an undeformed can, Fig. 4.12(a) and a can after HIP'ing, Fig. 4.12(b). From observation of the can in Fig. 4.12(b), it is clear that the deformation is not completely isostatic. There is limited deformation around the welds at the top and bottom of the can which creates a 'tree trunk' effect around the circumference of the HIP'ed can. Though the process is isostatic, deformation is rarely uniform due to the design of the can. Radial deformation in a can is greater than the axial deformation due to can shielding [84].

$$\sigma_{rr} > \sigma_{zz} \tag{4.3}$$

Furthermore, the can did not leak during the deformation process, indicating that the in-house developed canning/crimping process is a suitable process for canning Ti HDH powder for a non-melt consolidation process.

4.6 Consolidation of Canned Ti Powder

A powder product that is completely consolidated has formed metallurgical bonds at the prior particle boundaries. Even though the powder has been consolidated, there is still likely to be evidence of prior particle boundaries, as these would form new grain boundaries. Ultimately, proof of consolidation must come down to a microstructural analysis, and more importantly, the mechanical properties of the consolidated product. The porosity of the consolidated products is discussed in Section 4.6.1, microstructural

analysis of the extruded Ti HDH powder in Section 4.6.2 and the mechanical properties in Section 4.6.3. An image of an extruded structure of Ti HDH powder consolidated by direct powder extrusion is shown in Fig. 4.13.

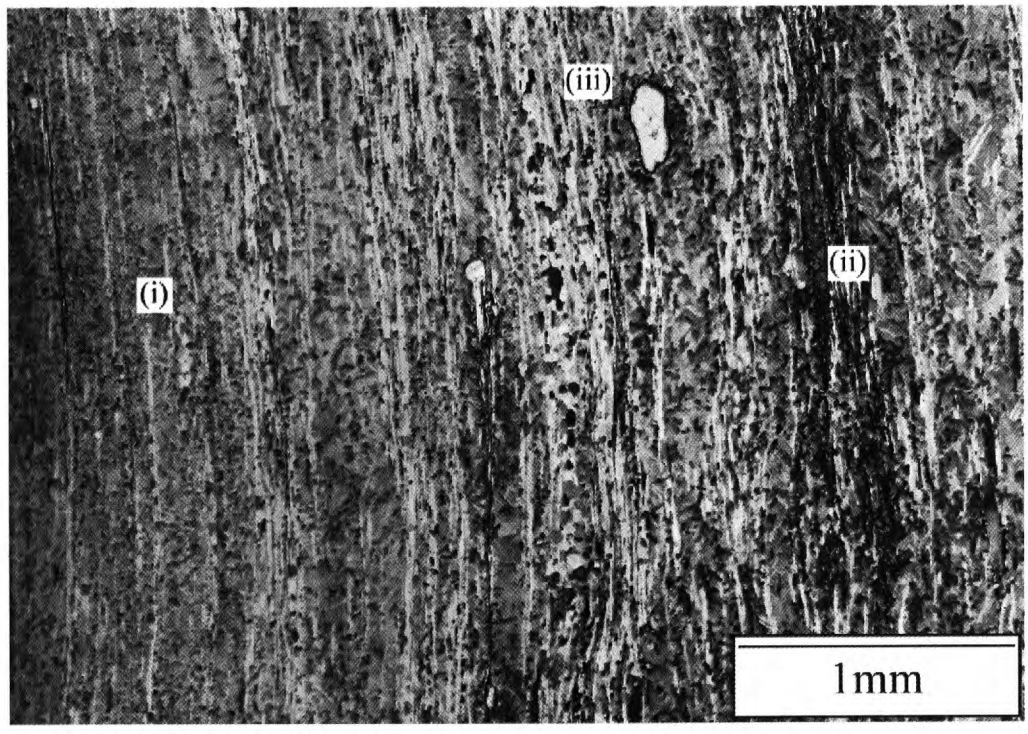


Fig. 4.13: Light micrograph illustrating an example of consolidated Ti HDH powder, region (i) equiaxed grains near the edge of the sample, region (ii) elongated grains towards the middle of the extrusion, region (iii) foreign particle

4.6.1 Analysis of Porosity in Consolidated Ti Powder

The porosity of each Ti HDH extrusion, degassed at various temperatures, is shown in Fig. 4.14(a-c), along with the corresponding image analysis of the porosity, Fig. 4.14(d-f). Each image of the porosity was taken from the middle of the extrusion after the material has reached equilibrium flow, i.e. from region (iii) in Fig. 4.8. The image analysis was performed using the software ImageJ. A threshold was taken for each image and an analysis performed on the thresholded image to determine the volume fraction of porosity and the average size of the pores.

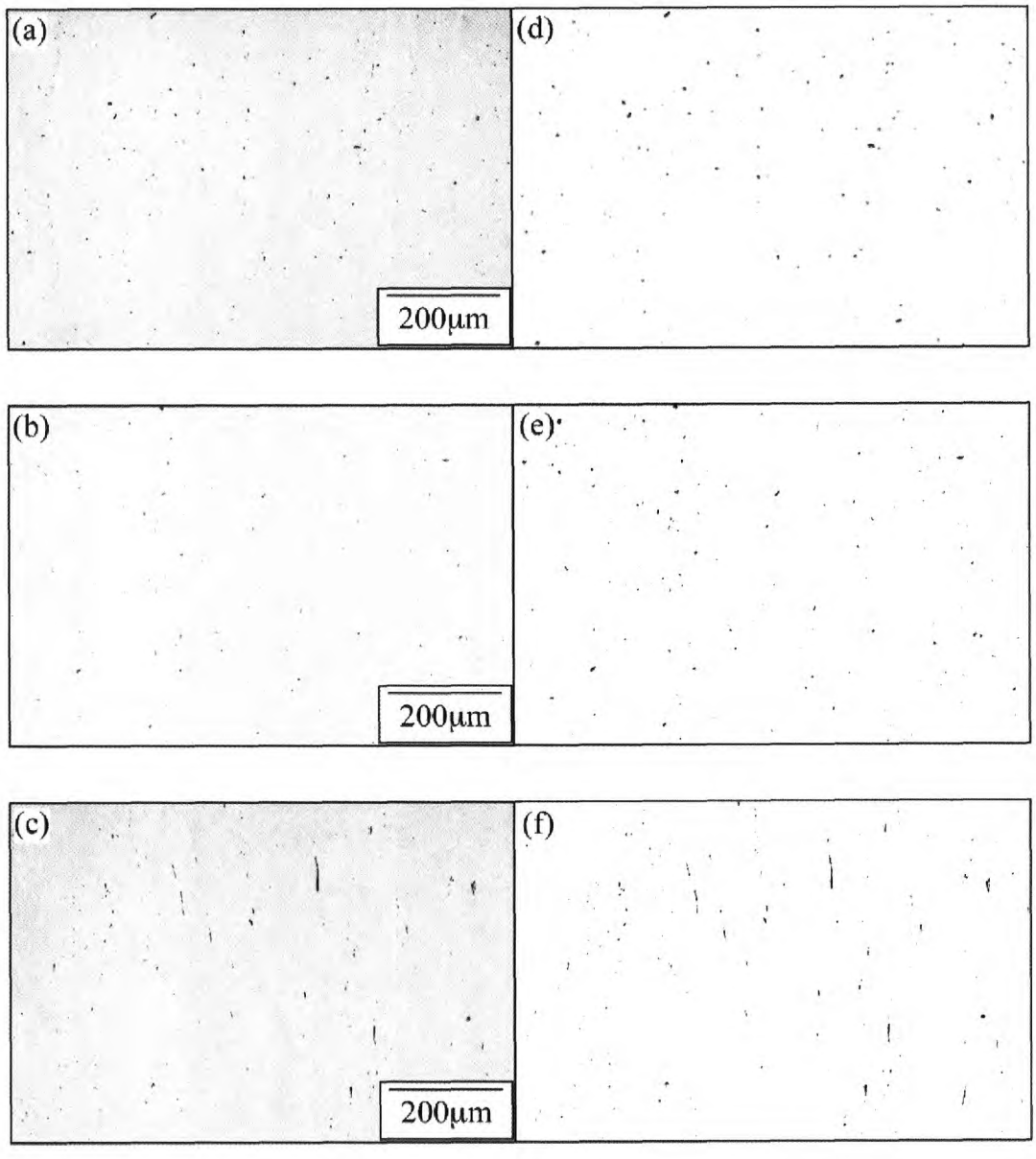


Fig. 4.14: Porosity distribution of degassed and extruded Ti HDH powder, (a) 900°C, (b) 700°C, (c) 500°C, corresponding image analysis of porosity (d) 900°C, (e) 700°C, (f) 500°C

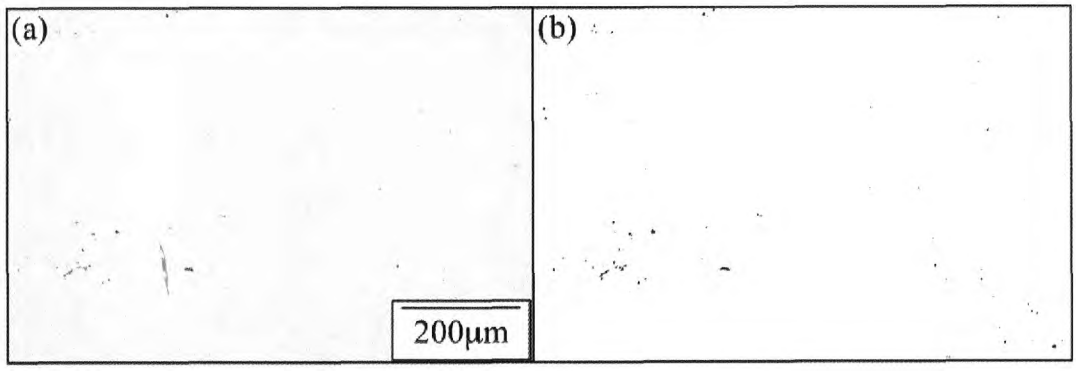


Fig. 4.15: (a) Porosity in canned, degassed and HIP'ed Ti HDH powder and (b) corresponding image analysis

The percentage porosity of each degassed and extruded can is shown in Table 4.8, along with the porosity of the HIP'ed Ti powder.

Table 4.8: Percentage porosity of extruded and HIP'ed Ti HDH powders

Degassing Temperature, °C	Process	Area Analysed, μm^2	Area Fraction Porosity	No. Pores	Average Porosity Size, μm^2
900	Extrusion	1174	0.22	240	4.893
700	Extrusion	1076	0.20	262	4.106
500	Extrusion	1246	0.23	328	3.800
300	HIP	361	0.084	107	1.435

The density of the extruded Ti powder is 99.8% for all the degassed and extruded samples. The HIP'ed billet has a density greater than 99.9%. It is clear that HIP'ing densifies the Ti powder to a greater degree than direct powder extrusion, when extruded at a ratio of 17:1. When powder is forced though the die, the powder particles weld, break and re-weld to form coherent metallurgical bonds and the porosity between the particles has effectively disappeared. HIP'ing reduces the porosity to less than 0.1%. It is extremely difficult to completely remove all porosity from a consolidated powder compact as the majority of densification that occurs during HIP'ing is from the rearrangement and localised plastic deformation stages of consolidation, reviewed in Section 2.4 on page 41. The majority of densification that occurs above approximately 99% is due to creep mechanisms and diffusion of atoms rather than plastic deformation. HIP'ing Ti HDH powder for 4 hours at 920°C almost completely removes porosity from the powder. HIP'ing Ti HDH powder for 2 hours at 920°C would most likely mean a greater degree

of porosity in the billet, though not proven here. HIP'ing is a process for which the majority of uses is to decrease the porosity in wrought products, though this does not completely eliminate porosity, it decreases the size of and distribution of the pores and improves fatigue properties.

The average pore size in the extruded sections, is 4.3 μm^2, which is significantly larger than the pore size in the HIP'ed material, which has a value of 1.4 μm^2. In terms of the consolidation of the material, HIP'ing consolidates Ti HDH powder to a greater extent than extrusion with a reduction ratio of 17:1. However, it is envisaged that extruding to a larger reduction ratio would decrease both the porosity distribution and size of the pores.

4.6.2 Microstructural Analysis of Consolidated Ti Powder

4.6.2.1 Microstructure of Ti HDH Consolidated *via* Extrusion and HIP'ing

Optical microscopy was performed on all the degassed and extruded Ti HDH powders, shown in Fig. 4.16.

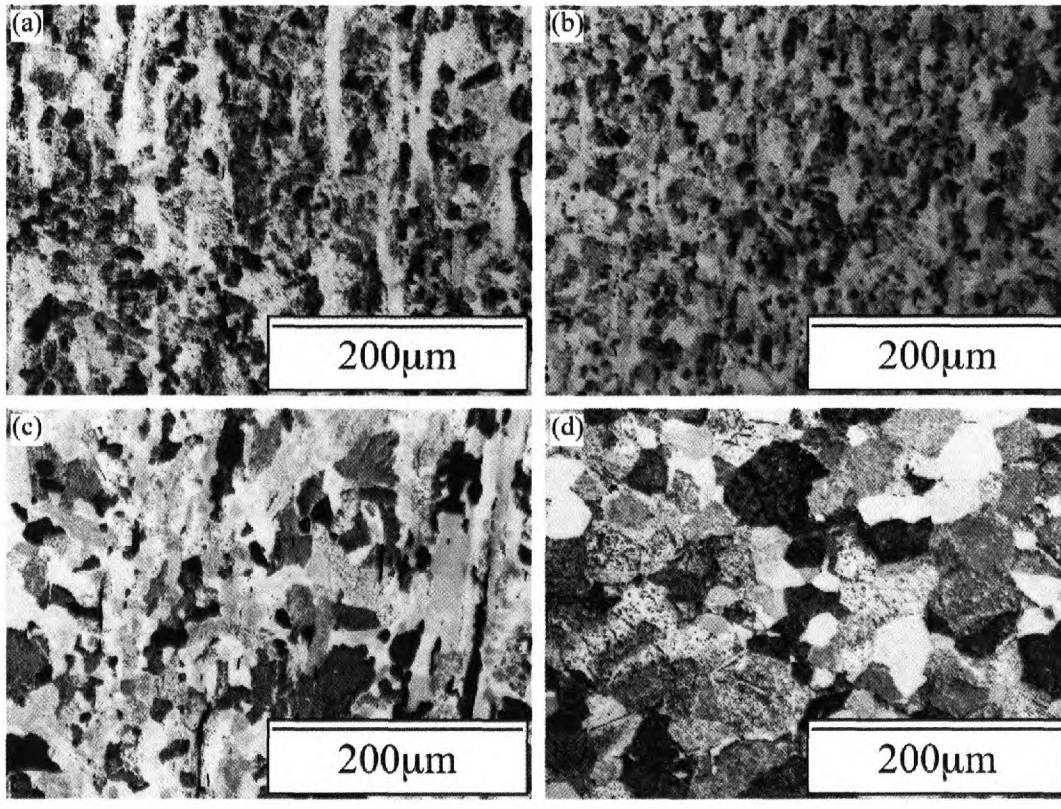


Fig. 4.16: Light micrographs of canned, degassed and extruded Ti HDH powder, degassed at (a) 500°C, (b) 700°C, (c) 900°C and (d) degassed at 300°C and HIP'ed at 920°C for 4 hours

Fig. 4.16(a-c) shows representative microstructures of Ti HDH powder degassed and extruded at 500°C (Fig. 4.16(a)), 700°C (Fig 4.16(b)) and 900°C (Fig. 4.16(c)). Fig. 4.16(d) shows the microstructure of Ti HDH powder degassed at 300°C and consolidated by HIP'ing at 920°C for 4 hours. The different microstructures observed in the extruded sections were observed in each sample, and the microstructures shown in Fig. 4.16(a-c) are representative of all the degassing conditions. In some regions of samples from all the degassing conditions, grains were elongated in the extrusion direction, other areas produced more equiaxed grains. Fig. 4.16(c) shows both elongated and equiaxed grains. From Fig. 4.16(a-c), it is believed that the degassing temperature does not affect the microstructure of consolidated Ti HDH powder. The average grain size in the consolidated powder which was originally degassed at 900°C is slightly larger than the material originally degassed at either 500 or 700°C, this is most likely due to the higher temperature soak, which enables for some grain growth to occur within grains in the powder particles. In all the extruded samples, the grains have either recrystallised or have partially recrystallised.

Fig. 4.16(d) shows the microstructure of Ti HDH powder degassed at 300°C followed by HIP'ing at 920°C. There are two differences between material that was extruded and HIP'ed. Firstly, the grains are all equaixed in the HIP'ed sample, as the material has not been extruded, which is to be expected. Secondly, the grain size in the HIP'ed is larger than the extruded material. Grain growth is is more prevalent in the β phase than in the α phase due to the increased self diffusion of the β phase. The β transus for CP-Ti alloys is approximately 915°C due to the increased interstitial content of CP-Ti alloys over 'pure'-Ti. The Ti HDH powder was HIP'ed at 920°C, which is just above the β transus, and so grain growth is expected. Although the β transus of these materials has not been established, it is thought that the powder was just above the β transus during HIP'ing. However, the growth is limited by the presence of grain boundary β that is present in most CP-Ti alloys. Grain boundary β is present due to the reasonably high Fe content in the powder which is rejected by the α to form β.

The temperature chosen for HIP'ing Ti HDH powder was based upon the temperature used for HIP'ing Ti-6Al-4V, which is 920°C as this provides approximately 50% α phase and 50% β phase. For CP-Ti grades, 920°C is just above the β transus, and so grain growth could occur. Though, consolidating in the β phase would be more beneficial as self diffusion in the β phase is considerably higher than the α phase.

4.6.2.2 Foreign Particles within the Powder

As can been seen in Fig. 4.17, foreign particles were observed in the consolidated Ti HDH powder. These particles were observed in all cases of consolidated powder and across the entire cross section of the consolidated Ti HDH powder. It is clear that the particles effect the microstructure of the consolidated Ti HDH powder. Acicular laths of α are observed emanating from the particle, indicating that there are β stabilising elements diffusing from the particle. It is believe that these particles were present in the as-recieved powder.

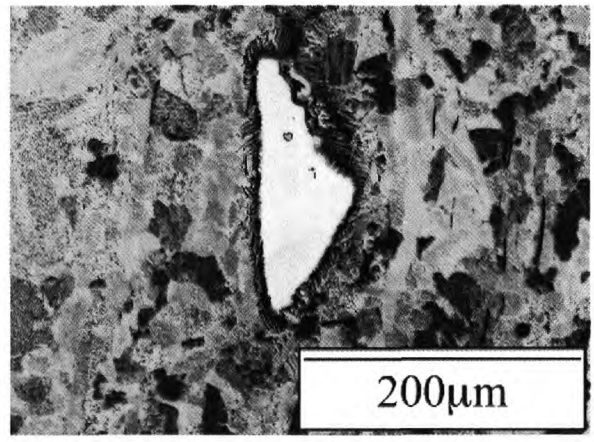


Fig. 4.17: Light micrograph illustrating iron rich foreign particle in the consolidated Ti HDH powder

In order to ascertain the composition of the foreign particle, chemical analysis was performed on the electron microscope, the X-ray energy dispersive spectroscopy (X-EDX) results for the particles are shown in Table 4.9.

Table 4.9: Chemical composition of foreign particle in the Ti HDH powder

Element	wt.%
Fe	4.40
Ti	94.23
Cr	0.45
Ni	0.92

An X-EDX scan of areas that did not contain such particles gave a 100% Ti composition. Clearly, a certain proportion of the powder particles have been contaminated by mainly Fe, but also Cr and Ni. It is thought that this contamination originates from the HDH

manufacturing process and not from the mild steel can or the Kroll reactor lining. During the HDH process, the powder mass is infused with hydrogen to form TiH_2 which is then easily pulverised. It is thought that the contamination is from this crushing/milling process when the powder is milled.

4.6.2.3 Oxygen Analysis on Extruded Canned Ti

An oxygen analysis was performed on the extrusion which was degassed at 500°C, extruded with a reduction ratio of 17:1. The oxygen content of this material was 1563 ppm, which is an average of three readings taken. It is clear that there is no pick up during the preheating prior to extrusion and as the Ti is canned, there is no pick up after the material has exited the die. It is encouraging that there is no oxygen pick up during the consolidation of canned titanium powder.

4.6.2.4 Interface with the Can

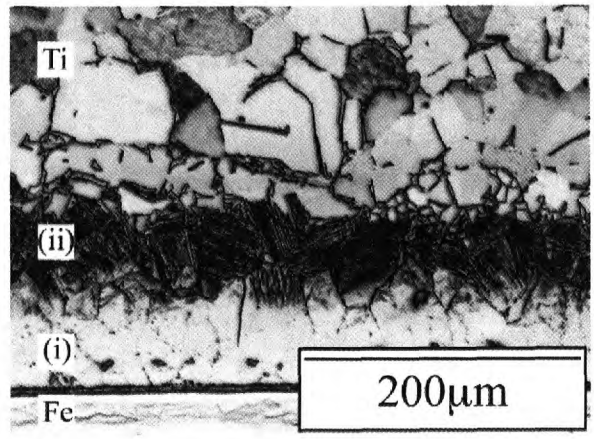


Fig. 4.18: Light micrograph of the interface between the mild steel can and the Ti HDH powder, after HIP'ing at 920°C for 4 hours

Fig. 4.18 shows the interface between the consolidated Ti and the mild steel can when HIP'ed at 920°C for 4 hours. Clearly, there is a reaction between the can and the consolidated Ti, which is approximately 200 μm in thickness, which is made up of two distinct layers. The first layer, Fig. 4.18(i) shows stabilised β grains which have an equiaxed morphology. Fe diffuses into the Ti from the can, and this stabilises the β phase. As the diffusion of Fe into the Ti proceeds, Fig. 4.18(ii), the morphology changes from stabilised β grains to an α+β morphology, with acicular laths of α in a β matrix.

The interfacial regions that inevitably form between the mild steel can and the consolidated Ti powder would need to be removed. However, the can, in both the HIP'ed and

extruded material, could serve to protect the Ti during further processing. As previously discussed in Section 2.1.4, the diffusion of oxygen in Ti is a serious problem when thermomechanical processing, a mild steel can would be an effective barrier to oxidation. It is believed that this interfacial reaction would be insignificant compared to any oxidation that the Ti would undergo.

A similar interface is observed in the encapsulated and extruded Ti HDH powder. The total interface is approximately 100 μm. The width of the interface is smaller that the HIP'ed sample due to the time at temperature. The HIP'ed sample was consolidated at above 900°C for 4 hours, the degassed and extruded samples were preheated only for 1 hour.

4.6.3 Mechanical Properties

Room temperature tensile tests were performed on the as extruded canned Ti rods. The extruded sections were machined to the specifications shown in Fig. 3.12 and the HIP'ed sample was machined to the specifications in Fig. 3.13. One sample was tested in each case. The ductility and ultimate tensile strengths are shown in Table 4.10.

Table 4.10: Ultimate tensile strength and ductility of degassed and extruded Ti HDH powder

Process	Degassing Temperature, °C	Ultimate Tensile Strength, MPa	Ductility %
Extrusion	500	587	11
Extrusion	700	676	9
Extrusion	900	586	8
HIP	300	539	9

Firstly, and most importantly, all the extrusions of canned Ti HDH powder have to some extent been consolidated, as every sample showed reasonably high ductility with increased ultimate tensile strengths over conventional CP Ti Grades. This is extremely promising and shows that there is potential in the direct extrusion of Ti powder for consolidation via non-melt processing without the need for some degree of compaction prior to consolidation. The tensile tests show a decrease in the ductility with increasing degassing temperature. The extrusion degassed at 500°C showed approximately 10% ductility and this dropped to slightly less than 8% ductility with powder degassed at 900°C. The ductility of ASTM CP Grade 2 Ti is 20% [82]. The decrease in ductility with increasing degassing temperature is most probably due to the increased oxygen content with increasing degassing temperature and also the high iron content particles observed

in the consolidated powder. It is known that both oxygen and iron decrease the tensile ductility while increasing the strength of the material.

4.7 Conclusions

Trials have been conducted to determine the optimum temperature for degassing Ti HDH powder. The microstructural and mechanical properties of degassed powder consolidated via direct powder extrusion have also been investigated. The following conclusions can be drawn from the presented data:

- The optimum degassing temperature for Ti HDH powder is 300°C to avoid recombination with evolved gases. As the powder is heated up, gases evolve from the power surfaces and exit the can. When the degassing temperature is low (300°C) the evolved gases are not absorbed into the Ti powder and are drawn out of the can. At higher temperatures, evolved gases can be re-absorbed by powder within the can. Although degassing at higher temperatures may be necessary to evolve off compounds such as TiH_2 or $MgCl_2$.

- The Ti HDH powder has been consolidated by shear that is applied to the powder during the extrusion process. The design of of the die means that the material undergoes constant welding, breaking and re-welding as the powder pass through the deformation zone until metallurgically sound bonds are created.

- The consolidation of canned Ti powder was achieved using direct powder extrusion without the need for pre-compaction, however, the economics of the process are questionable for short billets due to the front and back defects that were observed in the extrusion, and would thus have to be discarded.

- The consolidated Ti powder shows increased strength over conventional commercial purity of the same grade, but a lower ductility. The ductility decreases with increasing degassing temperature due to increased interstitial content. The low ductility is also affected by foreign particles within the consolidated powder. These particles were determined to be iron rich particles that are formed during the HDH process.

- The purity of the powder is extremely important in determining the final properties of the power, as the consolidated product is only as 'clean' as the starting powder feedstock. A method of purifying the powder prior to consolidation is necessary.

Chapter 5

The Consolidation of Compacted Titanium Powder

5.1 Summary

It has been shown in Chapter 4 that it is possible to consolidate canned and degassed Ti HDH powder *via* extrusion. This chapter details the effect of different reduction ratios on the consolidation of Ti HDH powder and a model of the extrusion process is presented. The heating of compacted Ti HDH billets, prepared by cold compaction, is examined with regards to a protective Deltaglaze glass coating and different atmospheres. The extrusion profile of the three different reduction ratios is examined, along with the characterisation of porosity and microstructure of extruded Ti HDH powder compacts. The finite element software package, Forge 2005, is used to match predicted extrusion pressures with the experimental ones. Forge 2005 is then used to predict pressure curves and temperature profiles across the extrusion width as the material exits the die.

5.2 Billet Heating

Ti HDH powder was compacted in a die to a pressure of approximately 320 MPa using a 'Tange' hydraulic press, as detailed in Section 3.4. To determine the optimum heating conditions, a number of the Ti HDH compacted billets powder were made, two were coated in Deltaglaze and one was left uncoated. The billets were placed in a preheated furnace at 900°C for 90 minutes in either an air or Ar atmosphere and then air cooled. The resultant oxygen contents are detailed in Table 5.1. An example of a compacted Ti

HDH powder billet is shown in Fig. 5.1.

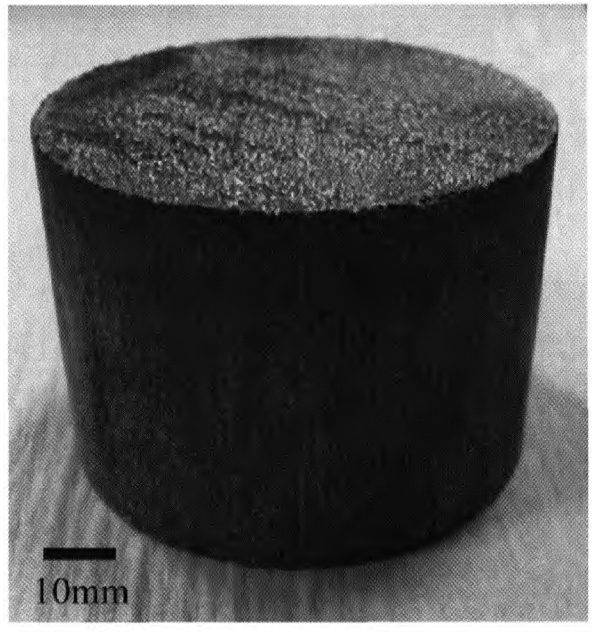


Fig. 5.1: Example of compacted Ti HDH, 72 mm diameter, powder billet

Table 5.1: Table of oxygen analysis with different heating conditions of Ti HDH powder compacts

Test No.	Compact Density, %	Atmosphere	Deltaglaze	Oxygen (Centre), wt.%	Oxygen (Surface), wt.%
1	80	Air	yes	0.47	6.79
2	80	Ar	yes	0.58	1.68
3	80	Ar	no	0.71	3.47

From Table 5.1, it is clear that there is significant oxygen pick up on the surface of all the samples. Whilst the data is complicated by the fact that the samples are air cooled leading to further oxygen pick-up during cooling the following conclusions can be drawn. In terms of surface pick-up the combination of an argon atmosphere and a Deltaglaze coating provides the best protection. In terms of oxygen pickup in the bulk of the compact it would appear that the presence of the Deltaglaze coating is critical and that argon alone does not fully protect the sample. It should be noted that a billet that was heated in air with no Deltaglaze coating was so oxidised that it was deemed unnecessary to test for oxygen content. For the extrusion trials the billets were Deltaglaze coated and heated in air. The oxygen contents measured in the extrusions were in the range 0.23 - 0.30 wt.%. These values are less than that obtained during the heating trials.

However for extrusion the billets were heated and immediately consolidated reducing the exposure time.

5.3 Extrusion

Ti HDH powder compacts, 72 mm in diameter, were prepared for extrusion, as described in Section 3.4. The measured density of the compacted Ti HDH powder billets, along with the reduction ratios utilised during the extrusion, are shown in Table 5.2.

Table 5.2: Ti HDH compact density with reduction ratio

Billet No.	Compact Density, %	Reduction Ratio
1	76	9:1
2	76	17:1
3	76	75:1

The extrusion conditions of the compacted Ti HDH billets are shown in Table 5.3.

Table 5.3: Extrusion conditions for Ti HDH powder compacts

Temperature:	900°C
Speed:	10 $mm.s^{-1}$
Loading Time:	10 s
Container Temperature:	280°C
Lubrication:	Graphite Dag
	Deltaglaze Glass
	Glass Pad

The extrusion pressure of the Ti HDH powder compacts extruded with different reduction ratios are shown in Fig. 5.2.

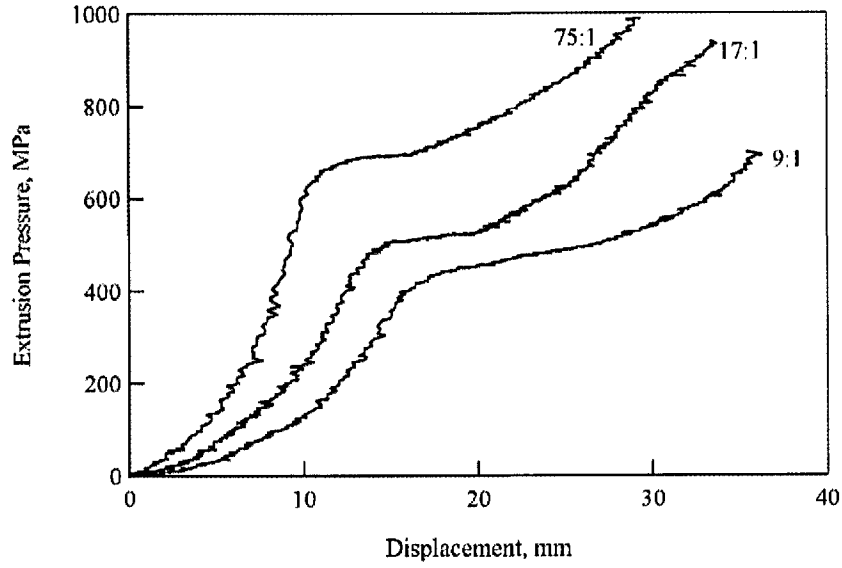


Fig. 5.2: Extrusion pressure vs displacement during extrusion of Ti HDH powder compacts at 900°C

The increase in pressure with displacement between 0 and 15 mm is due to the powder compact upsetting in the die container. The powder compacts are 76% dense and 72 mm in diameter and thus do not fill the die container. Before extrusion begins, the powder compact is upset to fill the die container, which has an internal diameter of 75 mm. At the onset of extrusion, the powder compact is nearly 100% dense but the particles are not well bonded together. The breakthrough pressures and maximum pressures for the Ti HDH powder compacts extruded under three reduction ratios, are shown in Table 5.4.

Table 5.4: Breakthrough and maximum pressures for Ti HDH powder compacts extruded under different reduction ratios

Billet No.	Reduction Ratio	Breakthrough Pressure, MPa	Maximum Pressure, MPa
1	9:1	441	690
2	17:1	510	934
3	75:1	690	983

Table 5.4 shows an increase in the breakthrough pressure with increasing reduction ratio when extruding Ti HDH powder compacts. There is an increase in the breakthrough pressure from 441 MPa at a reduction ratio of 9:1, to 690 MPa at a reduction ratio of 75:1. This increase in pressure is due to the increased force required to force the material though a smaller exit die diameter. As the reduction ratio increases, the size of the exit

hole decreases, which increases the amount of strain imparted to the material.

All three extrusion curves in Fig. 5.2, show increasing pressures with displacement. This is due to billet chilling as heat is lost to the container. The phenomenon of billet chilling has been explained in Section 4.4. In order to avoid billet chilling, heat loss from the billet to the container lining needs to be minimised, this can be achieved in two ways. Firstly, the billet can be insulated so that there is minimal heat loss from the billet to the container, and secondly, the container can be heated to the same temperature as the billet (isothermal conditions). In order to insulate the billet from excessive heat loss, a thermal insulator would need to be placed around the billet prior to extrusion. This could cause several problems, not just with billet heating, but also the extrusion itself. As has been shown in Chapter 4, the surface of the billet is drawn into the centre of the billet and forms the back end defect. If a thermal insulator were placed around the billet to insulate it from heat loss, this would cause the insulating jacket to be drawn into the extrusion. Since thermal insulating materials are frequently made out of oxides, this could cause significant contamination of the extrusion. The second option of extruding when both the container and the billet are the same temperature, so that there is no thermal gradient, also has several problems associated with it. The container would have to be manufactured out of a high temperature material, such as a nickel superalloy. This would significantly increase the costs of extruding titanium powder billets. Currently, the only viable method to minimise heat loss during extrusion of titanium components, is to perform the extrusion as fast as possible to limit the time that the billet has in contact with the container. The possibilities or increasing the die temperature and extrusion speed are examined in Section 5.5.

5.4 Consolidation of Compacted Ti HDH Powder

5.4.1 Analysis of Porosity in Consolidated Ti HDH Powder

Samples of each Ti HDH extrusion were sectioned in the longitudinal direction and examined using light microscopy. Unetched images of the three reduction ratio extrusion are shown in Fig. 5.3(a-c), with the corresponding image analysis images in Fig. 5.3(d-f).

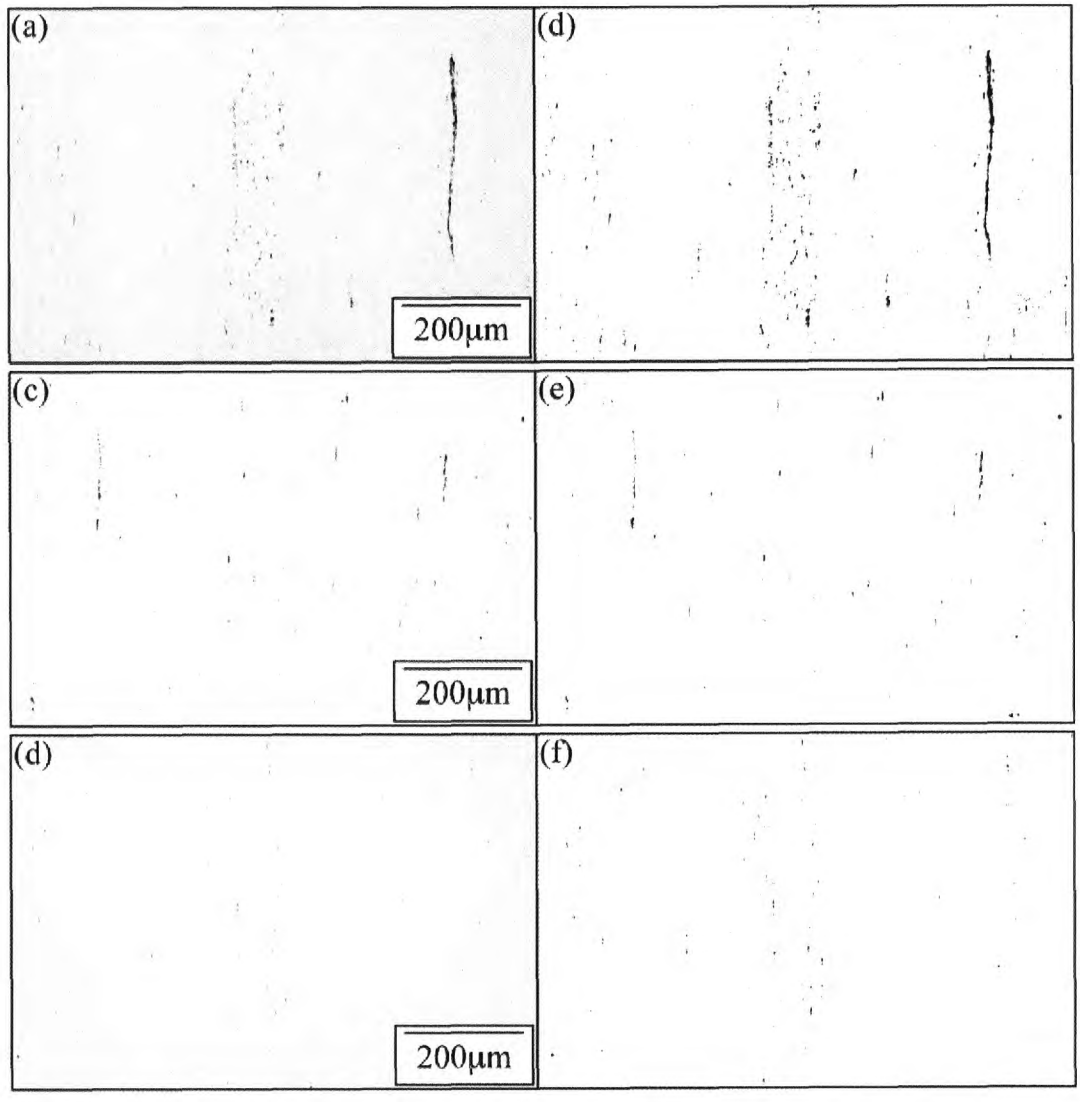


Fig. 5.3: Porosity distribution of compacted and extruded Ti HDH powder, (a) 9:1, (b) 17:1, (c) 75:1, corresponding image analysis of porosity (d) 9:1, (e) 17:1, (f) 75:1

Fig. 5.3 shows that the porosity in the R=9:1 extrude, Fig.5.3(a), is elongated in the extrusion direction. The pores in the R=17:1 condition, Fig.5.3(b), are still elongated in the extrusion direction, though less pronounced. In the R=75:1 condition, Fig.5.3(c), the pores are still elongated, though some evidence of the pores approaching an equiaxed morphology. There is a visible decrease in the volume fraction of porosity and also with the average size of pores in the samples with increasing reduction ratio. The volume fraction and the average size of porosity of the extrusions are shown in Table 5.5.

Table 5.5: Volume fraction and size of porosity of different reduction ratios of extruded Ti HDH powder compacts

Reduction Ratio	Area Analysed μm^2	Area Fraction Porosity	No. Pores	Average Porosity Size, μm^2
9:1	3416	0.65	705	4.84
17:1	674	0.12	179	3.76
75:1	347	0.06	192	1.81

The porosity with increasing reduction ratio is shown graphically in Fig. 5.4. The average size of porosity is shown on the same graph.

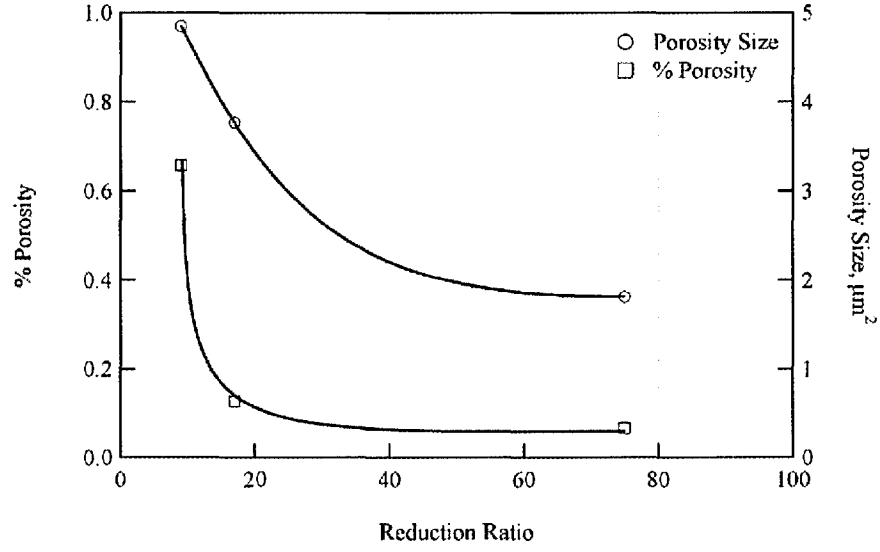


Fig. 5.4: Volume fraction of porosity and average size of pores with the reduction ratio of extruded Ti HDH powder compacts

The volume fraction of porosity decreases with increasing reduction ratio from 0.7 vol.% at a reduction ratio of 9:1 to 0.06 vol.% at a reduction ratio of 75:1. There is a similar trend in the average porosity size, from a size of 4.8 μm^2 at a reduction ratio 9:1 to a size of 1.8 μm^2 at a ratio of 75:1, though the decrease is less pronounced for the volume fraction of porosity. The decrease in volume fraction and size of porosity with increasing reduction ratio is due to the increasing degree of deformation that the material undergoes as the Ti HDH powder compact is forced though the die. As the reduction ratio increases, the amount of strain that the material undergoes increases dramatically. The strain induced during extrusion is defined as:

$$\varepsilon = \ln\left(\frac{A_c}{A_d}\right) \tag{5.1}$$

Where ε is the strain, A_c is the area of the container and A_d is the area of the die.

Table 5.6: The level of strain imparted to Ti HDH powder compacts when extruded at different reduction ratios

Reduction Ratio	Die Diameter, mm	Strain
9:1	25.0	2.20
17:1	18.0	2.85
75:1	8.6	4.32

The amount of strain generated increases with increasing reduction ratio. The Ti HDH powder particles experience more localised welding, breaking and re-welding as the powder compact is forced through the die. A greater degree of plastic deformation on the powder particles will shift the pore size to a smaller size distribution. Hence the smaller pore size and lower volume fraction of porosity with increasing reduction ratio. Clearly, the greater the reduction ratio, the greater the densification of the powder compact.

5.4.2 Microstructural Analysis of As-Extruded Ti HDH Powder

Light micrographs of the as extruded Ti HDH powders are shown in Fig. 5.5.

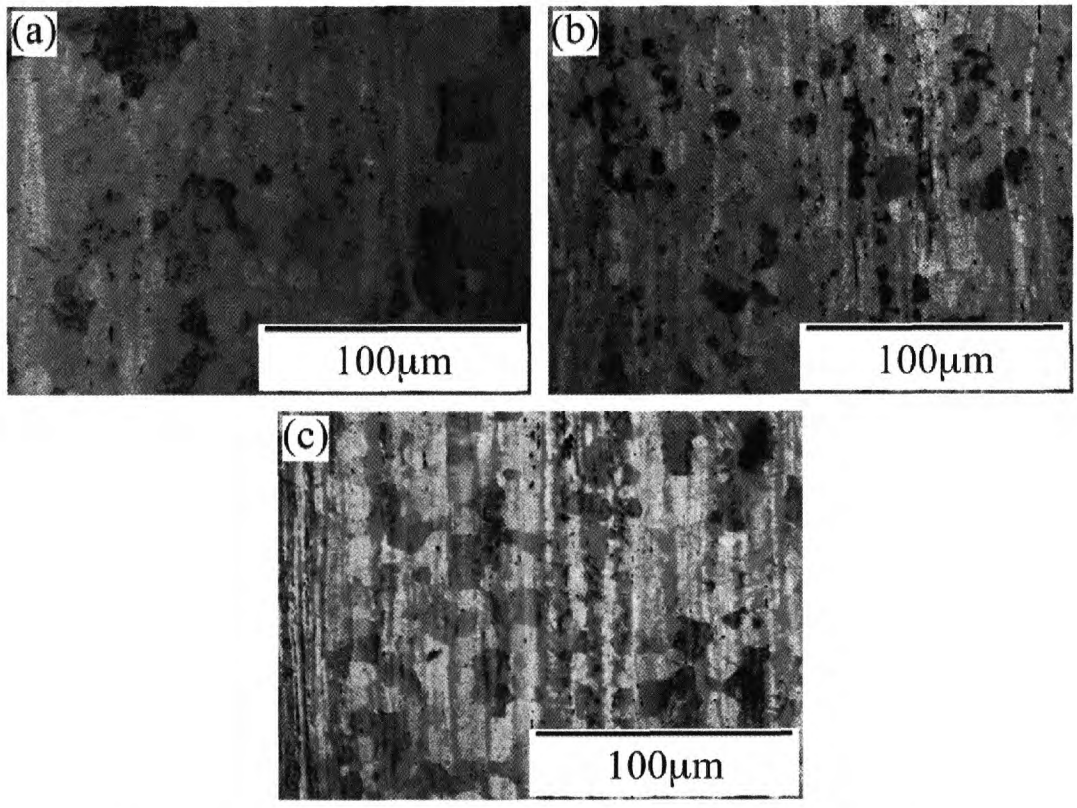


Fig. 5.5: Light micrographs of as extruded Ti HDH powder at different reduction ratio (a) R=9:1, (b) R=17:1 and (c) R=75:1

Fig. 5.5 shows micrographs of the extruded Ti HDH powders at different reduction ratios. All three extrusions show elongated grains in the extrusion direction. The grains in the 9:1 extrusion, Fig. 5.5(a), show partial recrystallisation. The R = 17:1 extrusion, Fig. 5.5(b), shows grains which have either recrystallised or have partially recrystallised, indicating sufficient deformation has occured for dynamic recrystallisation to occur. The R = 75:1 extrusion, Fig. 5.5(c), shows almost complete recrystallisation.

5.4.3 Mechanical Properties

Tensile tests were performed on specimens machined from the extrusion in the longitudinal direction. The specimen geometry is shown in Fig. 3.13. It is worth noting that the foreign particles observed in the canned and degassed Ti HDH powder, Chapter 4, were also observed in the microstructure of these materials. The presence of these inclusions is likely to significantly influence the mechanical properties of consolidated Ti HDH powder compacts, especially the fatigue properties, as inclusions can act as crack initiation sites.

Table 5.7: Tensile properties of compacted and extruded Ti HDH powder

Reduction Ratio	Ultimate Tensile Strength, MPa	Ductility, %
9:1	540	12
17:1	679	6
75:1	733	12

Table 5.7 shows the ultimate tensile strength (UTS) and elongation of the extruded Ti HDH powder compacts. The UTS increases with increasing reduction ratio, from 540 MPa at R = 9:1, to 733 MPa at R = 75:1. The ductility of the extrusions varies from 6 to 12%. The variation in the ductility is believed to be heavily influenced by the presence of the inclusions present within the microstructure. The UTS of all three extrusions is significantly higher than the UTS of ASTM Ti CP grade 2 alloys, which is approximately 340 MPa [21]. The increase in strength is due to the fine grain sizes that are obtained in the consolidated material, as well as the increased Fe and O content compared with wrought material.

5.5 Finite Element Modelling of Titanium Powder Extrusion

Finite element (FE) modelling of titanium powder billet extrusion was carried out to gain an insight into the extrusion pressure and exit temperatures of titanium powder extrusions, extruded under different conditions. A series of sensitivity studies were performed, using Forge 2005, to determine the effects of die temperatures, extrusion speeds and billet temperature.

5.5.1 Determination of Constants from Thermomechanical Data Analysis

The Norton-Hoff equation (Equ. 5.2) relates the flow stress of a material to the strain and strain rate and thus describes the rheology of the material under specific stress conditions. The Norton-Hoff equation can be simplified (when there is no strain hardening/softening) to:

$$\ln \sigma = \ln k + m \ln \dot{\varepsilon} + \frac{\beta}{T} \tag{5.2}$$

where σ is the flow stress, m is the strain rate sensitivity, k is a constant, $\dot{\varepsilon}$ is the strain rate, β is an energetic term related to the activation energy and T is the absolute

temperature. The Norton-Hoff rheology law works well with materials which strain harden or those for with negligible strain hardening and constant flow stress behaviour with strain. The Norton-Hoff law does not work well for materials which flow soften. Equ. 5.2 fits the form:

$$y = A + Bx_1 + Cx_2 \tag{5.3}$$

In order to model the extrusion process, rheological data for the material is required, which is inputted into the data file. The parameters required are determined from the compression testing at different temperatures and strain rates, which characterises the flow stress behaviour over a hot working regime, as detailed in Section 3.10.1. The flow curves obtained from the compression tests are shown in Fig. 5.6 and the steady state flow stress values from the compression tests are shown in Table 5.8. The compression samples were coated with boron nitride spray to minimised barrelling in the samples.

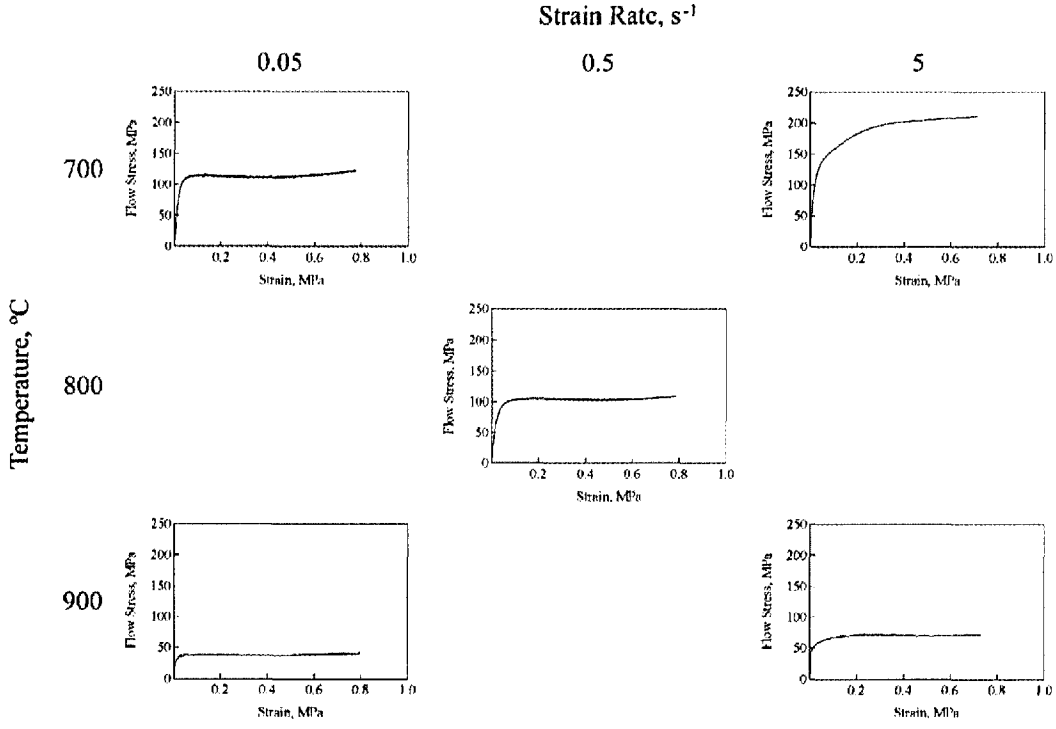


Fig. 5.6: Flow stress data for temperatures 700 - 900°C and strain rates of 0.05 to 5

Fig. 5.6 shows a steady state flow stress for all strain rates and temperatures, except at 700°C with a strain rate of 5 s^{-1}, where significant work hardening occurs. This form of the Norton-Hoff rheology law assumes no work hardening/softening, i.e. a steady state flow behaviour, so with the exception of lower temperatures and higher strain rates, the assumption of no strain hardening is accurate and thus the Norton-Hoff equation can be used to determine the rheology behaviour of the Ti HDH material.

Table 5.8: Flow stress data for Ti HDH powder, extruded at R=9:1, the units of the flow stress are in MPa

Temperature	Strain Rate		
°C	0.05	0.5	5
700	144	-	200
800	-	104	-
900	37	-	71

A regression analysis can be performed on the rheological data to obtain values for the constants $y(\ln k)$, $x_1(\beta)$ and $x_2(m)$ in Equ. 5.3, to determine the constants for the data file. These are summarised in Table 5.9.

Table 5.9: Flow stress regression data obtained from compression testing

Variable	Value	Coefficient
y-intercept	-1.14	$\ln k$
x var 1	6119	β
x var 2	0.132	m

In order to ascertain the accuracy of the regression data for constants in the Norton-Hoff equation (Equ. 5.2), the values can be put back into the equation to determine the predicted flow stress using the regression data. The correlation between the actual flow stress and the calculated flow stress, using the Norton-Hoff equation, Equ. 5.2, is shown in Fig. 5.7.

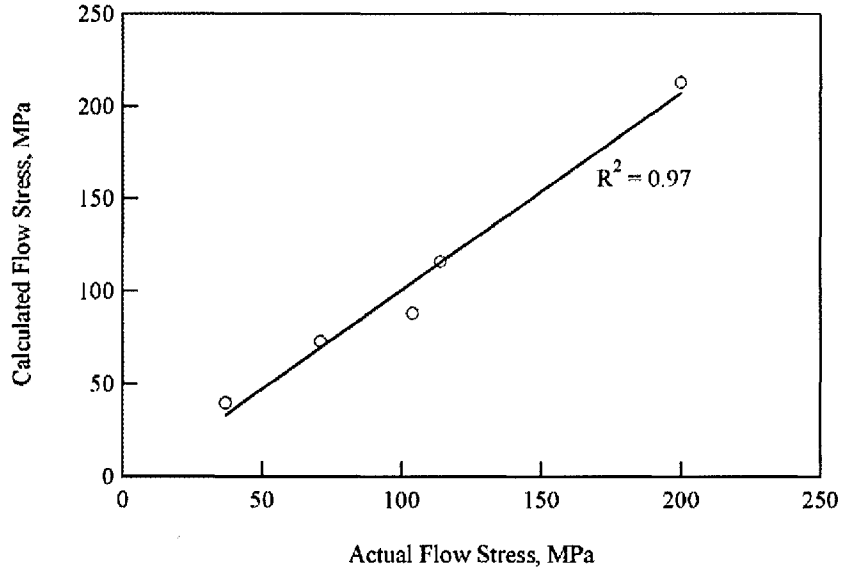


Fig. 5.7: Correlation between the predicted and experimental flow stress, using the Norton-Hoff Equation

With an R^2 value of 0.97, there is an accurate fit for the predicted flow stress data that is required for the Forge 2005 data inputs. The remaining data for the physical and thermal inputs for Forge 2005 are summarised in Table 3.4. Several simulations were run to determine the influence of extrusion conditions on the flow stress and exit temperature, the different simulation conditions are summarised in Table 5.10.

Table 5.10: Simulation conditions for Forge 2005 modelling of Ti HDH powder compacts

Simulation Number	Die Temp °C	Billet Temp °C	Extrusion Speed, $mm.s^{-1}$
1	280	900	10
2	280	900	3
3	280	900	15
4	500	900	10
5	900	900	10
6	280	800	10

Each simulation was performed with three reduction ratios, R = 9:1, R = 17:1 and R = 75:1.

5.5.2 Predicted Extrusion Pressure

A series of sensitivity studies were performed to determine the predicted extrusion pressure with various extrusion conditions. While all material constants have been determined, the remaining variable input for Forge 2005 is the heat transfer coefficient.

5.5.2.1 Determination of Heat Transfer Coefficient

The heat transfer coefficient is a measure of heat conduction at an interface. The greater the value, the greater the heat transfer across the interface. It is an important parameter as it effectively determines the amount of billet chilling that occurs between the billet and the container lining, and thus greatly effects the extrusion pressure. The recommended value for metal-to-metal contact is 10,000 $Wm^{-2}K^{-1}$ [85], though a value of 7500 $Wm^{-2}K^{-1}$ has been proposed specifically for Ti, as Ti has an inherently low thermal conductivity [81]. A sensitivity analysis was performed in Forge 2005 to infer the heat transfer coefficient. It was determined that a value of 4250 $Wm^{-2}K^{-1}$ is more appropriate for the extrusion of Ti HDH powder coated in Deltaglaze glass, rather than the previously reported values of either 10,000 or 7500 $Wm^{-2}K^{-1}$. This is to account for the insulating characteristics of Deltaglaze glass on the Ti power compact. The Deltaglaze glass insulates the interface between the billet and the container so that less heat is transferred from the billet to the container, thus the heat transfer coefficient is lowered.

A comparison between the experimental and predicted extrusion pressure (simulation number 1), using a value of 4250 $Wm^{-2}K^{-1}$ for the heat transfer coefficient, are shown in Fig. 5.8.

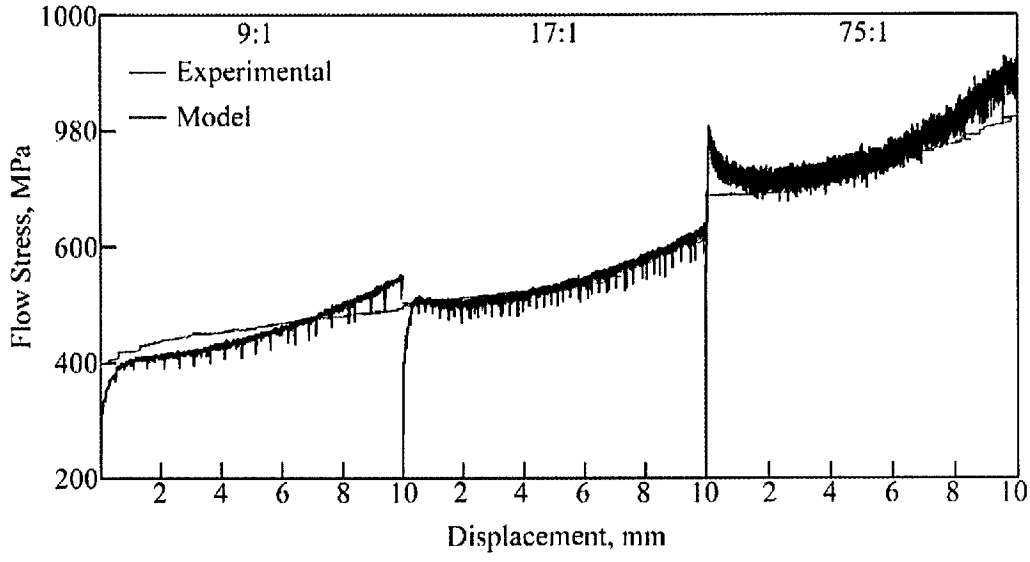


Fig. 5.8: Experimental and predicted extrusion pressure, with a heat transfer coefficient of 4250 $Wm^{-2}K^{-1}$ for three different reduction ratios (a) 9:1, (b) 17:1 and (c) 75:1

5.5.2.2 Speed

Simulation runs 2 and 3 in Table 5.10, show the conditions used in the FE model to predict the extrusion pressure and exit temperature of different extrusion speeds. The two speeds selected were 3 and 15 $mm.s^{-1}$. The slower speed represents a more typical extrusion speed for Al alloy extrusions (although not in the isothermal condition), and the higher speed represents the maximum speed of the extrusion press used in the experiments.

The predicted extrusion pressure for extrusion speeds of 3 $mm.s^{-1}$ and 15 $mm.s^{-1}$ are shown in Fig. 5.9.

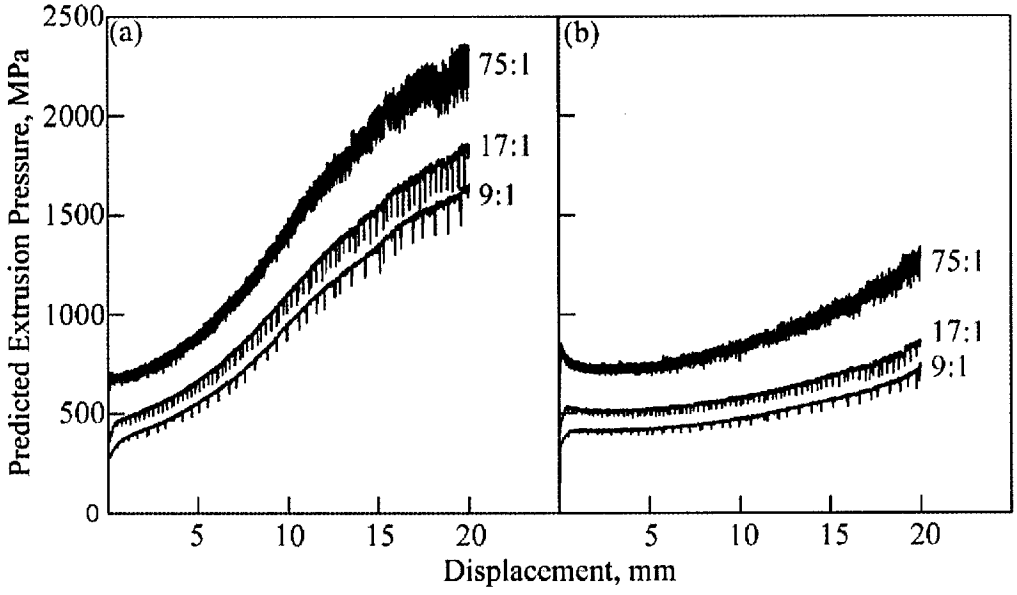


Fig. 5.9: Predicted extrusion pressure of Ti HDH powder compacts, with different extrusion speeds (a) 3 mm.s^{-1} and (b) 15 mm.s^{-1}, for reduction ratios of 9:1, 17:1 and 75:1

From Fig. 5.9, there is a clear difference between the different extrusion speeds on the billet chilling and thus the extrusion pressure. An extrusion speed of 3 mm.s^{-1} shows considerable billet chilling, so much so that extrusion of titanium powder compacts at this speed becomes almost impossible as the maximum press capacity is reached soon after extrusion begins. The maximum press capacity is approximately 1200 MPa for a 75 mm diameter container. An extrusion speed of 15 mm.s^{-1} still exhibits billet chilling, but to a much lesser extent, due to less contact time between the billet and the container. The breakthrough pressures of the two conditions increases with increasing speed. At a reduction ratio of 9:1, the breakthrough pressure is 320 MPa at a speed of 3 mm.s^{-1}, whereas with an extrusion speed of 15 mm.s^{-1}, the breakthrough pressure increases to 405 MPa. Although there is a significant increase in the breakthough pressure, the increase is small compared to the increase in extrusion pressure due to billet chilling. With the current extrusion conditions, outlined in Table 5.3, it is clear that a fast extrusion speed is necessary for the extrusion of titanium powder compacts with a lower temperature container, to limit the billet chilling time.

5.5.2.3 Die Temperatures

A sensitivity study was performed to determine the effect of die temperature on the extrusion pressure. Simulation runs 4 and 5 in Table 5.10, show the FEM conditions for modelling the effect of die temperature on the extrusion pressure of Ti HDH powder ex-

trusion. The two die temperatures chosen were 500 and 900°C. The lower temperature die represents the maximum useable temperature of H13 steel, and the higher temperature represents the ideal container temperature to eliminate billet chilling during the extrusion of titanium powder compacts, i.e. isothermal conditions. The predicted extrusion pressure of the two die temperatures are shown in Fig. 5.10.

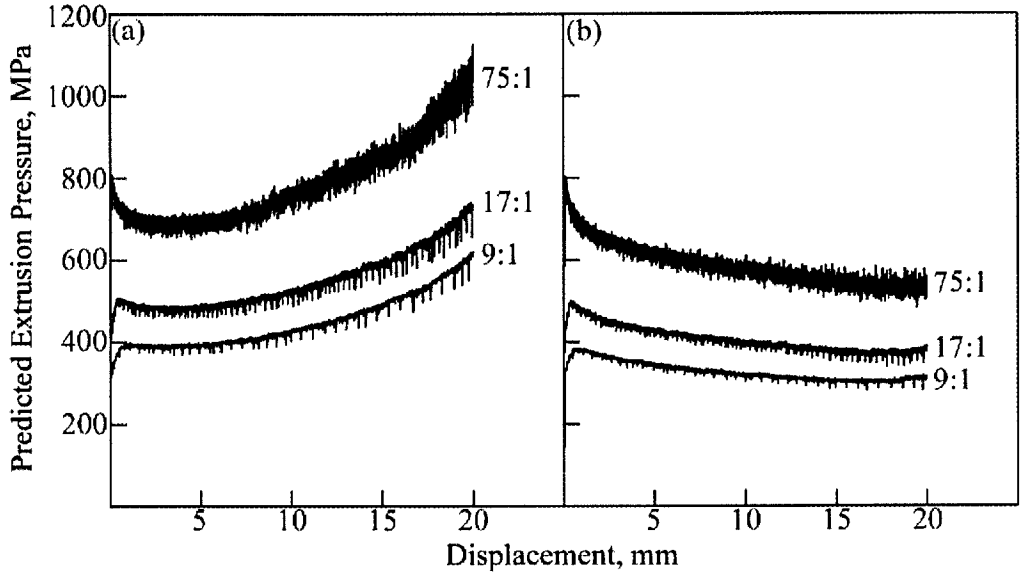


Fig. 5.10: Predicted extrusion pressure with different die temperatures, (a) 500°C and (b) 900°C, the reduction ratios are shown in the figure

The predicted extrusion pressure with both 500 and 900°C die temperatures in Fig. 5.10 are less than the experimental extrusion pressures shown in Fig. 5.2. This is expected as, in reality, there is less billet chilling than predicted due to the lower thermal gradient across the billet liner interface.

The billet still chills when the container is at 500°C as the temperature of the billet is still considerably greater than the container temperature. When the temperature of the container is the same as the billet, the extrusion pressure exhibits a more 'conventional extrusion profile', i.e. as the extrusion proceeds, the extrusion pressure steadily decreases as the friction between the billet and the container steadily reduces.

An interesting feature of billet chilling is that there is a theoretical maximum billet height which can be extruded before the load capacity of the press is reached, due to the gradually increasing flow stress as the billet chills. The greater the billet height, the more the billet chills. The experimental extrusions and the simulations were run with reasonably short billet heights and the increase in extrusion pressure during extrusion, due to billet chilling, effectively determines the maximum billet length that can be extruded before the press load capacity is reached. The effect of increasing reduction

ratio compounds this problem. However, increasing the container temperature to the theoretical maximum of 500°C minimises this problem and on this basis, it is likely that billets nearly twice the length could be extruded before the press capacity is reached.

5.5.2.4 Billet Temperature

Simulation number 6 in Table 5.10 details the conditions employed to test the effect of billet temperature on the flow stress during extrusion. Fig. 5.11.

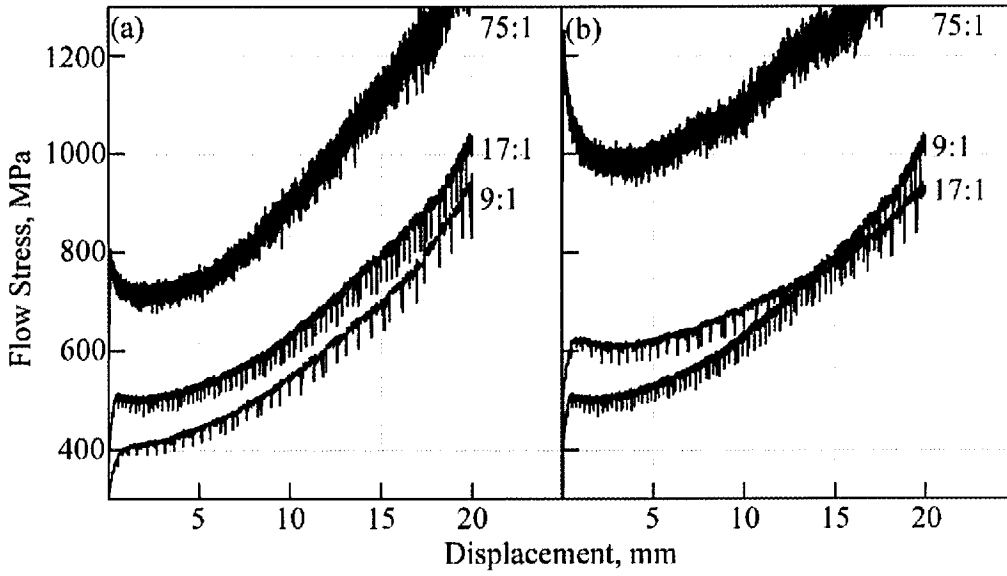


Fig. 5.11: The predicted extrusion pressure of Ti HDH powder compacts at different billet temperatures (a) 900°C and (b) 800°C

According to Fig. 5.11, the lower starting temperature of 800°C shows an increased breakthrough pressure compared with an initial billet temperature of 900°C for all reduction ratios. However, there is less billet chilling in the 800°C case due to the lower thermal gradient between the billet and the container. The extrusion pressures of the two starting billet temperatures are comparable up to approximately 20 mm for the reduction ratios 9:1 and 17:1. Above this displacement, the extrusion pressures for the 800°C initial billet temperature reach that of the 900°C initial billet temperature, due to the increasing billet chilling. It would be possible to extrude short lengths of Ti HDH powder at lower initial billet temperatures. At the higher reduction ratio, the extrusion pressures for the lower billet temperature is higher than that of the 900°C starting billet temperature and quickly exceeds 1200 MPa after a displacement of 15 mm. It would be difficult to extrude to higher ratios with such low temperatures.

5.5.3 Predicted Temperature Profiles Across the Extrusion Width

The FE model can be used to determine material point history during the simulated extrusion. In order to monitor the exit temperature, three data points were selected: on the surface, in the centre of the extrusion and a mid-point between the surface and the centre. These were all one millimetre below the die exit. The location of these points are schematically shown in Fig. 5.12.

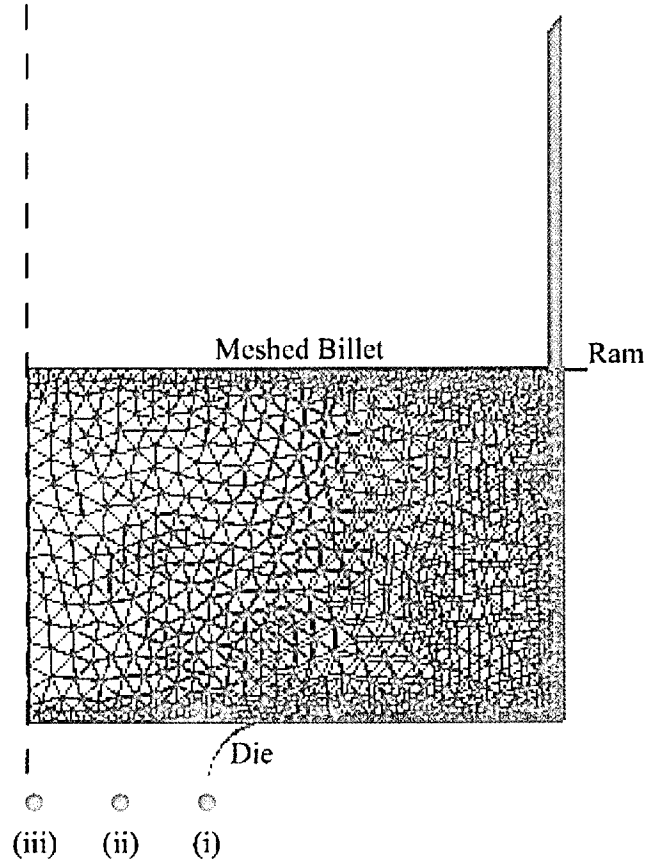


Fig. 5.12: Meshed billet with the material history points from the 9:1 reduction ratio die, (i) surface, (ii) midpoint and (iii) centre of the extrude width

5.5.3.1 Extrusion Conditions

The surface temperature is an important factor when the Ti HDH extrusion exits the die. This is because if the temperature is above the β transus, the material will absorb oxygen through the surface an order of magnitude higher than in the α regime, as illustrated in Fig. 2.6. If the material is below the β transus, oxygen will be absorbed, but at a rate significantly lower than if the surface is above the β transus. Simulations were run using the experimental extrusion conditions to determine the temperature profiles across the extrusion width as the material exits the die. An example of a temperature output file

is shown in Fig. 5.13.

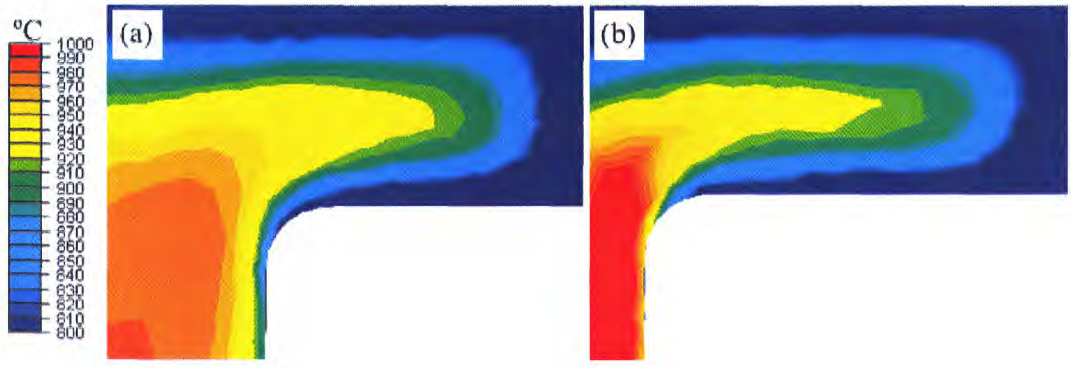


Fig. 5.13: Output data showing the temperature variations in the extrude, half way through the extrusion stroke, (a) R = 9:1 and (b) R = 75:1, the temperature key is shown in the figure

The predicted surface temperatures of the Ti HDH extrusions as they exit the die, for three different reduction ratios, are shown in Fig. 5.15. The exit temperatures of the surface, midpoint and centre for the three reduction ratios, from the experimental extrusion condition calculations, are shown in Fig. 5.14.

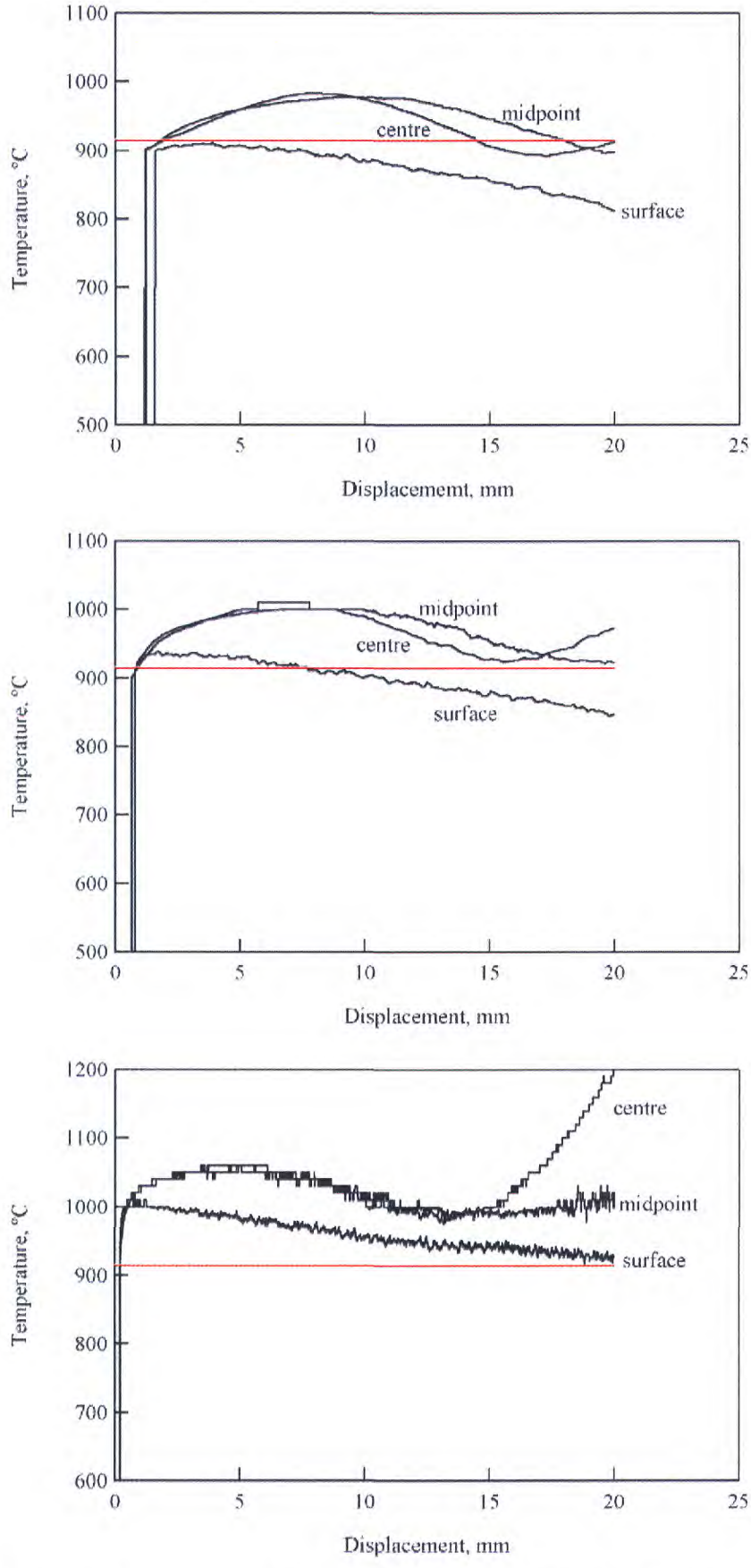


Fig. 5.14: Temperature profiles across the extrusion width, (a) R = 9:1, (b) R = 17:1 and (c) R = 75:1, the red lines in each graph indicate the nominal β transus for CP Ti grade 2 alloys

Fig. 5.14 shows the temperature profiles across the extrusion width. The surface temperatures for all reduction ratios is lower than the midpoint point or the centre points, which are approximately the same for the majority of the extrusion. The surface temperatures for the three reduction ratios are plotted in Fig. 5.15.

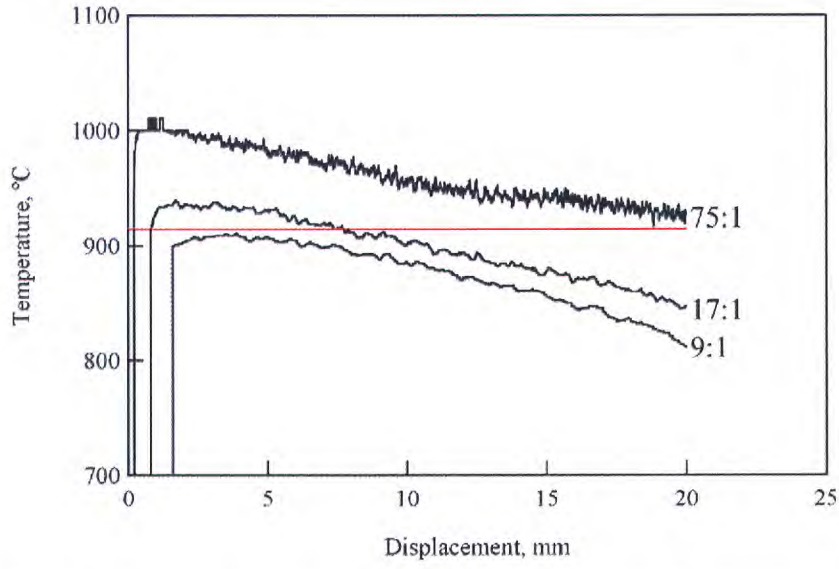


Fig. 5.15: The predicted surface temperatures as the Ti HDH extrusions exit the die, the red line indicates the nominal β transus temperature for Ti CP grade 2 alloys

Fig. 5.15 shows the surface exit temperatures from simulations of the extrusion conditions, the reduction ratios are shown on the figure. The exit temperature for all three reduction ratios rises to a maximum very quickly, and then steadily drops as the extrusion proceeds. The lowest reduction ratio, R=9:1, shown in Fig. 5.15, shows that the surface exit temperature never reaches the β transus (which is ~915°C for CP Ti grade 2 alloys [79]). The surface exit temperature for the R=17:1 reduction ratio in Fig. 5.15, has a maximum temperature of 939°C, although the surface exit temperature only stays above the β transus for a short time. The R=75:1 simulated extrusion, Fig. 5.15(c), shows a surface exit temperature which is above the β transus for the entire operation. The diffusion coefficients between 700 and 1100°C are shown in Fig. 2.6. A measure of how far something diffuses into a material is the diffusion length, which is defined as:

$$L_{diff} = \sqrt{Dt} \tag{5.4}$$

Where L_{diff} is the diffusion length, D is the diffusion coefficient and t is time. The values The diffusion length can be plotted to against temperature to determine the distance for which oxygen diffuses into titanium, using the diffusion coefficient data for α and β Ti shown in Fig. 2.6, this is shown in Fig. 5.16

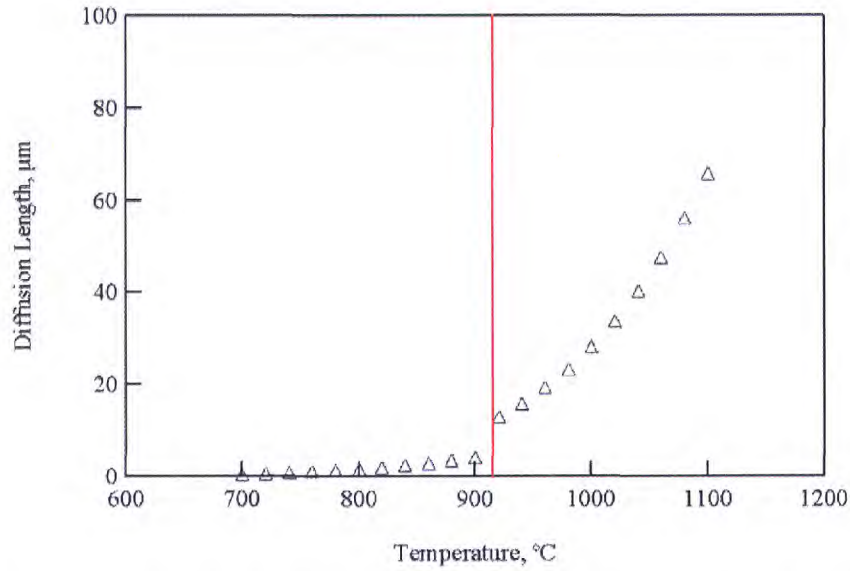


Fig. 5.16: The diffusion length of O in Ti, after t = 300 s, the red line indicates the nominal β transus for CP Ti grade 2 alloys

As illustrated in Fig. 5.16, the diffusion of oxygen in titanium is considerably greater above the β transus, when using the diffusion coefficients shown in Fig. 2.6 and activation energies shown in Equ. 2.6 (for α-Ti) and Equ. 2.7 (for β-Ti). Though it is clear that diffusion is an order of magnitude greater in the β phase, the quantitative accuracy is questionable to the varying values reported for the diffusion coefficients and activation energy for diffusion of oxygen in titanium [86]. Other factors which will effect the diffusion of oxygen in titanium are the levels of impurities in the material and the α-case that forms on the surface. Also, interstitial alloying elements such as Fe will slow the O diffusion in Ti.

Due to the increased diffusion length of O in Ti, the O content would be expected to rise when the surface of the extrude is above the β transus, as shown in Fig. 5.15. In this case, severe oxidation would be expected as oxygen diffusion would be prevalent along the entire length of the extrusion. The two extrusions performed at a lower reduction ratio would expect to pick up some oxygen at the front ends of the extrusions, as the titanium is still extremely hot, however given that the surface is in the α regime, the oxygen pick up would be an order of magnitude lower compared to the R=75:1 reduction ratio condition, using the available data in Fig. 5.16. However, the calculated values for the diffusion length of α in to Ti is still only 70 μm even at 1100°C for 5 minutes. This is insignificant when compared to the extrusion width, so no increase in oxygen content would be expected in the core of the extrusion.

The glass pad, which is placed between the die and the billet, which is primarily used

to protect the die during the extrusion, coats the extrude and thus provides a certain degree of protection from the atmosphere after the material has left the die. At higher reduction ratios, and hence faster exit speeds, it is not possible for the glass pad to produce a continuous layer on the surface of the extrude, leading to higher oxidation at higher reduction ratios. In order to reduce oxidation of the extrusion surface as the material exits the die, a protective atmosphere, such as Ar, would be required, to minimise surface contamination.

This analysis would suggest that the oxidation of the Ti extrudate after the material has left the die is small compared to the oxidation of the Ti compact during pre-heating. It is more important to heat the Ti compact in such a way as to reduce oxidation of the Ti powder during preheating than preventing oxidation of the surface of the extrudate after the material has exited the die.

5.5.3.2 Extrusion Speed

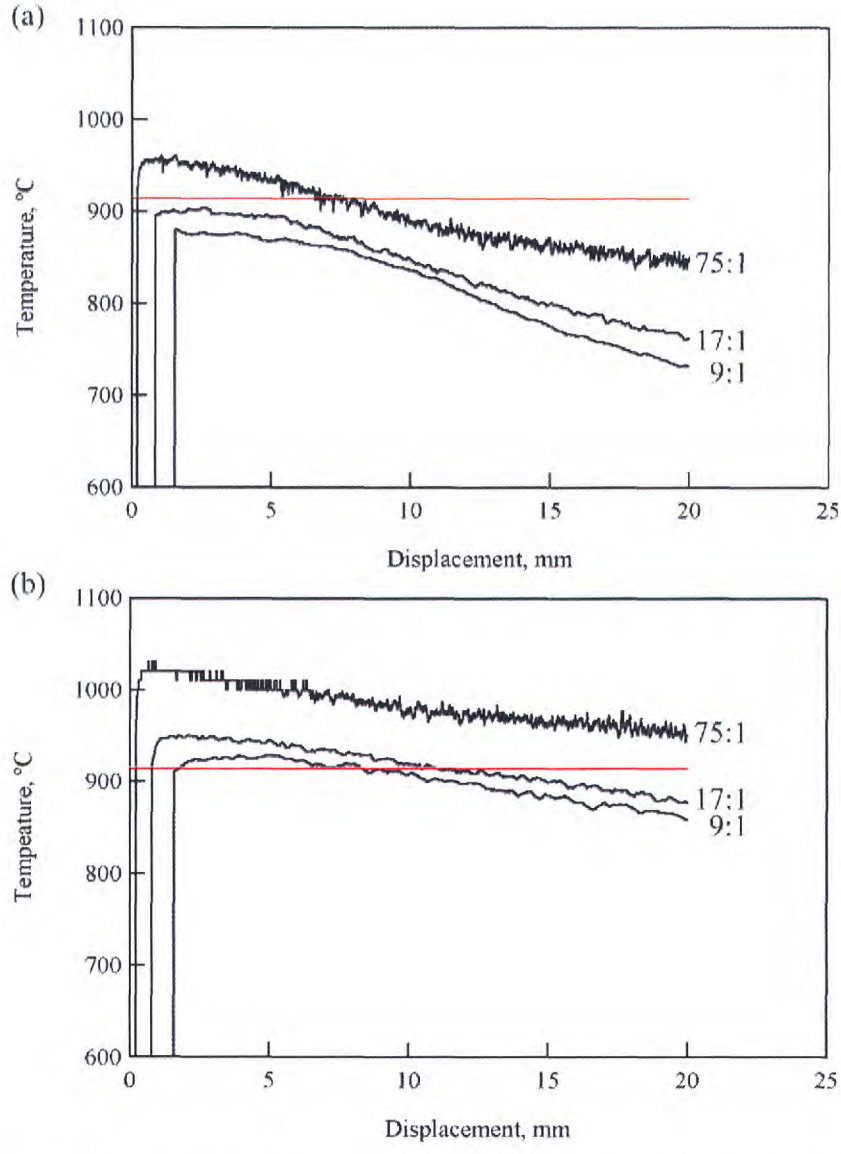


Fig. 5.17: The variation in the exit surface temperature extrusion speed (a) 3 $mm.s^{-1}$ and (b) 15 $mm.s^{-1}$, the red lines in each graph indicates the nominal β transus for Ti CP grade 2 alloys

Fig. 5.17 shows the surface exit temperatures of different extrusion speeds. The slower speed surface exit temperature is significantly lower for all the reduction ratios than for the faster extrusion speed. The lower reduction ratios never reach the β transus, and the 75:1 reduction ratio only stays above the β transus for a short time. In fact, the lowest reduction ratio extrusion exit surface temperature does not even reach the initial billet temperature of 900°C due to the significant billet chilling that occurs. The fast extrusion speeds reach significantly higher surface exit temperatures. These high

surface exit temperatures have significant implications for current extrusion conditions employed commercially.

5.5.3.3 Die Temperatures

Fig. 5.18 shows the surface exit temperatures for the two different die temperatures, 500°C, Fig. 5.18(a) and 900°C, Fig. 5.18(b).

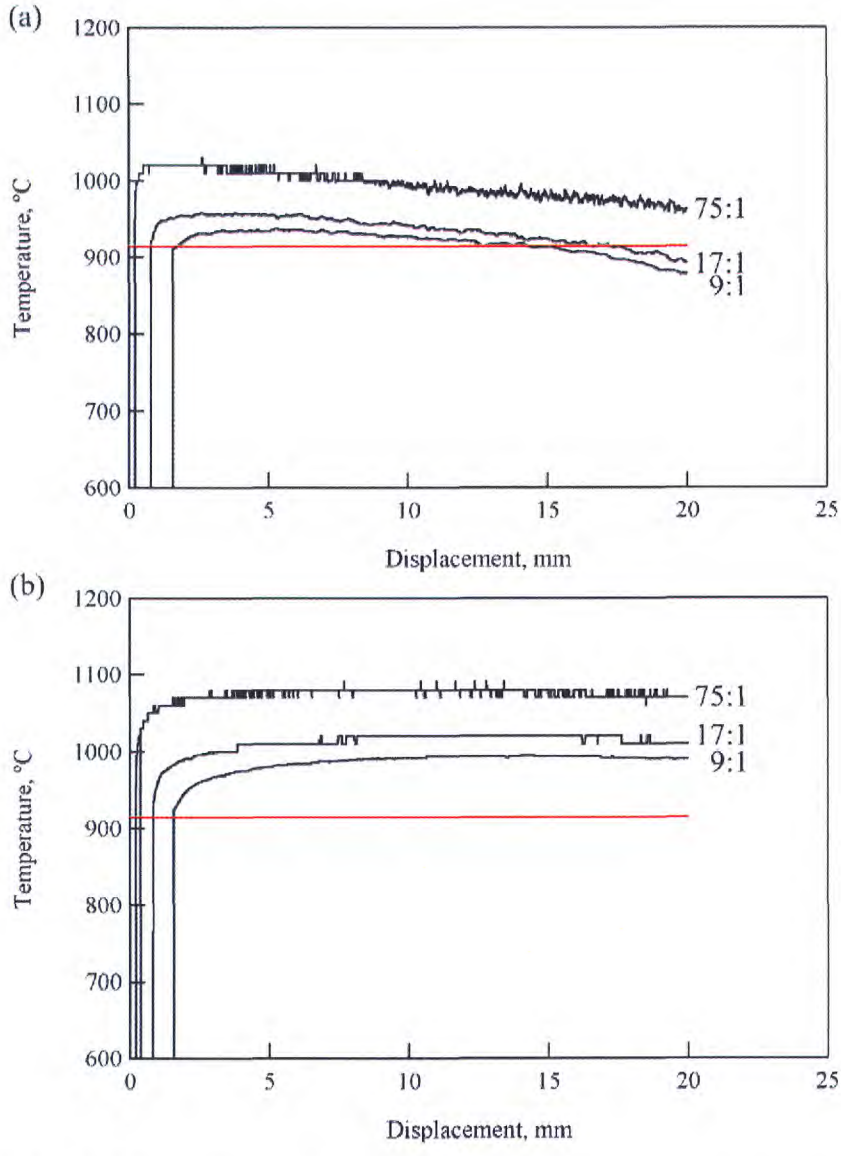


Fig. 5.18: The variation in the exit surface temperature with reduction ratio with different die temperatures (a) 500°C and (b) 900°C, the red lines in each graph indicate the β transus for Ti CP grade 2 alloys

Comparing the surface exit temperature of the extrusion conditions and an increased die temperature, clearly there is an increase in the surface exit temperature for all reduction

ratios when employing either a 500 or 900°C die temperature. At lower reduction ratios and with a die temperature of 500°C, the surface exit temperature eventually decreases to below the β transus after 15 mm, although the majority of the extrusion is above the β transus and significant oxygen pick up would be expected. At high reduction ratios, the surface exit temperature remains above the β transus for the entire length of the extrusion. At the higher die temperature of 900°C, the surface exit temperatures for all the reduction ratios, remain well above the β transus, and, once again, significant oxygen pick up would be expected.

5.5.3.4 Billet Temperature

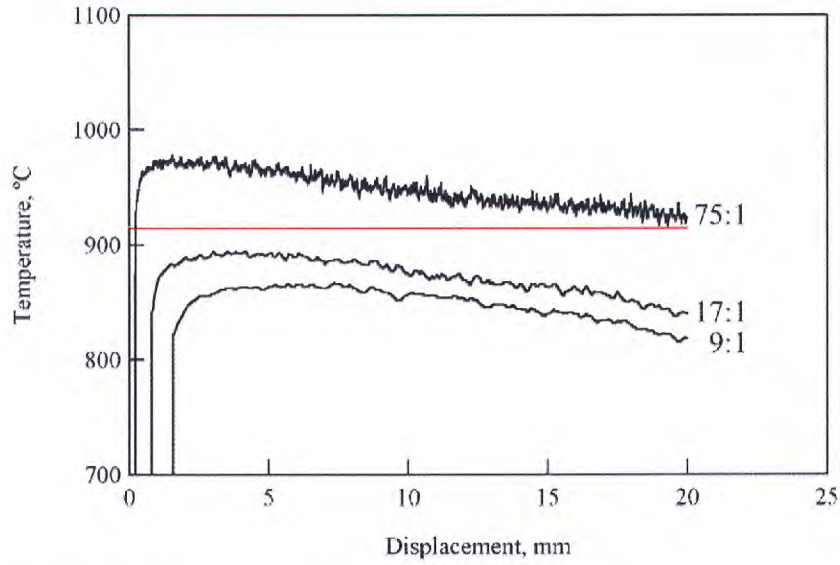


Fig. 5.19: The variation in the exit surface temperature with an initial billet temperature of 800°C, the red line indicates the β transus for Ti CP grade 2 alloys

The variation of the exit surface temperature for an initial billet starting temperature of 800°C is shown in Fig. 5.19. Comparing Fig. 5.19 with the surface exit temperatures in Fig. 5.15, it is clear that the surface exit temperatures are lower than with an initial starting billet temperature of 900°C. The lower reduction ratios never reach the β transus. The higher reduction ratio surface exit temperatures show the same profiles as the higher initial billet starting temperature, but only at slightly lower temperatures.

At the present time, the only viable way to realistically extrude titanium is with fast extrusion speeds as to avoid large extrusion pressures. However, Fig. 5.17 shows that this produces variations in the surface exit temperature along the length of the billet. It is likely that this would therefore lead to differences in the oxygen contamination along the extrusion length. Not only are there temperature variations along the length, the

temperature profiles in Fig.5.14, show that there are also temperature variations across the width of the extrusion. This would have detrimental effects on the microstructure, not only along the length of the billet, but also across the width of the extrusion as microstructure is extremely sensitive to the temperature of deformation.

5.5.4 Limitations of Finite Element Modelling

Finite element modelling using the Norton-Hoff rheology law assumes no work hardening/softening in the material, i.e. steady state flow behaviour. It is shown in Fig. 5.6 that this in not the case for lower temperatures with higher strain rates and thus the material data is not completely accurate. Therefore billet chilling can potentially lead to some work hardening during the extrusions, which could account for the inaccuracies in the predicted extrusion pressure.

The Norton-Hoff equation is based on 100% dense monolithic material which is similar in composition and microstructure, i.e. the rheological behaviour is similar across the billet width. Ti powder compacts differ in one respect. The powder compacts are not 100% dense. The initial starting density of the powder billets is 76%. However, the billets are compacted to near full density during the upsetting stage of extrusion, although the powder particles are poorly bonded as the particles have not yet experienced any shear. In the case of powder compacts, the upset billet can be considered to be monolithic in its flow behaviour.

5.6 Conclusions

In this chapter, the consolidation of Ti HDH powder compacts *via* extrusion has been investigated, with particular reference to the reduction ratio employed during the extrusion. A model, using the software programme Forge 2005 was utilised to simulate various extrusion conditions on the flow stress and exit temperatures of Ti HDH powder compacts. The rheological data for constants in the model were obtained from compression testing. In the present work, the following conclusions can be drawn for the presented data:

- The optimum heating conditions for Ti powder compacts is in an Ar atmosphere with a Deltagalze glass coating. This is to ensure the minimal amount of oxygen pick up during preheating. Oxidation has been reported for compacts preheated with Detlaglaze in an air atmosphere. The source of the oxygen contamination is likely to include the Deltaglaze glass coating itself.

- Ti HDH powder compacts have been consolidated *via* the shear deformation that occurs in the extrusion process. The strength of the Ti extrudate increases with increasing reduction ratio, however there are variations in the ductility due to the presence of inclusions in the starting powder feedstock. The ultimate tensile strength is greater in all cases than Ti CP grade 2 alloys. This is due to the fine grain size obtainable with powder consolidation.

- The mechanical properties of Ti HDH powder compacts compares with Ti HDH which has been canned and degassed of the same reduction ratio.

- The value of 4250 $Wm^{-2}K^{-1}$ has been shown to be a reasonable constant for the heat transfer coefficient for Deltaglaze glass coatings, for use in Forge 2005 simulations.

- Modelling the extrusion process has shown that the phenomenon of billet chilling, due to the thermal gradient which exits between the billet and the die, to be a problem of Ti extrusion. This can be overcome, partly by fast extrusion speeds using current extrusion presses, but also by increasing the container temperature to reduce the thermal gradient.

- FE modelling of the extrusion process to determine the surface exit temperatures, has shown that the reduction ratio dramatically increases the exit temperature. For the extrusion conditions used in the experimental procedures, the surface exit temperatures are increased above the β transus of CP Ti grade 2 alloys. The pre-heating of the Ti compact prior to extrusion is more important that the potential oxygen pick up after the material has exited the die.

- With the extrusion of titanium, there is a balance between the extrusion speed and the billet/die temperature, which needs to be controlled to avoid excessive extrusion pressures and exit temperatures.

- FE modelling of the extrusion process for Ti HDH powder compacts has shown the optimum processing conditions would involve extrusion with isothermal conditions, i.e. a similar container temperature to the billet temperature to limit billet chilling and therefore variations in extrusion temperature along the extrusion length and a slow speed, to limit variations in the temperature across the extrusion width.

Chapter 6

Thermomechanical Processing of Ti-6Al-4V+TiB Composites

6.1 Summary

In this chapter, the thermomechanical processing of titanium matrix composites is presented and discussed. The mechanical properties of Ti-6Al-4V + 20 vol.% TiB manufactured *via* a solid state processing route have been established with reference to a heat treatment to fully convert TiB_2 to the reinforcement phase TiB. X-ray diffraction (XRD) was performed to prove full conversion of TiB_2 to the reinforcement phase, TiB. A texture analysis has also been performed on Ti-6Al-4V + 20 vol.% TiB sample to determine the orientation of the TiB reinforcement in relation to the Ti-6Al-4V matrix. A comparison of the α phase texture is made with monolithic Ti-6Al-4V.

6.2 Characterisation of Ti-6Al-4V and TiB_2 Powder

The mechanically alloyed (MA'ed) materials used in this chapter were supplied by Aerospace Metals Composites, Farnborough, UK. The suppliers for the titanium alloy powder and TiB_2 are shown in Section 3.2.

The Ti-6Al-4V gas atomised powder is spherical and approximately 100 - 120 μm in diameter. The spherical nature and small diameter of the powder allows for a greater packing density. The TiB_2 is approximately 5 μm in diameter.

6.3 Processing Route for Ti-6Al-4V + 20 vol.% TiB

The processing route for the composites is described in Section 3.9.1 on page 67. An unreinforced variant of gas atomisted (GA) Ti-6Al-4V was also manufactured for comparison using the same processing conditions as the Ti MMCs. The mechanical alloying process, described in Section 4.6.3 on page 94, intimately mixes the two powders until there is a solid solution of one element in the other. Godfrey [59] has investigated the effects of mechanical alloying on the distribution of TiB_2 in titanium and determined that it is extremely difficult to get an even distribution in Ti-6Al-4V even after long milling times. It is also unlikely that there is a complete solid solution of TiB_2 in the Ti matrix. Apart from the information in Section 3.9.1, little is known on the mechanical alloying process as it is proprietary. It is thought that the uneven distribution of TiB_2 in the Ti-6Al-4V would resemble the layered structure shown in Fig. 2.11(c), and not the homogeneous distribution shown in Fig. 2.11(e).

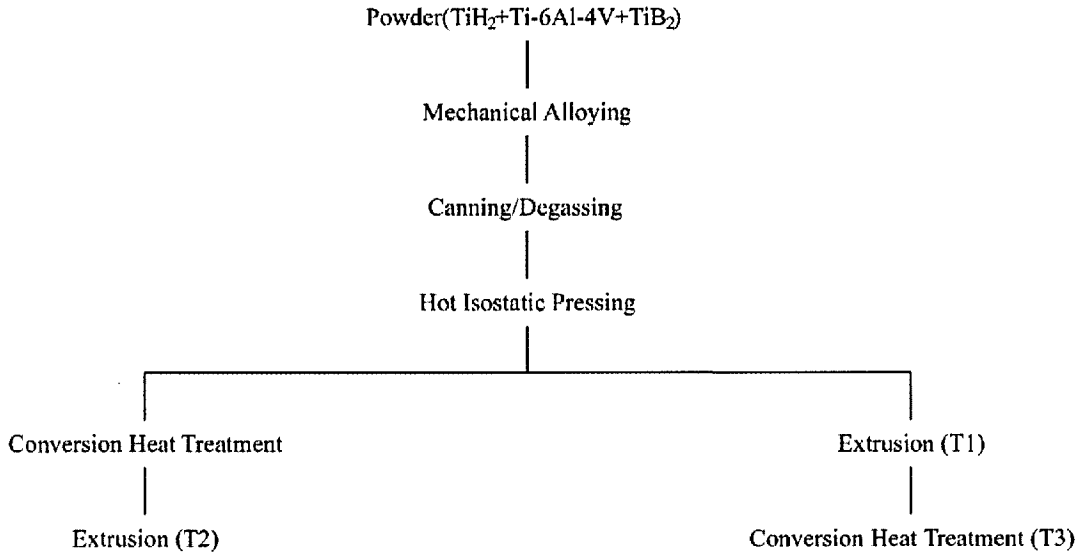


Fig. 6.1: Thermomechanical processing route for Ti-6Al-4V+TiB composites; the heat treatment conditions T1, T2 and T3 are described in Table 6.1

12.8 wt.% TiB_2 was mechanically alloyed with GA Ti-6Al-4V powder and 6.4 wt.% TiH_2 powder. 12.8 wt.% TiB_2 was chosen as this converts to 20 vol.% TiB upon complete conversion. It is also important to note that 6.4 wt.% Ti (in the form of TiH_2) was added to the powder mix. This is due to the fact that for every mole of TiB_2 which reacts with the Ti-6Al-4V matrix, 2 moles of TiB are formed, from the reaction:

$$TiB_2 + Ti \rightarrow 2TiB \tag{6.1}$$

If no extra Ti were added (on the left hand side of the equation), Ti would be consumed from the matrix in the reaction and so the matrix would become lean in Ti, thus the

matrix would become richer in the alloying elements. TiH_2 also has the benefit of breaking up the agglomerates that form during the mechanical alloying process from the welding, breaking and rewelding that occurs. This is due to the H in the TiH_2 which permeates along grain boundaries and embrittles the agglomerate. This is a similar effect to the hydride-dehydride process described in Section 2.2.2. It is important to note that due to the presence of TiH_2 in the material, the powder was degassed at 800°C. Although, the necessity to degas at elevated temperatures, to remove H from the powder mass, has not been established. An alternative to this process could be to add pure Ti and mechanically alloy the powders in a H atmosphere.

The three different conditions of the composites are examined. These are described in Table 6.1.

Table 6.1: Heat treatment conditions for the conversion heat treatment (CHT) of TiB_2 to TiB, pre and post extrusion

Heat Treatment	Condition	Temperature, °C	Time, hours
T1	Non-CHT then extruded	-	-
T2	CHT then Extruded	1200°C	4
T3	Extruded then CHT	1200°C	4

CHT is the conversion heat treatment, which is at 1200°C for 4 hours. This is the heat treatment, applied to the material, to fully convert the TiB_2 to TiB. T2 was conversion heat treated in a vacuum furnace and was nitrogen blast quenched. T3 was conversion heat treated in an argon atmosphere and then water quenched. The T2 heat treatment was carried out at AMC, T3 was heat treated at Imperial College London.

6.4 As Extruded Ti-6Al-4V + 20 vol.% TiB

6.4.1 Extrusion of Ti MMCs

Ti-6Al-4V and Ti-6Al-4V + 20 vol.% TiB billets were extruded using the techniques described in Section 3.5.2, into rods of approximately 1 m in length, Fig. 6.2.



Fig. 6.2: Extrusions of Ti-6Al-4V-TiB

The extrusion conditions for the Ti, Ti-6Al-4V and T-6Al-4V+TiB composites are shown in Table 6.2. The extrusion loads for the titanium alloy composites are shown in Table 6.3. For comparison, Ti HDH and Ti-6Al-4V are included (both processed and extruded under the same conditions).

Table 6.2: Extrusion conditions for CP Ti, Ti-6Al-4V and Ti-6Al-4V + 20 vol.% TiB

Material	Heat Treatment Condition	Extrusion Temperature, °C	Extrusion Speed, mm/s
Ti HDH	T1	950	2.5
Ti-6Al-4V	T1	1000	5
Ti-6Al-4V + 20 vol.% TiB	T2	1060	5
Ti-6Al-4V + 20 vol.% TiB	T1	1000	5

The T3 condition is the same as the T1 condition during the extrusion as the conversion heat treatment for T3 is after the thermomechanical processing.

Table 6.3: Breakthrough and maximum loads for CP Ti, Ti-6Al-4V and Ti-6Al-4V + 20 vol.% TiB

Material	Heat Treatment Condition	Breakthough Load, MPa	Maximum Load, MPa
Ti HDH	T1	196	841
Ti-6Al-4V	T1	473	836
Ti-6Al-4V-20TiB	T2	825	1000
Ti-6Al-4V-20TiB	T1	825	1000

The breakthrough pressure for the Ti HDH powder is 196 MPa. This increases to 473 MPa for Ti-6Al-4V. When 20 vol.% TiB is added to the Ti-6Al-4V, the extrusion load increases to 825 MPa. There is no difference between the T1 condition and the T2 condition in the extrusion pressure. The increased breakthrough pressure for Ti MMCs is due to the increased flow stress of the Ti MMCs, due to the increased stiffness of the reinforcing phase. There is no difference between the T1 and T2 conditions due to the materials having the same volume fraction of reinforcement phase. All the extrusions exhibit increasing pressure with displacement. This is due to billet chilling, i.e. heat is transferred from the billet to the container. The problem of billet chilling when extruding titanium alloys and composites has been explained previously in Section 4.4. However, it is clear that it is possible to extrude these materials, although the pressures required are significantly larger than those required for monolithic alloys. The increase in the load that is required to extruded these composites has important implications in the required extrusion press capacity.

The container material of the press used in this study is made of H13 steel. This material is useful up to 500°C, however it cannot be used above this temperature due to overageing. A more suitable material to manufacture the container out of would be a nickel (Ni) superalloy. Ni superalloy materials can be used up to 1000°C, and although this would be a considerably more expensive option; it would be a more appropriate material, as a higher temperature container would lead to less billet chilling and therefore a lower overall flow stress. The ideal case would be to have the container at the same temperature as the billet so that no billet chilling occurs, i.e. isothermal conditions. This is the case for the majority of Al extrusions. If the container temperature could be increased sufficiently, there would be significantly more scope to change the process variables, such as the die design and extrusion speed. Ideally, extrusions should be carried out under isothermal conditions.

In order to confirm the presence of TiB_2 in the T1 condition, X-ray diffraction (XRD) was performed on both conditions, T1 and T2, in the transverse direction. The XRD trace for the non-conversion heat treated composite (T1 condition) is shown in Fig. 6.3 and for the conversion heat treated composite (T2 condition) in Fig. 6.4. All the peaks were identified using powder diffraction files obtained from the International Centre for Diffraction Data cards, as described in Section 3.7.4.

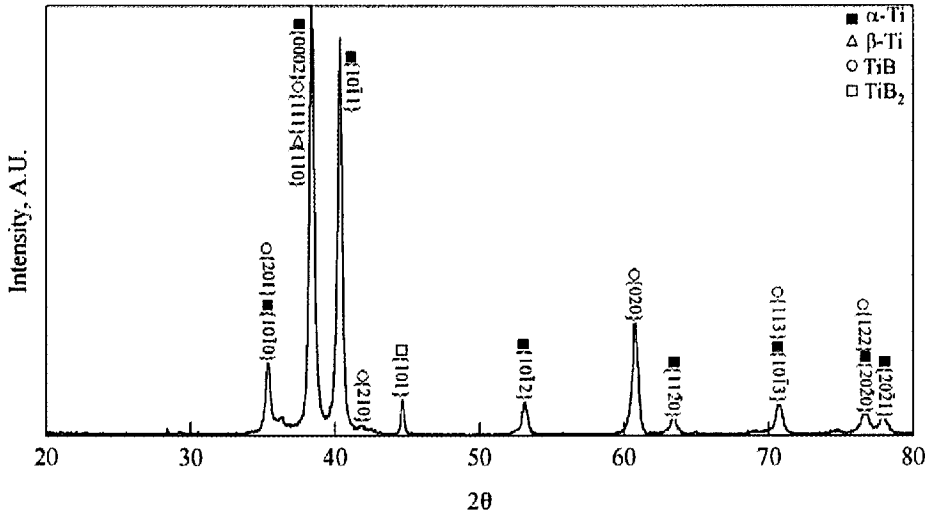


Fig. 6.3: X-ray diffraction trace of extruded Ti-6Al-4V + 20 vol.% TiB, T1 condition, transverse direction, the $\{101\}_{TiB_2}$ peak at 44.6° shows residual TiB_2

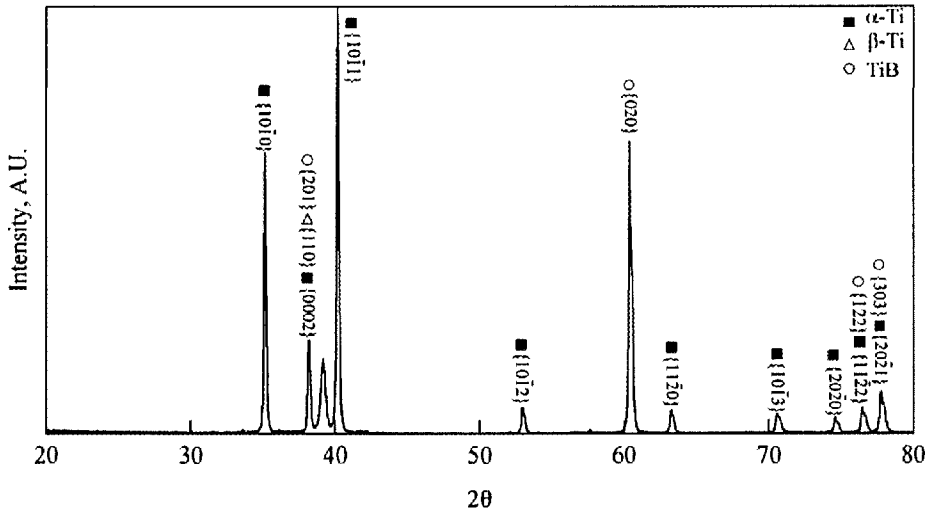


Fig. 6.4: X-ray diffraction trace of extruded Ti-6Al-4V + 20 vol.% TiB, T2 condition in the transverse direction, conversion heat treatment converts the remaining TiB_2 to TiB

Fig. 6.3 confirms the presence of TiB_2 in the T1 condition from the $\{101\}_{TiB_2}$ peak at 44.6°. After heat treating at 1200°C for 4 hours (T2 condition) prior to extrusion,

Fig. 6.4, the $\{101\}_{TiB_2}$ peak at 44.6°, disappears suggesting complete transformation of TiB_2 to TiB after HIP'ing and CHT. No other TiB_2 peaks were observed, and there are two reasons as to why this is the case. Firstly, there is a small volume fraction of TiB_2 in the material as the majority has already transformed to TiB during the HIP'ing process. Secondly, other TiB_2 peaks overlap with peaks from the other phases in the material, such as the α-Ti and TiB peaks.

The $\{010\}_{TiB_2}$ is the 100% peak for TiB_2 in untextured materials, which means that it is the most likely peak to be visible if the phase is present. However, it is known that for textured materials, XRD traces are not accurate in terms of the peak height. The peak positions are determined by the d-spacing and so as there are impurities in this material, the peak positions are also not accurate. Thus, the XRD traces shown in Figs. 6.3 and 6.4 are not accurate in terms of the peak heights and thus the volume fraction of the different phases in the material cannot be measured by this method. This has been confirmed by an XRD trace of the Ti MMC in the T1 condition taken from the longitudinal direction, Fig. 6.5. Despite these inaccuracies, it is believed that complete transformation of TiB_2 to TiB has occurred.

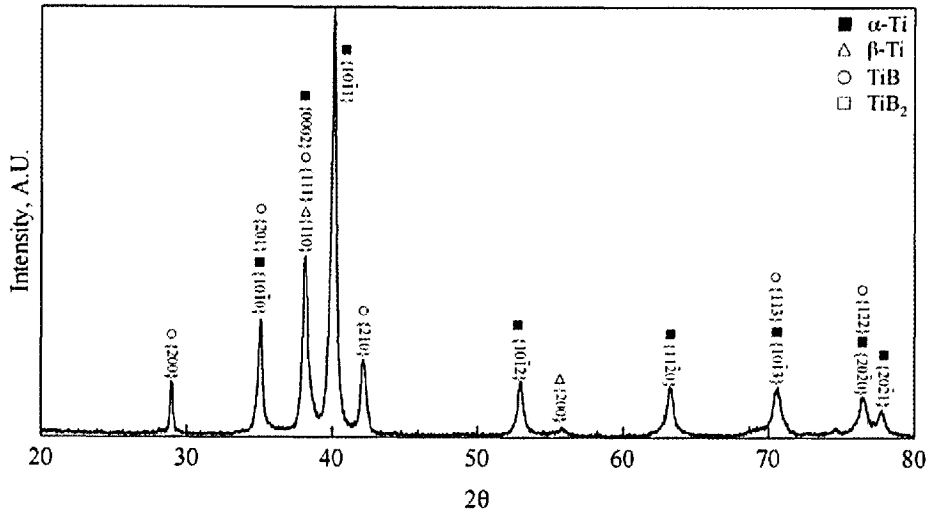


Fig. 6.5: X-ray diffraction trace of extruded Ti-6Al-4V-20 vol.% TiB, T1 condition in the longitudinal direction, showing the disappearance of the $\{101\}_{TiB_2}$ peak at 44.6°

In Fig. 6.5, the $\{101\}_{TiB_2}$ peak at 44.6° disappears, which would indicate that there is no TiB_2 in the T1 condition, however this is not the case as it has been shown in Fig. 6.3. Care must be taken when determining the phases present in these materials. It has been shown that the transverse direction is the optimal face for XRD analysis, for these materials, which have been extruded.

From the XRD traces in Figs. 6.3, 6.4 and 6.5, almost all the α-Ti, β-Ti, TiB_2 and TiB peaks overlap, and thus is it extremely difficult to determine exactly which phases are present within the material. In order to determine the phases present and the d-spacings with more accuracy, a more accurate detector is needed.

6.4.2 Microscopy of Ti MMCs

Light microscopy was performed on the Ti MMCs in both the T1, T2 and T3 conditions in the longitudinal direction, the resultant micrographs are shown in Fig. 6.6.

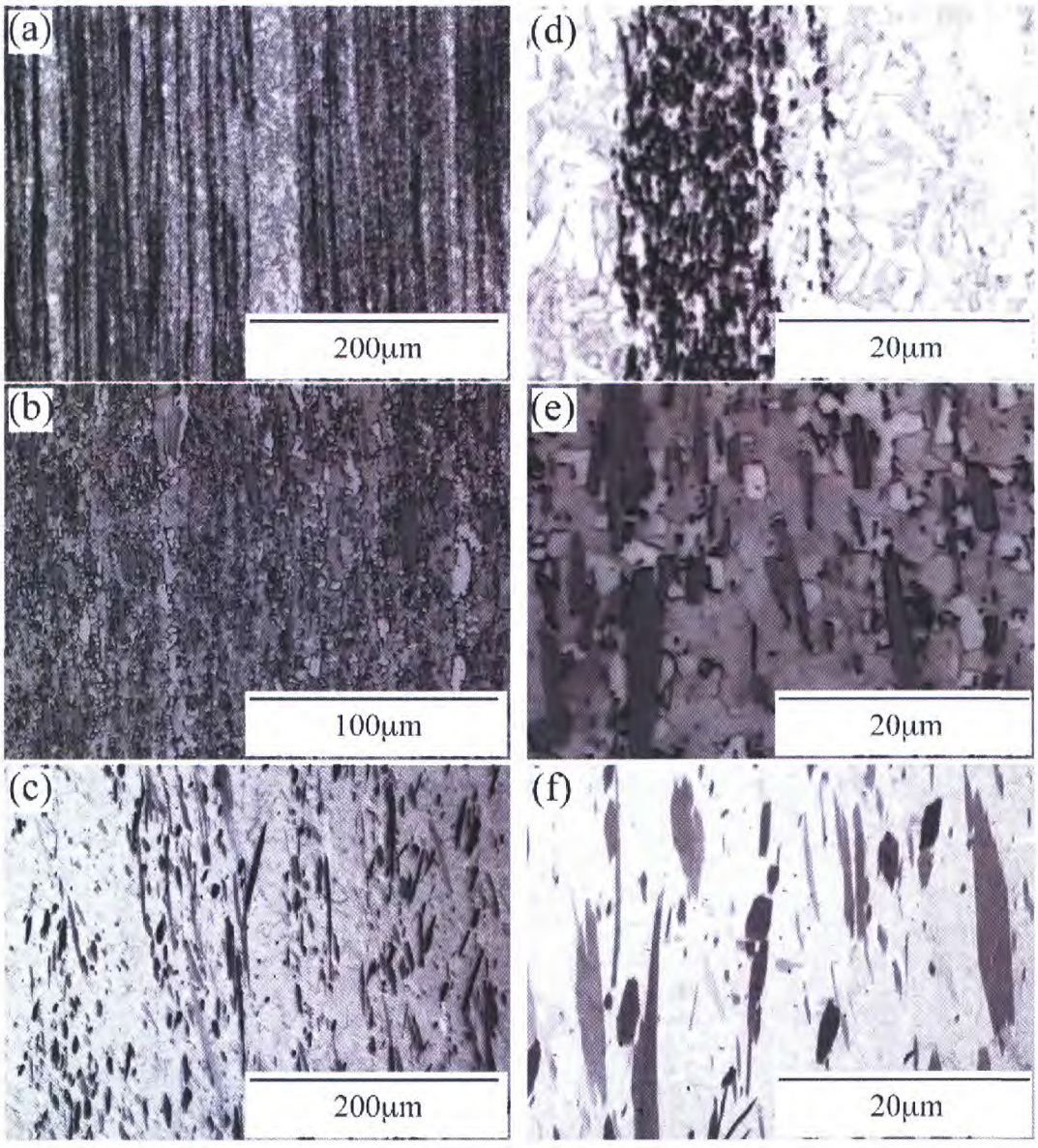


Fig. 6.6: Optical micrographs of the as extruded titanium composites, (a) T1, (b) T2, (c) T3, with corresponding high magnification images (d) T1, (e) T2 and (f) T3

Both the Ti MMCs in the T1 condition, Fig. 6.6(a), and T2 condition, Fig. 6.6(b), show that the TiB needles rotate to align with the extrusion direction, after extrusion. The TiB needles in the T1 condition are considerably smaller than the TiB needles in the T2 and T3 condition. When the composite is conversion heat treated after extrusion, T3 condition shown in Fig. 6.6(c), the TiB needles grow, which are of a similar size to the TiB needles formed in the T2 condition. This is due to the fact that in the T2 and T3 conditions, the materials have been heat treated at the same temperature and the same time. The morphology of the TiB needles in the three conditions are summarised in Table 6.4.

The distribution of the TiB in the T1 condition is heterogeneous. Comparing the higher magnification micrographs in the T1 condition, Fig. 6.6(d) and T2 condition, Fig. 6.6(e), there is a clear difference in the size and the distributions of the TiB needles. The T2 condition, Fig 6.6(e), shows a more homogeneous distribution of TiB than the T1 condition, Fig. 6.6(d), in which there is a definite 'streaking' structure of the reinforcing phase, clearly observed in Fig. 6.6(a). This effectively means that there are regions of the material in which there is essentially 100% reinforcement and other regions in which there is no reinforcement. After extrusion, the TiB/TiB_2 reinforcement, in the T1 condition, are extremely close together, illustrated in Fig. 6.6(d). There are, however, regions of heterogenity in the T2 condition, however these were much less frequent. A region of heterogenity is shown in Fig. 6.7(a).

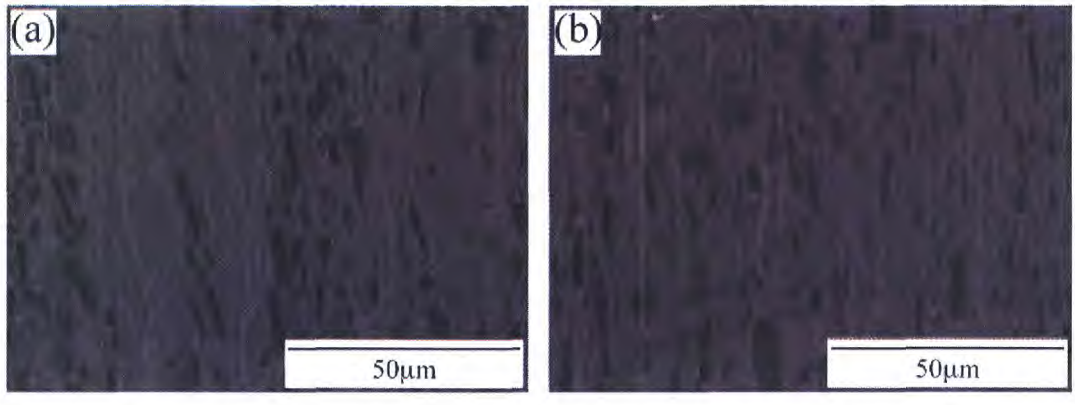


Fig. 6.7: Backscattered electron micrographs of Ti-6Al-4V + 20 vol.% TiB (a) region of heterogeneous TiB reinforcement and (b) region of homogeneous reinforcement

Fig. 6.7(a) shows that there are also regions of heterogeneity in the T2 condition, with regards to the TiB reinforcement, although these regions were far less common in the T2 condition compared to the T1 condition.

Table 6.4: Morphology of TiB needles in the three different heat treatment conditions, T1, T2 and T3

Heat Treatment Condition	Length, μm	Aspect Ratio
T1	1-5	3:1
T2	5-20	10:1
T3	5-20	10:1

The size of the TiB reinforcements in the T1 condition are approximately 1-5 μm in length and an aspect ratio of approximately 3:1. The TiB size in the T2 condition, Fig. 6.6(e), is significantly larger than the T1 condition, Fig. 6.6(d), being approximately 5-20 μm and an aspect ratio of approximately 10:1. The TiB size in the T2 and T3 condition has increased dramatically over the T1 condition due to grain growth of the TiB needles during the high temperature heat treatment at 1200°C for 4 hours. The size of the needles in the T3, Fig. 6.6(f) condition, which has been conversion heat treated post extrusion, exhibits needles of a similar size to the needles in the T2 condition, which was conversion heat treated prior to extrusion. The needles in the T3 condition retain the 'streaking' that is observed in the T1 condition, shown in Fig. 6.6(a) and Fig. 6.6(c).

In order to understand why the TiB grows as needles from the TiB_2, it is necessary to understand the crystal structure of TiB and the conditions in which it forms. TiB is characterised by zig-zag chains of boron atoms parallel to the 'b' direction with each boron atom lying in the centre of six Ti atoms. B atoms, in this case, form along the [010] direction, and to account for the stoichiometry, the columns of prisms are connected at their edges, Fig. 2.10(c). The prisms therefore form boron-free pipes. Growth normal to planes containing metal and boron atoms, in the same stoichiometry, should be faster than growth involving alternate planes of boron and titanium. It is also suggested that planes with a higher density of strong bonds (boron-boron >boron-metal >metal-metal) will grow at a faster rate. Thus the [010] direction should grow at a faster rate and so the TiB grows as needles [87].

This heterogeneous distribution and smaller size of TiB needles in the T1 condition is due to the mechanical alloying process. The starting materials are titanium alloy powder, TiH_2 and TiB_2 powder. These are then mechanically alloyed. During this process, the TiB_2 is supposed to be taken into a super saturated solid solution, however, the distribution of the reinforcing phase is still not homogeneously distributed throughout the titanium alloy powder [59] and it is extremely unlikely that the TiB_2 is in solid solution. The final powder material is similar to the layered structure, illustrated in

Fig. 6.8(a). The ideal case for the powder product after mechanical alloying is shown in Fig. 6.8(b).

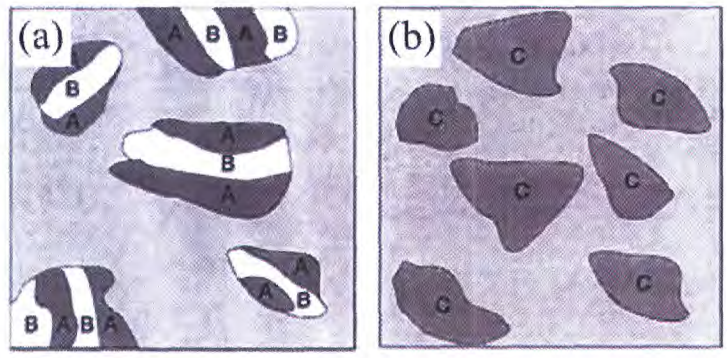


Fig. 6.8: Mechanical alloying, showing the (a) layered structure observed in Ti-TiB composites and (b) the optimal distribution of reinforcement phase, the alloy is in solid solution

When the powder is HIP'ed at 920°C for 2 hours, the conversion of TiB_2 to TiB starts to occur, the TiB grows into the Ti alloy matrix as needles, seen in Fig. 2.10. At this point, the TiB_2 and the Ti alloy matrix are anisotropic so the needles grow in all directions. The distribution of the needles, however, is heterogeneous due to the layered structure of reinforced areas and unreinforced areas, so when the material is extruded the TiB needles are aligned in streaks. This is illustrated in Fig. 6.9.

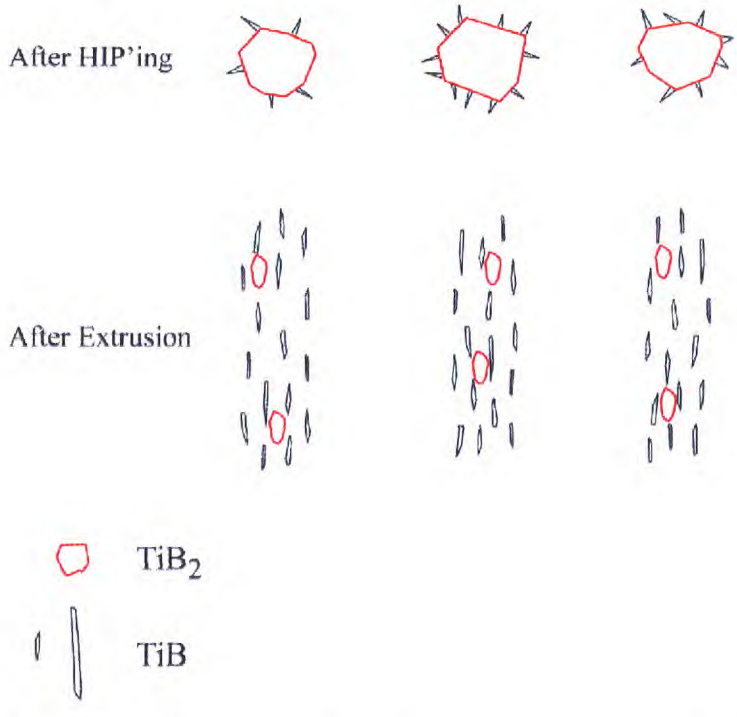


Fig. 6.9: Schematic illustration of TiB/TiB_2 distribution in the T1 condition

When the conversion heat treatment is applied to the material prior to extrusion, the needles grow further into the matrix as the material is still anisotropic, distributing the needles thoughout the matrix so that when the material is extruded, there is a much more homogenous distribution of the needles. This is illustrated in Fig. 6.10.

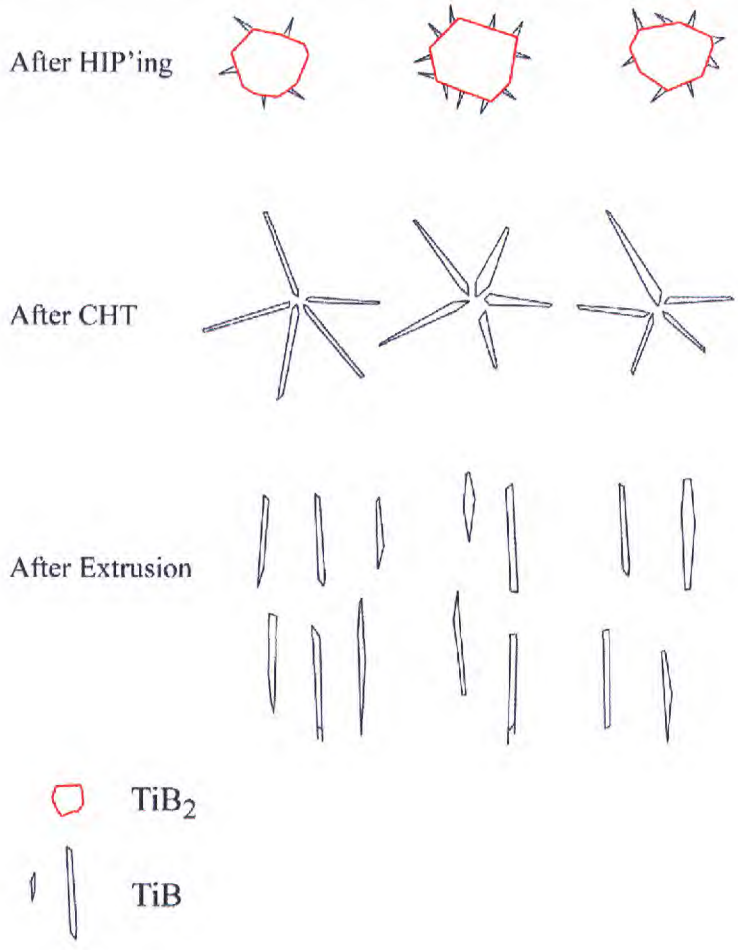


Fig. 6.10: Schematic illustration of the TiB distribution in the T2 condition

The reinforcement phase in these materials is needle shaped, however it has been reported that it could be possible to obtain a lower aspect ratio reinforcement phase by a low temperature anneal between 400 and 700°C before the HIP'ing cycle [87]. The reinforcement phase is reported to be approximately 100 nm in size and equaixed, with few needle shaped TiB particles. Although this is only reported for materials which have been manufactured *via* a rapid solidification (RS) technique. This is due to the diffusion of B atoms along different directions in the Ti matrix. At lower temperatures, the rate determining factor is the diffusion of B atoms, which is considerably lower than at higher temperatures. Thus, the difference in diffusion kinetics along different directions will depend on the supply of B atoms rather than the diffusion coefficients of a particular direction. In addition, the nucleation of TiB is favoured due to the instability of B in

super saturated solid solution. Thus the consumption of B atoms in the formation of many TiB nuclei makes TiB growth even more difficult. Therefore, the difference between the growth rates in different directions will be substantially reduced and the TiB will be nearly equiaxed. At higher temperatures and with a large supply of B atoms in solid solution, diffusion of B along the [010] direction will be dominant due to the increased diffusion coefficients at elevated temperatures, ~800°C.

In order to fully convert the TiB_2 to TiB, it is necessary to heat treat the material at 1300°C [59]. A conversion heat treatment prior to extrusion has been shown to produce a more homogeneous distribution of TiB reinforcement. Micrographs of the Ti MMC which has been conversion heat treated after extrusion (T3 condition) are shown in Fig. 6.6(c) and (f). During the conversion heat treatment, the Ti-6Al-4V microstructure is entirely β, as the material is at 1200°C, which is approximately 200°C above the β transus of monolithic Ti-6Al-4V. Monolithic Ti-6Al-4V would expect to have excessive grain growth at 1200°C for 4 hours. This is beneficial for these composites as the material still retains a fine grain size even after heat treating at 1200°C as the TiB needles pin the grain boundaries so that there is minimal growth. During the heat treatment, the TiB grows from the TiB_2 into the β. TiB has been shown to grow from the TiB_2, however, the effect of the β phase orientation has not been established. The light micrograph of the Ti-6Al-4V + 20 vol.% TiB in the T2 condition (conversion heat treated prior to extrusion) shows that the TiB penetrates though α and β grains when observed after extrusion.

There is a clear difference in the size of the TiB in the T1, Fig. 6.6(a), and T3, Fig. 6.6(c), conditions. This transformation has been reported to take 8 hours at 1300°C [59]; however it is shown that it is unnecessary to have such a high conversion temperature. The TiB needles have substantially grown during the conversion heat treatment post extrusion at 1200°C for 4 hours. The driving force for the TiB grain growth is the reduction in surface area to volume ratio between the matrix and the reinforcement. The mechanism for this grain growth is unlikely to be Oswald Ripening as this requires smaller particles to re-dissolve into the matrix, allowing larger particles to grow at the expense of smaller ones. The solubility of B in Ti is reported to be low at all temperatures and so the energy required to re-dissolve B in Ti would be significantly larger than the surface energy differences between larger and smaller particles. However, the microstructure in the T1 condition, Fig. 6.6(b), shows that the TiB particles are in contact with each other, which would significantly lower the energy required for diffusion B.

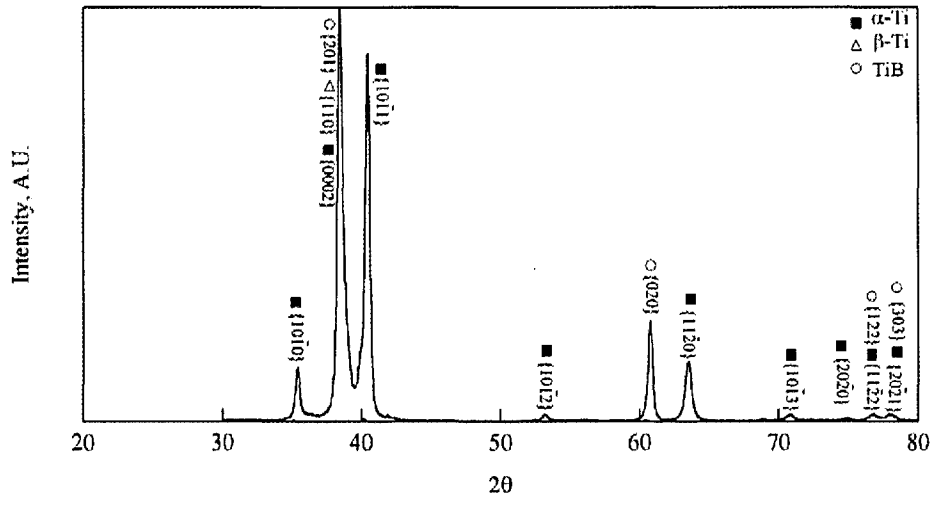


Fig. 6.11: XRD trace of Ti-6Al-4V + 20 vol.% TiB in the T3 condition, transverse direction

The as extruded Ti MMC in the T1 and T2 conditions has been analysed in Section 6.4. Fig. 6.11 shows an X-ray diffraction trace of the T3 condition, suggesting the $\{101\}_{TiB_2}$ peak at 44.6° disappears. Complete transformation, therefore, of the TiB_2 to TiB, occurs after 1200°C for 4 hours in an Ar atmosphere and can occur after thermomechanical process (extrusion). The small TiB needles and TiB_2 particles agglomerate together to form large TiB needles within the titanium matrix, Fig. 6.6(f). The TiB needles still retain some of the in-homogeneous distribution of the TiB reinforcement as in the as extruded composite, Fig. 6.6(c). During industrial scaling up, it would be necessary to determine the optimum conversion heat treatment conditions before conversion heat treating. The temperature/time relationship should be determined to obtain the optimal transformation temperature for both mechanical and economical benefits.

The Ti-6Al-4V matrix converts to fine scale lath-like α martensite upon quenching from 1200°C, Fig. 6.6(f). Aside from ageing the material at ~600°C to form a lamella microstructure, it would be impossible to convert the microstructure to a bi-modal or equiaxed microstructure without subsequent hot working high in the $\alpha+\beta$ phase field. This CHT is essentially a heat treatment on the matrix to form a lamella microstructure, illustrated in Fig. 2.7(b). Conversion heat treating the material post extrusion is not only detrimental for the reinforcement size, but also limits the microstructural possibilities.

In order not to limit the microstructural possibilities, and to obtain the best homogeneity of TiB needles, it is thought that the optimum processing conditions for Ti-TiB composites is to conversion heat treat the composite prior to any further thermomechanical heat treatments. The CHT, prior to any thermomechanical processing, also acts as

a homogenisation treatment, above the β transus, which is essential for bi-modal and equiaxed microstructures, illustrated in Fig. 2.7(a) and (b).

6.5 Mechanical Properties

Tensile testing of the Ti MMCs was performed by AMC using BS EN10002-1 testing conditions, these are outlined in Section 3.9. The extrusions were tested in the as-extruded condition using the tensile specimen geometry shown in Fig. 3.14. The stiffness and ultimate tensile strength are shown in Figs. 6.12, the ductility is shown in Fig. 6.13. A comparison between the T1 and T2 conditions is shown in Table 6.5

Table 6.5: Mechanical properties of Ti-6Al-4V+20 vol.% TiB, in both the T1 and T2 conditions

Material	Heat Treatment	Modulus, GPa	UTS, MPa	Ductility, %
Ti-6Al-4V	T1	116	1066	15.8
Ti-6Al-4V+10TiB	T1	143	922	0.62
Ti-6Al-4V+20TiB	T1	164	736	0.45
Ti-6Al-4V+20TiB	T2	160	880	0.58

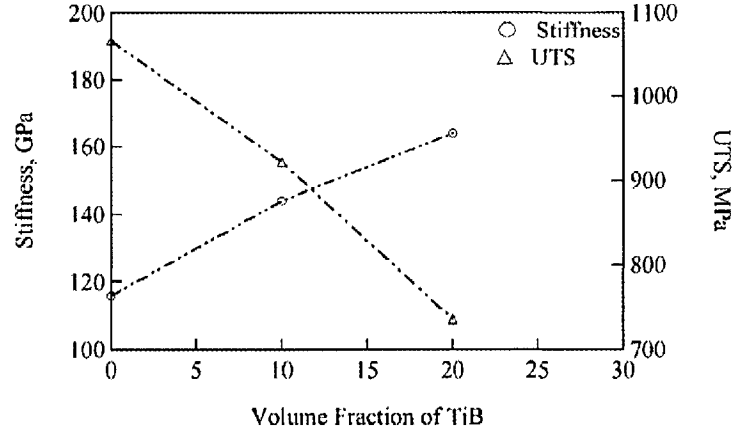


Fig. 6.12: Effect of the volume fraction of TiB on the stiffness and UTS of Ti-6Al-4V + 20 vol.% TiB in the T1 condition

Fig. 6.12 shows that the stiffness of the composites increases dramatically with increasing TiB content. The un-reinforced variant has a stiffness of 116 GPa. When 10 vol.% TiB is added to the alloy, the stiffness increases by 20% to 143 GPa. Increasing the TiB volume fraction to 20 vol.% again increases the stiffness by 41% over the un-reinforced variant to 160 GPa. These values compare reasonably well with the predicted values

shown in Table 2.4.

Load is transferred across the matrix/reinforcement interface, and as the TiB is significantly stiffer than the matrix (approximately 340% stiffer), there is a general increase in the stiffness of the material. Conversely, the UTS decreases with increasing volume fraction of TiB reinforcement, shown in Fig. 6.12.

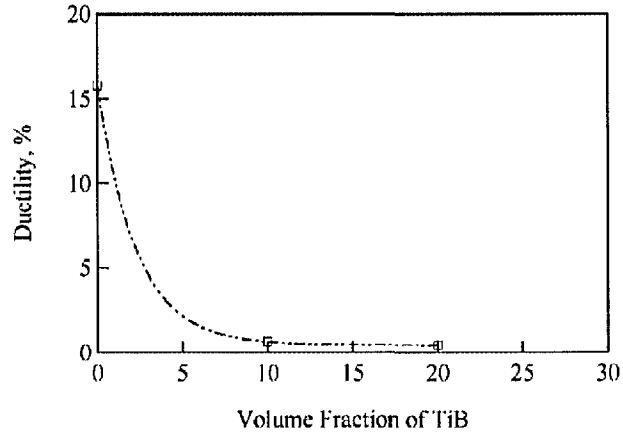


Fig. 6.13: Effect of the volume fraction of TiB on the ductility of Ti-6Al-4V + 20 vol.% TiB in the T1 condition

The decrease in the ductility, shown in Fig. 6.13, and UTS, shown in Fig. 6.12, of the composites are inextricably linked. As the reinforcement volume fraction increases, the ductility decreases dramatically from 15.8% to 0.64% with a 10 vol.% reinforcement and 0.45% with 20 vol.% TiB. In the as extruded condition, these composites are extremely brittle and would be unsuitable for the vast majority of engineering applications. The decrease in ductility is due to the addition of extremely brittle ceramic reinforcements, though there is little difference in the ductility between the addition of 10 or 20 vol.%. The UTS of the composites decreases with decreasing ductility due to the lack of work hardening that the material undergos. It is known that in metal matrix composites, the stress is not uniformly distributed between the matrix and the reinforcement. With respect to whisker reinforced composites, applied stress in the composite can be less than the yield stress of the matrix but in some areas, i.e. in the area around the reinforcement tip, the stress can be much greater than the yield stress [50]. If the stress around the needles is above the ultimate tensile strength, then the material will fail in a brittle manner. Due to the strong interface between the TiB and the Ti-6Al-4V, the interface is not conducive to plastic processes, and so the interface is brittle anyway.

It is unclear as to what influence the TiB has on the presence of dislocations in the material. When, for example, SiC particles are added to an Al alloy (e.g. AA2124), the presence of the fine SiC particles increases the dislocation density around the particles

due to the thermal mismatch between the SiC and the Al matrix, this promotes the nucleation of strengthening precipitates and thus the ageing process is accelerated [88]. The presence of TiB in Ti-6Al-4V should not suffer from this problem as both materials have a similar coefficient of thermal expansion and there is a very clean interface between the reinforcement phase and the matrix. Also, the ageing treatments between the two metals are quite different. With Al alloys, strengthening precipitates are nucleated during the ageing process; with Ti alloys, in particular Ti-6Al-4V, hot working, recrystallisation and ageing processes are used to optimise the α+β structure and morphology, rather than to precipitate intermetallic strengthening phases.

Table 6.6: Specific stiffness of Ti-6Al-4V and Ti-6Al-4V + 20 vol.% TiB, the values for a steel alloy are also included as a comparison

Material	Heat Treatment	Modulus, GPa	Specific Stiffness,
Ti-6Al-4V	T1	116	26
Ti-6Al-4V+20TiB	T1	164	36
Ti-6Al-4V+20TiB	T2	160	35
Steel	-	210	26

From Table 6.6, clearly the specific stiffness of these Ti alloy composites, manufactured for this piece of research, exceeds that of steel. There is clearly potential for these composites to compete with steels in terms of the stiffness requirements.

6.6 Texture

Texture measurements were taken on Ti-6Al-4V + 20 vol.% TiB in the T2 condition.

6.6.1 α Phase

The texture of the α phase in Ti-6Al-4V + 20 vol.% TiB has been analysed and compared with monolithic Ti-6Al-4V.

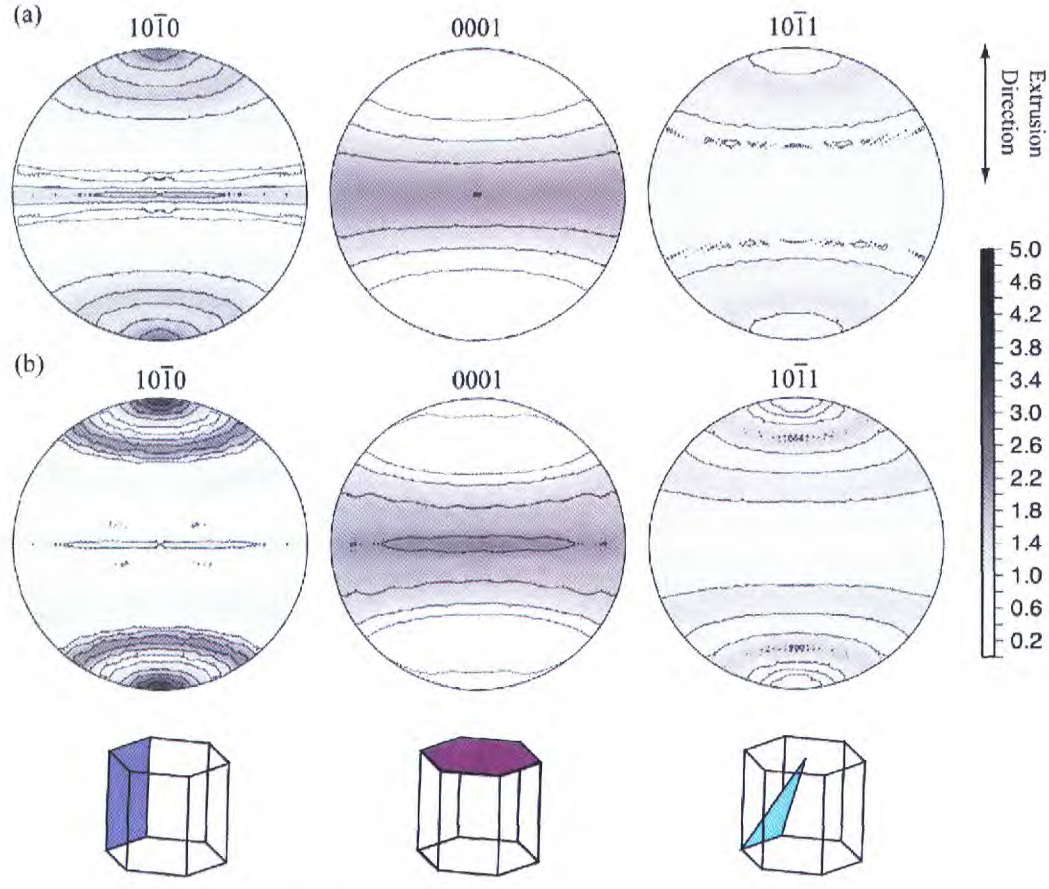


Fig. 6.14: Texture of α phase in (a) Ti-6Al-4V + 20 vol.% TiB and (b) monolithic Ti-6Al-4V

Fig. 6.14(a) shows the texture of Ti-6Al-4V + 20 vol.% TiB and monolithic Ti-6Al-4V, Fig. 6.14(b). The α phase in both variants shows a circular symmetric texture, which is expected in an extruded material, with both variants showing a $\{10\bar{1}0\}$ fibre texture. The difference between the two variants is the degree of texture. The composite, Fig. 6.14(a), shows less texture than the monolithic variant in Fig. 6.14(b). The TiB affects the texture of the material. During extrusion of the monolithic variant, the grains can rotate freely as there is nothing impeding grain rotation to align in the $\{10\bar{1}0\}$ plane. During extrusion of the composite, the TiB needles rotate to align in the extrusion direction, the TiB needles pin grain boundaries and so the grains can not rotate as freely as in the monolithic variant and as such there is less texture shown in the composite with respect to the α phase.

6.6.2 TiB

The texture of the TiB obtained from raw data files is shown in Fig. 6.15. It was not possible to generate proper pole figures as there was no orthorhombic file available in

popLA, so just the raw data is presented here to give an indication of the texture of the TiB phase.

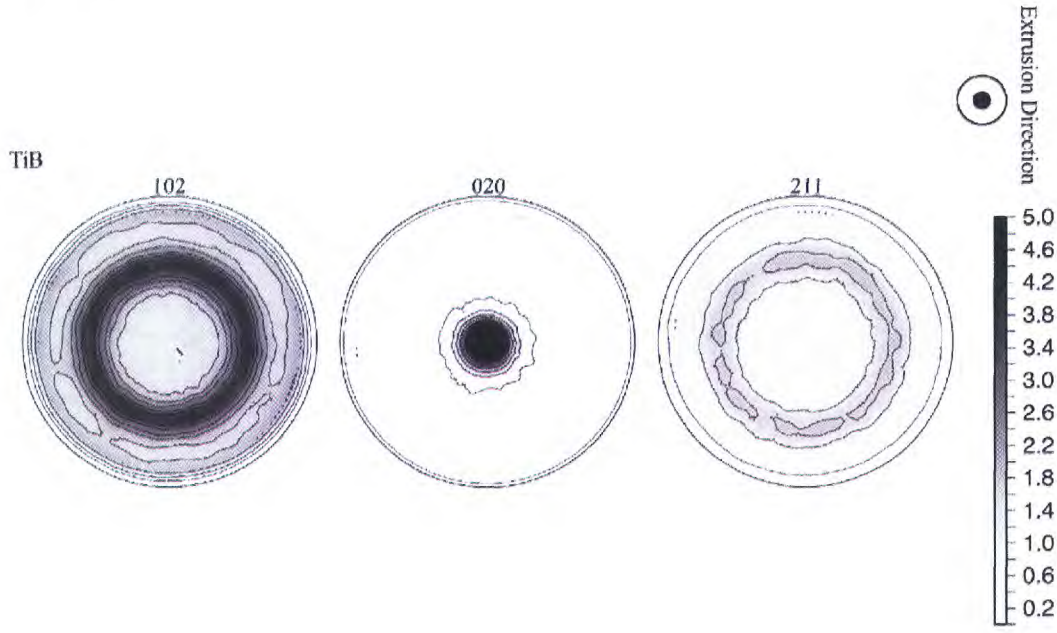


Fig. 6.15: TiB texture raw data file

Fig. 6.15 shows the texture of the TiB phase in the extrusion direction. The TiB is strongly aligned in the 020 direction. This is also the direction that the needles grow in, confirming that needles rotate to align in the extrusion direction. The TiB is significantly stiffer than the Ti-6Al-4V matrix and so rotate to align with the extrusion direction and they inhibit free rotation of the α grains.

6.7 Conclusion

In this chapter, the thermomechanical processing of a titanium alloy composite has been investigated. The Ti-6Al-4V + 20 vol.% TiB composite was manufactured *via* a non-melt processing route and a subsequent thermomechanical processing route applied. A conversion heat treatment to convert the TiB_2 to TiB was applied to the composite both before and after extrusion. The mechanical properties of the composites has also been evaluated. The following conclusions can be drawn from the presented data:

- A non-melt processing route can be utilised to manufacture Ti alloy composites reinforced with TiB. The starting Ti alloy powder feedstock material used in this piece of work was gas atomised powder, to further reduce the costs, a suitable

alternative source of cheap feedstock powder would be necessary, possibly following a blended elemental approach.

- Most of the conversion of TiB_2 to TiB occurs during the HIP'ing stage, however a conversion heat treatment at 1200°C for 4 hours is required to fully convert the reinforcement phase. The TiB_2 converts to TiB with a conversion heat treatment pre and post extrusion.

- The distribution of the reinforcement phase is inhomogeneous if no conversion heat treatment is applied to the composite. A conversion heat treatment pre-extrusion homogenises the distribution of the reinforcement phase after extrusion. The conversion heat treatment post extrusion maintains a degree of the inhomogeneous distribution of TiB.

- Significant grain growth of the TiB occurs during the conversion heat treatment at 1200°C, either before or after extrusion.

- The mechanical properties of the composites show increased stiffness when TiB is added to the Ti-6Al-4V matrix, however there is a drastic reduction in the ductility. If these materials are to be used in applications, an improvement in the ductility is required.

- The texture of the α phase in both monolithic and reinforced material has been established. The texture of the both the monolithic material and the composite shows a fibre texture in the $\{10\bar{1}0\}$ plane. The α phase texture in the monolithic material is stronger than the composite due to the TiB restricting grain rotation during extrusion.

Chapter 7

Conclusions and Further Work

7.1 Conclusions

The results in this thesis suggest that titanium powder can be consolidated *via* extrusion, which has been either canned and degassed, or cold compacted. The initial starting density of the powder is independent of the final extrusion density as the billets upset to nearly 100% density before the onset of extrusion. The consolidation of canned titanium *via* extrusion compares well with more traditional processes such as hot isostatic pressing. During extrusion of canned titanium powder, the front end of the extrudate experiences little deformation, forming a defect which is approximately 1/3 the length of the extrusion. The back end defect, common in all extrusions, were also observed in the canned material. This defect was formed from the mild steel can encapsulating the titanium powder. Although consolidation of the powder has been achieved, the economics of consolidation of canned titanium powder *via* extrusion is questionable due to the presence of these defects.

Although there is little published research on the effect of degassing preparations of titanium powders, the majority of degassing procedures employed, especially in the degasssing of titanium alloy composites, have tended to use higher temperatures. The degassing of titanium powder has yielded results that show it is unnecessary to degas above 500°C. At these lower temperatures, the diffusion of oxygen into the titanium powder is extremely low and hence interstitial pick up is minimised.

Titanium powder, which has been pre-compacted at room temperature, can also be consolidated *via* extrusion, with a greater degree of densification with increasing reduction ratio due to the increased strain that s imparted to the titanium powder as it is extruded.

The mechanical properties of compacted and extruded billets compares well with both canned and extruded, and HIP'ed titanium powder. The manufacturing method to produce the HDH titanium powder forms embrittling inclusions in the powder mass which are present in the consolidated powder product. These inclusions affect the ductility of the consolidated titanium powder and it is likely that these inclusions would effect other mechanical properties, such as the fatigue strength.

Rheology data for titanium powder was obtained by compression testing cylinders sectioned from a low reduction ratio extrusion of titanium powder. A regression analysis was performed to obtain data for the material file for Forge 2005 simulations. A sensitivity analysis has been performed and a value of 4250 $Wm^{-2}K^{-1}$ for the heat transfer coefficient for the billet/tooling interface with a Deltaglaze layer, has been established. A series of simulations has been performed to determine the effect of different extrusion conditions on the extrusion pressure and exit temperatures with different reduction ratios.

Billet chilling, due to the thermal gradients between the billet and the container, causes an increase in the flow stress of the titanium, and hence a rise in the extrusion pressure during extrusion of titanium powder compacts. A series of studies was conducted to predict the extrusion pressure of titanium powder compacts under different extrusion conditions. It was found that the speed of extrusion has a profound effect on the extrusion pressure compared with either the billet temperature or the die temperature. Billet chilling leads to temperature variations, during deformation through the dead metal zone, which could significantly alter the microstructure in titanium alloys. It is found that increasing the die and container temperature decreases this billet chilling, so that slower extrusions can be performed. However, if titanium alloy extrusions are to become completely isothermal, a container, with a similar temperature to the billet, would need to be developed. This would add significant costs to any titanium extrusion process.

A finite element model can be used to determine the material point history during the simulated extrusions. Surface temperature profiles were measured during the FE simulations and it has been shown that the surface exit temperature increases on leaving the die. Under the experimental conditions, the surface exit temperature for the low reduction ratios (R = 9:1 and 17:1), the exit temperature is only above the β transus for a short time, whereas the exit temperature for a high reduction ratio stays above the β transus for the entire length of the extrusion. Significant oxidation of the Ti compact billet occurs during preheating for extrusion, and although the surface exit temperature of the material is above the β transus for higher reduction ratios, the diffusion length of oxygen into α and β phases is minimal compared with the oxidation which occurs prior to extrusion.

The thermomechanical processing of Ti-6Al-4V + 20 vol.% TiB has been examined with reference to a conversion heat treatment on the reinforcing phase, to convert the constitutent powder, TiB_2, to the reinforcing phase, TiB *via* an *in situ* reaction with the Ti matrix. The composites was manufactured via a non-melt processing route, and the conversion heat treatment applied both before and after extrusion. Although it is found that the majority of the conversion of TiB_2 to TiB needles occurs during the hot isostatic pressing, i.e., when the powder is consolidated, there is still some residual TiB_2 which is converted during a high temperature heat treatment. The distribution of the reinforcement phase was found to vary with when the conversion heat treatment is applied. When conversion heat treating before extrusion, a much more homogeneous distribution of TiB needles is observed compared with conversion heat treating after the extrusion. However, the TiB needles grow during the heat treatment to approximately 10 μm in length, whereas they are significantly smaller if the composite is not conversion heat treated prior to extrusion.

The stiffness of the composites is significantly improved over a monolithic variant prepared in the same manner. This is attributed to the stiffness of the reinforcing phase. However, the ductility and ultimate tensile strength of the composites are severely reduced, so much so that, in their current condition, would be quite unsuitable for engineering applications.

A texture analysis was performed on the Ti-6Al-4V + 20 vol.%TIB composite, as well as on the monolithic variant to determine the effect of the TiB on the α phase in the Ti-6Al-4V. Both variants show a circular symmetric fibre texture aligned in the $[10\bar{1}0]$ direction. The TiB pins grain rotation and so the texture of the composite shows a more random texture than the monolithic Ti-6Al-4V. The TiB reinforcement shows a strong alignment in the 020 direction.

7.2 A Note on Titanium Powder

The titanium industry, and especially the powder titanium industry, has been receiving renewed interested in recent years [89], partly due to the inherent specific properties of titanium and its alloys, but also due to governmental directives to reduce fuel consumption and become more environmentally friendly. Non-melt processing of titanium powder is an important part of producing a step change in the economics of titanium and its alloys. If components can be manufactured from titanium which has never been melted (from reduction of the ore to the final component), then the costs can potentially be brought down to acceptable levels for non-traditional titanium industries. These materials are unlikely to find use in the aerospace industry as they will not have been triple

vacuum arc melted, which is a requirement in this industry. The automotive sector, for example, is not going to require such rigorous standards as the aerospace industry.

The cost of titanium powder, however, remains an issue, which at the present has not been addressed. Atomisation routes are notoriously expensive and it is difficult to produce titanium alloys in this way; however, recent advances in the extraction of titanium metal from its ores has led to the commercialisation of two non-melt reduction processes which could produce powder products. The first being International Titanium Powder (ITP), using a continuous version of the Hunter process, and more recently, Metalysis, using the FFC Cambridge Process.

The properties of the powders produced from these non-melt reduction processes have yet to be established, especially contaminants formed during the reduction, most notably, the use of $CaCl_2$ in the FFC Cambridge process. In the Kroll process, the $MgCl_2$ is distilled off, however this is unlikely to occur when using $CaCl_2$ unless high vacuums are employed, due to the vapour pressure of $CaCl_2$ being several orders of magnitude lower than $MgCl_2$. The preparation of these powders, e.g. degassing, is thus vitally important prior to consolidation. Other potential problems are the powder shape, given that the FFC Cambridge process forms sintered pellets, it is likely that a non-melt powder production process, such as the HDH process, is required to manufacture the powder from the FFC Cambridge process. This would produce angular particles which have inferior flow properties compared with spherical powders. Contamination during the HDH process could also be a potential problem. It remains to be seen whether the problems of producing powders *via* these processes can be overcome. Due to the massive demand for titanium powder, it is believed that there will be a market for these materials, even if it is just as a research product.

The potential problem with the ITP process is that the feedstock material is $TiCl_4$, the price of which is dominated by the pigment industry. The use of $TiCl_4$ also introduces another step into the process, which is unnecessary if Ti can be produced directly from TiO_2.

Titanium powder metallurgy is also receiving interest in near-net-shape processing techniques [90], such as press sintering and metal injection moulding, to further reduce to the cost of downstream processing, such as machining. The ability to manufacture complicated geometry's with little or no further processing is an attractive manufacturing technique for the titanium industry.

7.3 Further Work

The work presented in this thesis has proven that titanium powder can be consolidated *via* non-traditional non-melt processes for titanium powder. It would be useful to determine whether it would be possible to use a continuous consolidation process, such as conform (continuous extrusion), to consolidate the powder feedstock material. This would make the consolidation process far more economically viable. It would also be interesting to determine whether other possible consolidation routes, such as direct particle rolling, could be used to produce other shaped products. Cheap sheet material made from consolidated titanium powder would be a very attractive to industries, such as water purification plants. It is vital that a considerable quantity of powder produced by these novel reduction methods is manufactured so that consolidation trials can be conducted on this powder. The consolidation of cheap titanium powder feedstock, however, relies on a source of cheap feedstock material which is manufactured using non-melt processes, such as the FFC Cambridge process. There are currently very few companies pursuing these routes. Although there is no reason as to why more traditional titanium, i.e. Kroll sponge, can not be used for direct consolidation, it is vital that these non-melt processes are brought to fruition.

Titanium metal produced *via* consolidation processes from powder feedstock is the first step in the production of affordable titanium products, however, the consolidation of titanium alloys would be considerably more useful. Therefore consolidation of constituent powders for alloys should be attempted to determine whether a homogeneous mixture of the different powders can be obtained.

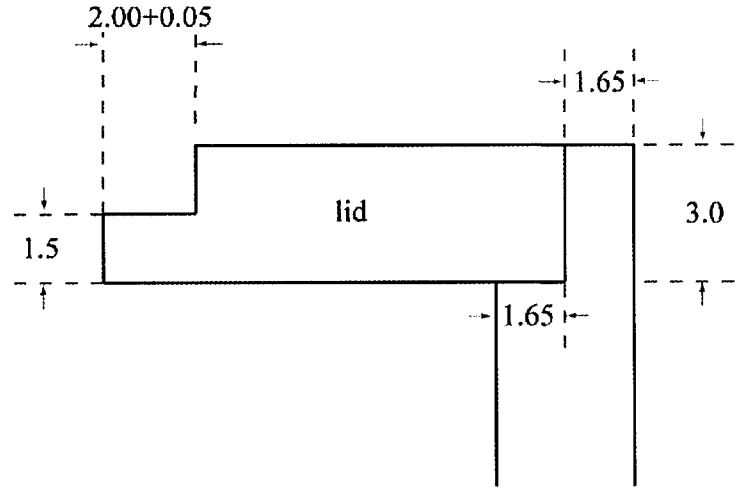
Finite element modelling of the consolidation of titanium powder has shown that improvements in the design of the extrusion press is vital if these processes are to be used to consolidate titanium powder. For example, the heating of titanium could be improved by the use of an induction furnace and the introduction of an inert atmosphere. The container material also needs modifying so that the container temperature and the die temperature are the same as the billet temperature to eliminate billet chilling. To extrude under isothermal conditions, an extremely slow extrusion speed is necessary. In order for this to happen, billet chilling needs to be eliminated and thus the container temperature needs to be raised.

The texture of the α has been determined, both in monolithic Ti-6Al-4V and in Ti-6Al-4V + 20 vol.% TiB, however a complete analysis of the TiB phase has not been established and it would be interesting to determine the texture of the TiB relative to the α, both before and after extrusion. For an analysis of the TiB phase, an orthorhomic WIMV file is required in popLA.

During the course of this thesis, several industrial partners have begun projects in the consolidation of titanium powder. Although the specific details are proprietary, the two industry projects have resulted from the work presented in this thesis are in association with Norsk Titanium, Norway and Aerospace Metals Composites, UK. Norsk Ti are interested in the consolidation of Kroll titanium sponge for the production of Ti alloy wires. Aerospace Metals Composites are researching the possibilities of producing Ti alloy composites via non-melt processing routes.

Appendix A

Appendix



all units are in mm

Fig. A.1: Lid design

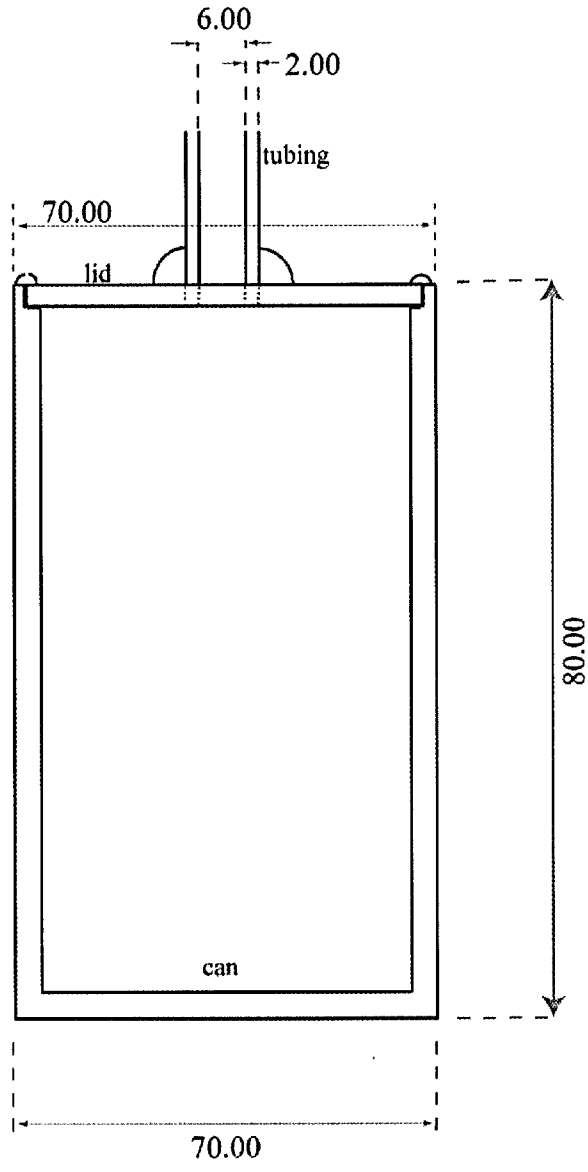


Fig. A.2: Can design

References

[1] E. Kraft, "Titanium: Past, Present and Future," Tech. Rep. Subcontract 4000013062, US Department of Energy and Oak Ridge National Laboratory, 2002.

[2] R. Wilson, N. Stone, and M. Gibson, "Extrusion of CP grade titanium powders eliminating the need for hot pre-compaction via hot isostatic pressing," *Materials Science Forum*, vol. 534-536, pp. 801–804, 2007.

[3] J. Sejournet and J. Delcroix, "Glass lubrication in the extrusion of steel," *Lubrication Engineering*, vol. Nov-Dec, p. 389, 1955.

[4] J. Norley, *The extrusion of Ti-6Al-4V*. PhD thesis, Imperial College London, 1985.

[5] T. Sheppard and P. Chare, "The extrusion of atomized aluminium powders," *Powder Metallurgy*, vol. 15, no. 29, pp. 17–41, 1972.

[6] P. Chare and T. Sheppard, "Powder extrusion as a primary fabrication process for Al-Fe alloys," *Powder Metallurgy*, vol. 16, no. 32, pp. 437–458, 1973.

[7] T. Sheppard and D. Raybould, "On load and temperature rise during the extrusion of superpure Al, Al-Zn and Al-Zn-Mg alloys," *Journal of the Institute of Metals*, vol. 101, pp. 33–44, 1973.

[8] P. Chare and T. Sheppard, "Densification and properties of extruded Al-Zn-Mg atomised powder," *International Journal of Powder Metallurgy*, vol. 10, no. 3, pp. 203–215, 1974.

[9] T. Sheppard and H. McShane, "Production of an aluminium-rich magnesium silicide alloy from atomized powder," *Powder Metallurgy*, no. 3, pp. 126–133, 1967.

[10] T. Sheppard and P. Chare, "On thermal activation during extrusion of metal powders," *Powder Metallurgy*, vol. 18, no. 35, pp. 1–14, 1975.

[11] T. Sheppard and A. Greasley, "Densification and pressure requirements during the extrusion of air-atomized tin bronze powders," *Powder Metallurgy*, no. 1, pp. 26–35, 1977.

[12] T. Saito, "The automotive application of discontinuously reinforced TiB-Ti composites," *Journal of Metals*, vol. May, pp. 33–36, 2004.

[13] C. Leyens and M. Peters, eds., *Titanium and Titanium Alloys - Fundamentals and Applications*. Wiley-VCH, 2003.

[14] M. Hunter, "Metallic titanium," in *General, Physical and Inorganic*, pp. 330–335, 1910.

[15] W. Kroll, "The production of ductile titanium," in *General Meeting*, pp. 35–47, 1940.

[16] "Annual report," tech. rep., Deutsche Titan, 2006.

[17] H. Flower, "Microstructural developments in relation to hot working of titanium alloys," *Materials Science and Technology*, vol. 6, pp. 1082–1092, 1990.

[18] R. Boyer, G. Welsch, and E. Collings, *Materials Properties Handbook: Titanium Alloys*. ASM International, 1994.

[19] I. Polmear, *Light Alloys*. Edward Arnold, 3 ed., 1989.

[20] H. Boyer and T. Gall, eds., *Metals Handbook*. ASM, 2005.

[21] M. Donachie, *Titanium - A Techincal Guide*. ASM International, 2nd ed., 2000.

[22] S. Lampman, *ASM Handbook*, vol. 2. ASM International, 1990.

[23] G. Lutjering and J. WIlliams, *Titanium*. Springer, 2003.

[24] M. A. Imam, R. Armstrong, B. Rath, and R. Judy, "Sustained load cracking and the plastic strain rate effect in titanium alloys containing hydrogen," in *Titanium Science and Technology* (G. Lutjering, U. Zwicker, and W. Bunk, eds.), vol. 4, (Munich, Germany), pp. 2487–2494, Deutsche Gesellschaft Fur Metallkunde E.V., 1984.

[25] R. Jaffee and I. Campbell, "The effect of oxygen, nitrogen and hydrogen on iodide refined titanium," *Transactions of the Metallurgical Society of AIME*, vol. 185, pp. 646–654, 1949.

[26] W. Finlay and J. Snyder, "Effects of three interstitial solutes on the mechanical properties of high purity, alpha titanium," *Journal of Metals*, vol. 188, no. Feb, p. 277, 1950.

[27] C. Ouchi, H. Iizumi, and S. Mitao, "Effects of ultra-high purification and addition of interstitial elements on properties of pure titanium and titanium alloy," *Materials Science and Engineering A*, vol. 243, no. 1-2, pp. 186–195, 1998.

[28] D. Simbi and J. Scully, "The effect of residual interstitial elements and iron on mechanical properties of commercially pure titanium," *Materials Letters*, vol. 25, pp. 35–39, January 1995.

[29] G. Dieter, *Mechanical Metallurgy*. McGraw-Hill, SI Metric Edition ed., 1988.

[30] V. Stolyarov, Y. T. Zhu, T. Lowe, and R. Valiev, "Microstructure and properties of pure Ti processed by ECAP and cold extrusion," *Materials Science and Engineering A*, pp. 82–89, 2001.

[31] J. Murray, *Phase Diagrams of Binary Titanium Allloys.* ASM International, 1987.

[32] R. Wasilewski and G. Kehl, "Diffusion of nitrogen and oxygen in titanium," *Journal of the Institute of Metals*, vol. 83, pp. 94–104, 1954.

[33] C. Rosa, "Diffusion of nitrogen and oxygen in titanium," *Metallurgical Transactions*, vol. 1, pp. 2517–2522, 1970.

[34] K. Dring, *Electrochemical Reduction of Titanium Dioxide in Molten Calcium Chloride.* PhD thesis, Imperial College London, 2005.

[35] H. Nakajima and M. Koiwa, "Diffusion in titanium," *Iron and Steel Institute of Japan International*, vol. 31, no. 8, pp. 757–766, 1991.

[36] S. Semiatin, P. Fagin, M. Glavicic, I. Sukonnik, and O. Ivasishun, "Influence on texture on beta grain growth during continuous annealing of Ti-6Al-4V," *Materials Science and Engineering A*, vol. 299, pp. 225–234, 2001.

[37] G. Lutjering, "Influence of processing on microstructure and mechanical properties of $\alpha + \beta$ titanium alloys," *Materials Science and Engineering A*, vol. 243, pp. 32–45, 1998.

[38] M. Peters and G. Lutjering, "Control of microstructure and texture in Ti-6Al-4V," in *Titanium '80* (H. Kimura and O. Izumi, eds.), vol. 2, pp. 925–935, 1980.

[39] M. Balshin and S. Kiparisov, *General Principles of Powder Metallurgy.* Mir Publishers, Moscow, 1980.

[40] S. Tsukerman, *Powder Metallurgy.* Pergamon Press, London, 1965.

[41] C. Azevedo, D. Rodrigues, and F. Beneduce Neto, "Ti-6Al-4V powder metallurgy via the hydrogenation-dehydrogenation (HDH) process," *Journal of Alloys and Compounds*, vol. 353, pp. 217–227, 2003.

[42] R. M. German, *Powder Metallurgy Science.* Metal Powder Industries Federation, 1984.

[43] V. Arunachalam and R. Sundaresan, *Materials Science and Technology: A Comprehensive Treatment*, vol. 15: Processing of Metals and Alloys, ch. 4. VCH, 1991.

[44] Z. Fan, A. Miodownik, L. Chandraskaran, and M. Ward-Close, "The young's moduli of in-situ Ti/TiB composites obtained by rapid solidification processing composites

obtained by rapid solidification processing," *Journal of Materials Science*, vol. 29, pp. 1127–1134, 1994.

[45] E. Kraft, "Economic analysis of the application of emerging reduction technologies to mill products production," in *Cost-Affordable Titanium - Symposium dedicated to Professor Harvey Flower* (F. H. Froes, M. A. Imam, and D. J. Fray, eds.), (Charlotte, North Carolina, USA), pp. 27–34, TMS, 2004.

[46] G. Z. Chen, D. J. Fray, and T. Farthing, "Direct electrochemical reduction of titanium dioxide to titanium in molten calcium chloride," *Nature*, vol. 407, pp. 361–364, 2000.

[47] R. Anderson, W. Ernst, L. Jacobsen, D. Kogut, and J. Steed, "Commercialization of the armstrong process for producing titanium alloy powder," in *Cost-Affordable Titanium - Symposium Dedicated to Professor Harvey Flower* (F. H. Froes, M. A. Imam, and D. J. Fray, eds.), pp. 121–126, TMS, 2004.

[48] A. Benish, A. Sathaye, P. Nash, R. Anderson, and T. Zwitter, "Characterization and use of armstrong process titanium powder," *Advances in Powder Metallugy and Particualte Materials*, vol. 3, no. 10, pp. 61–71, 2005.

[49] T. Saito, "A cost effective P/M titanium matrix composite for automotive use," *Advanced Performance Materials*, no. 2, pp. 121–144, 1995.

[50] T. Clyne and P. Withers, *An introduction to metal matrix composites.* Cambridge University Press, 1993.

[51] X.-H. Lu, Y. Yang, B. Huang, X. Luo, and Y. Liu, "Reaction diffusion in continuous SiC fibre reinforced Ti matrix composite," *Transactions of Nonferrous Metals Society of China*, vol. 17, no. 1, pp. 27–43, 2007.

[52] S. Tamirisa and D. B. Miracle, "An overview of titanium alloys modified with boron," in *Ti-2007 Science and Technology* (M. Niinomi, S. Akiyama, M. Hagiwara, M. Ikeda, and K. Maruyama, eds.), vol. 1, pp. 737–740, The Japan Institute of Metals, 2007.

[53] Z. Ma, S. Tjong, and L. Gen, "In-situ Ti-TiB metal-matrix composite prepared by a reactive pressing process," *Scripta Materialia*, vol. 42, pp. 367–373, 2000.

[54] J. Brandstötter and W. Lengauer, "Multiphase reaction diffusion in transition metal-boron systems," *Journal of Alloys and Compounds*, vol. 262-263, pp. 390–396, 1997.

[55] B. Decker and J. Kasper, "The crystal structure of TiB," *Acta Crystallographica*, vol. 7, pp. 77–80, 1954.

[56] M. Hyman, C. McCullough, J. Valencia, C. Levi, and R. Mehrabian, "Microstructure evolution in TiAl alloys with B additions: Conventional solidification," *Metallurgical Transactions A*, p. 1847, 1989.

[57] S. Whang, "Rapidly solidified titanium alloys for high-temperature applications," *Journal of Materials Science*, vol. 21, pp. 2224–2238, 1986.

[58] S. Tamirisakandala, R. Bhat, D. B. Miracle, S. Boddapati, R. Bordia, R. Vanover, and V. Vasudevan, "Effect of boron on the beta transus of Ti-6Al-4V alloy," *Scripta Materialia*, vol. 53, pp. 217–222, 2005.

[59] T. Godfrey, *Production, microstructure and tensile properties of mechanically milled titanium-boron alloys.* PhD thesis, Imperial College London, Department of Materials, Imperial College London, 2001.

[60] T. Godfrey, P. Goodwin, and M. Ward-Close, "Titanium particulate metal matrix composites, reinforcement, production methods and mechanical properties," *Advanced Engineering Materials*, vol. 2, no. 3, pp. 85–92, 2000.

[61] R. Gardiner, P. Goodwin, S. Dodd, and B. Viney, "Non-equilibrium synthesis of new materials," *Advanced Performance Materials*, vol. 3, pp. 343–364, 1996.

[62] J. Silk, *The influence of secondary processing conditions on the mechanical properties and microstructure of a particle reinforced aluminium matrix composite.* PhD thesis, Imperial College London, 2008.

[63] R. Heckel, "An analysis of powder compaction phenomena," *Transactions of the Metallurgical Society of AIME*, vol. 221, pp. 1001–1008, 1961.

[64] T. Penrice, "Compacting of powders using moulds made from reversible gels," *Powder Metallurgy*, no. 1/2, pp. 79–84, 1958.

[65] M. Stromgren, H. Astrom, and K. Easterling, "The effect of interparticle contact area on the strength of cold-pressed aluminium powder compacts," *Powder Metallurgy*, vol. 16, no. 32, pp. 155–165, 1973.

[66] M. Galanty, P. Kazanowski, P. Kansuwan, and W. Misiolek, "Consolidation of metal powders during the extrusion process," *Journal of Materials Processing Technology*, vol. 125-126, pp. 491–496, 2002.

[67] Y. Lee and M. Peters, "Effect of degassing treatment on microstructure and mechanical properties of PM Ti-6Al-4V," in *Titanium '99* (I. Gorynin and S. Ushkov, eds.), vol. 3, (St-Perterburg, Russia), pp. 1805–1812, CRISM "Prometey", 1999.

[68] C. Shakespeare and D. Oliver, "The hot extrusion of metal powders," *Powder Metallurgy*, vol. 7, no. 14, pp. 202–212, 1964.

[69] B. Eastwood and D. Robins, "Some properties of tin prepared from tin powder by extrusion," *Powder Metallurgy*, vol. 7, no. 14, pp. 99–112, 1964.

[70] P. Roberts and B. Ferguson, "Extrusion of metal powders," *International Materials Reviews*, vol. 36, no. 2, pp. 62–79, 1991.

[71] G. Sachs and W. Eisbein, "Power consumption and mechansim of flow in the extrusion process," *Deutsche Materialprüfungsanstalten Mitteilungen*, vol. 16, pp. 67–96, 1931.

[72] R. Thackray, *Flow effects during the extrusion of aluminium alloys.* PhD thesis, Imperial College London, 2000.

[73] C. Pearson and R. Parkins, *The Extrusion of Metals.* Chapman and Hall, 2nd ed., 1961.

[74] H. Atkinson and S. Davies, "Fundamental aspects of hot isostatic pressing: An overview," *Metallurgical and Materials Transactions A*, vol. 31A, no. 12, pp. 2981–3000, 2000.

[75] D. Delo and H. Piehler, "Early stage consolidation mechanisms during hot isostatic pressing of Ti-6Al-4V powder compacts," *Acta Materialia*, vol. 47, no. 9, pp. 2841–2852, 1999.

[76] M. Bocanegra-Bernal, "Hot isostatic pressing (HIP) technology and it's applications to metals and ceramics," *Journal of Materials Science*, vol. 39, pp. 6399–6420, 2004.

[77] F. H. Froes, D. Eylon, G. Eichelman, and H. Burte, "Developments in titanium powder metallurgy," *Journal of Metals*, 1980.

[78] *Forge Modelling Project - Report FMP - 7.* Universtity of Bath, School of Mechanical Engineering, 1994.

[79] "http://www.timet.com/index_new.htm," May 2008.

[80] M. Jackson, *Microstructural evolution of titanium alloys during isothermal subtransus forging.* PhD thesis, Imperial College London, 2002.

[81] D. Damodaran and R. Shivpuri, "Prediction and control of part distortion during the hot extrusion of titanium alloys," *Journal of Materials Processing Technology*, vol. 150, pp. 70–75, 2004.

[82] "http://www.matweb.com/search/datasheet.aspx?matid=14259," May 2008.

[83] O. Kubaschewski and C. Alcock, *Metallurgical Thermochemistry.* Pergamon Press, Oxford, 5th ed., 1979.

[84] J. Besson and M. Abouaf, "Behaviour of cylindrical HIP containers," *Internation Journal of Solid Structures*, vol. 28, no. 6, pp. 691–702, 1991.

[85] "Forge2, version 2005, Transvalor S.A., France," 2005.

[86] Z. Liu and G. Welsch, "Literature survey on diffusivities of oxygen, aluminium and vanadium in alpha titanium, beta titanium and rutile," *Metallurgical Transactions A*, vol. 19, pp. 1121–1125, 1988.

[87] Z. Fan, L. Chandraskaran, M. Ward-Close, and A. Miodownik, "The effect of preconsolidation heat treatment on TiB morphology and mechanical properties of rapidly solidified Ti-6Al-4V-XB," *Scripta Metallurgica et Materialia*, vol. 32, no. 6, pp. 833–838, 1995.

[88] B.-C. Ko and Y.-C. Yoo, "The effects of ageing treatment on the microstructure and mechanical properties of AA23124 hybride composites reinforced with both SiC whiskers and SiC particles," *Composites Science and Technology*, vol. 59, no. 5, pp. 775–779, 1999.

[89] R. Mehta, "Powder metallurgy processing for low-cost titanium," *Materials World*, vol. July, 2008.

[90] S. Samuel, S. Nag, T. Scharf, and R. Banerjee, "Wear resistance of laser-depositied boride reinforced Ti-Nb-Zr-Ta alloy composites for orthopedic implants," *Materials Science and Engineering C*, vol. 28, pp. 414–420, 2008.